Development and Performance Evolution of Medium-Pressure Plasma Process for Surface Modification of Fused silica

A thesis submitted

in partial fulfillment of the requirements

for the degree of

Doctor of Philosophy

By

Hari Narayan Singh Yadav

Roll No.-196103013

Department of Mechanical Engineering

Indian Institute of Technology Guwahati

Guwahati –781039, Assam, India

June, 2024

Department of Mechanical Engineering
Indian Institute of Technology Guwahati
Guwahati-781039, Assam,
INDIA

CERTIFICATE

It is certified that the work contained in the thesis entitled "**Development and Performance Evolution of Medium-Pressure Plasma Process for Surface Modification of Fused silica**", submitted by **Hari Narayan Singh Yadav**, Roll No. **196103013** to the Indian Institute of Technology Guwahati for the degree of Doctor of Philosophy has been carried out under my supervision in the Department of Mechanical Engineering, Indian Institute of Technology Guwahati. This work has not been submitted elsewhere for any other degree or diploma award.

Date: 01-06-2024

Dr. Manas Das

Department of Mechanical Engineering

Indian Institute of Technology Guwahati

Guwahati-781039, Assam, India

Declaration

I declare that this written submission represents my idea in my own words, and where others' ideas or words have been included, I have adequately cited and referenced the original sources. I also declare that I have adhered to all principles of academic honesty and integrity and have not misrepresented, fabricated, or falsified any idea/data/fact/source in my submission. I understand that any violation of the above will cause disciplinary action by the institute and can also evoke penal action from the sources that have thus not been properly cited or from whom proper permission has not been taken when needed.

Date: 01-06-2024

Hari Narayan Singh Yadav
Roll No.: 196103013

Dedicated to

My Family

ACKNOWLEDGEMENT

I would like to take this opportunity to pay my deep sense of respect and sincere gratitude to my supervisor, Dr. Manas Das, Department of Mechanical Engineering, Indian Institute of Technology Guwahati, Guwahati-781039, Assam, for his invaluable advice, resourceful guidance, inspiring instructions, active supervision and constant encouragement without which it would not have been possible for me to reach to this point.

I also wish to thank my doctoral committee members, Dr. Swarup Bag, Dr. Prasenjit Khanikar, and Dr. Chandan Das, for their guidance, moral support, and encouragement of my ideas in the subject as well as other areas of innovation. I must not miss the opportunity to thank all the professors of the Mechanical Engineering Department, Indian Institute of Technology Guwahati, whose motivation and timely help molded me in all possible ways.

I would also like to thank Dr. Sam Dayala Dev, Dr. Enni Krishna, Smt. Sreelakshmy K, Shri P B Narayana Kutty, and Shri Sukumaran K D, thank you for your support in carrying out my work at ISRO Inertial Systems Unit (IISU) Thiruvananthapuram. I am very thankful to workshop superintendent Mr. N. K. Das and workshop technicians Mr. Gokul Das and Mr. Dulumoni Das for their help in fabricating my experimental setup. I would like to acknowledge the Central Instrument Facility (CIF) of IIT Guwahati for its kind assistance in carrying out my research work.

Last but not least, I am deeply indebted to my parents for the sacrifices they have borne to ensure the fulfillment of my dreams. I would like to thank my family for their support and motivation during my Ph.D.

The time I spent with all my seniors and friends at IIT Guwahati, Dr. Manjesh Kumar, Dr. Abhinav Kumar, Dr. Keili Durgaprasad, Dr. Ambrish Singh, Dr. Atul Singh Rajput, Anand Mohan Pandey, Ranajit Mahanti, Aakash Tyagi, Ravi Prakash, Udit Kumar, and Kanak Jindal who made my life enjoyable and memorable on the campus.

Above everything, I thank my GOD for blessing me with wisdom and good health throughout this endeavor.

Hari Narayan Singh Yadav

Abstract

Glass has become essential in everyday life. Our modern society uses glass as a key material in thousands of products, ranging from simple glass bottles to sophisticated information technology (IT) systems. The pace of innovation in glass is accelerating due to progress in understanding glass physics and chemistry, combined with modern analytic and control technologies. Due to its unique properties, fused silica finds many applications among glass materials as a passive and active optical system. It is widely used as high-power lenses and windows for astronomy, microlithography, laser material processing, and high-power laser applications. But fused silica optics plays an active role in the inertial sensors category for aerospace applications. The refractive-based ring laser gyroscope and freeform hemispherical resonator shell have ultra-smooth, complete internal reflecting corner optics, essential for vibratory gyroscopes and fused silica substrate applications. These applications demand damage-free fused silica optics. But the brittle nature of the fused silica poses a challenge for manufacturing industries.

Conventional contact type of machining induces damage to the fused silica surface and significant damage incurred at the subsurface. Hence, a quantum of research is carried out to eliminate subsurface damage of fused silica optics by various non-conventional methods. Among the non-conventional methods, atmospheric plasma processing emerged as a deterministic process for polishing fused silica optics. The atmospheric plasma processing method requires a high-precision mechanism for processing a freeform optical application; moreover, achieving uniform machining is a challenge. Similarly, low-pressure plasma processing can process the entire optics simultaneously without precision mechanization. The physical action of the ions at low pressure damages the surface topography of the optical surface. Medium-pressure plasma processing carries the energy advantage of the low-pressure plasma system and chemical reactivity as atmospheric plasma processing.

A novel non-contact medium-pressure plasma nano-finishing technique is being developed to augment or replace chemo-mechanical polishing (CMP) techniques for finishing such microstructures. The developed process uniformly polishes the complex-shaped gyro, i.e., a hemispherical resonator shell fabricated with fused silica by an ultrasonic milling process. A combination of plasma polishing and cleaning processes is used to achieve sustained polishing of the hemispherical shell. It is essential to understand the brittle damages, such as surface cracks and plastic deformation, that can occur on the surface of

hard, brittle materials like glass ceramics, fused silica, etc. The novelty of the present medium-pressure plasma process is that it combines the isotropic material removal capability of low-pressure plasma and the atomistic material removal capability of atmospheric-pressure plasma. This process can simultaneously polish entire complex 3D surfaces, including cavities where no tool or beam can reach.

The present study designed and developed a medium-pressure plasma polishing (MPPP) setup for finishing optical materials. The MPPP plasma process consists of mass flow controllers for precise control of helium (i.e., processing gas), sulfur hexafluoride (i.e., reactive gas), and oxygen (i.e., catalytic gas). The system also consists of a gas dosing valve for controlling the total pressure of the plasma chamber. The pumping system can reduce the chamber pressure during machining. Further, an experimental investigation of atomistic material removal using a medium-pressure plasma process on a fused silica surface is carried out. The effects of plasma polishing factors, such as gas composition, pressure ratio, total pressure, and RF power, on fused silica's material removal rate (MRR) have been investigated while conducting a series of experiments at each parameter. The material removal rate has been improved up to 0.1004 mm^3/min at the optimized process parameters, i.e., gas composition of 90:10, pressure ratio of 1:1, total pressure of 5 mbar, and RF power of 80 W. Raman spectroscopy analysis provides clear evidence of a reduction in strain bonds after plasma processing. Further Raman spectroscopic results show that the average ratio (at different depths) improves from 1.88 before plasma processing to 2.12 after plasma processing, enhancing 13% reduction in damaged and strained layers after plasma processing on the substrate surface.

The plasma system effectively improves the surface finish, material removal rate (MRR), the percentage change in surface roughness, and subsurface defects. Material removal rate (MRR) and percentage improvement in R_a (% ΔR_a) are significantly affected by RF power, total pressure, gas composition, pressure ratio, and machining time. A low-RF power and higher total pressure resulted in lower MRR, and a high RF power with lower total pressure resulted in a higher % ΔR_a. The MRR increases with increased substrate dimension because of the increased contact area between radicals and surface atoms. Also, the MRR decreases with the increase in the total pressure of the plasma chamber. The highest and lowest MRR achieved at a total pressure of 5 mbar and 30 mbar are 0.040 mm^3/min for the substrate dimension of 45×5×2 mm^3 and 0.006 mm^3/min for 5×5×2 mm^3 substrate dimension.

Moreover, FESEM analysis shows that the grain size was reduced and remained regular in shape after plasma processing. The elements Si, O, C, and F appear on the plasma processed surface, showing the reaction occurring during plasma processing. Further studies are focused on the variation of MRR and % ΔR_a with process parameters. Regression and statistical analysis for MRR and % ΔR_a with different power, pressure ratio, and total pressure are performed to find a suitable relationship between input and output parameters. The optimized MRR and % ΔR_a values are 0.012 mm^3/min and 3.59% for RF power, pressure ratio, and total pressure of 60 W, 3, and 14.3 mbar, respectively. The obtained desirability is 74.90%.

Moreover, a comparative analysis of the surface finish between the coarse machined and lapped surfaces of the fused silica substrates has been investigated using medium-pressure plasma polishing (MPPP) and wet chemical etching (WCE). In MPPP, the surface roughness linearly increases with increased material removal depth, i.e., up to 30 μm at a total pressure of 5 mbar for the coarse machined surface. Similar results are also observed at 10 mbar pressure; however, the percentage change in surface roughness is lower than 5 mbar. Further, it has been observed that at 20 mbar pressure, the surface roughness linearly increases up to 20 μm depth, and beyond that, surface roughness remains constant. The lapped surface also follows a similar trend in MPPP. However, the percentage increase in surface roughness of the lapped surface is lower than that of the coarse machined surface. MPPP is suggested for finishing lapped surfaces instead of coarse surfaces. The percentage increase in surface roughness is 84.8% and 98.81% on coarse machined surfaces and 69.23% and 892.3% on a lapped surface using MPPP (at 20 mbar pressure) and wet chemical etching, respectively.

During the plasma polishing of freeform and complex surface, i.e., prism, the area surface roughness (S_a) is increased from 0.54 nm to 2.61 nm (at 5 mbar total pressure) and 0.53 nm to 0.57 nm (at 20 mbar total pressure) without any surface contamination. A higher surface roughness value is observed at 5 mbar total pressure than 20 mbar. The experimental study was carried out at different pressures and RF power to evaluate the plasma process while comparing the wet chemical etching process. The buffered hydrofluoric acid and sulfuric acid composition is optimized to achieve a similar MRR as a plasma process. The experiments were repeated three times for different initial surface roughness values for both wet chemical etching and plasma processing. The results suggested that the wet chemical process significantly damages the surface roughness after processing. Hence,

plasma processing replacing the hazardous chemical process can reduce the optics' labor-intensive polishing time and cost.

Table of Contents

List of Figures

List of Tables

NOMENCLATURE

S_a	Average surface roughness entire area
R_a	Center-line average surface roughness
$Å$	Angstrom
T_e	Electron temperature
n_e	Electron density

Acronym

AFF	Abrasive flow finishing
Al_2O_3	Aluminium oxide
ANOVA	Analysis of variance
DOE	Design of experiment
CMG	Chemo-mechanical grinding
EDS	Energy-Dispersive X-Ray spectroscopy
FESEM	Field emission scanning electron microscope
MAAFM	Magnetically assisted abrasive flow machining
MAF	Magnetic abrasive finishing
MFAF	Magnetic field-assisted finishing
MRAFF	Magnetorheological abrasive flow finishing
MRF	Magnetorheological finishing
MRR	Material removal rate
R-MRAFF	Rotational magnetorheological abrasive flow finishing
RSM	Response surface methodology
SiC	Silicon carbide
XPS	X-Ray Photoelectron spectroscopy
XRD	X-ray Diffraction
APPJ	Atmospheric pressure plasma jet
AFF	Abrasive flow finishing
MAF	Magnetic abrasive finishing
MRAFF	Magnetorheological abrasive flow finishing
MFP	Magnetic float polishing
MRF	Magnetorheological finishing
SSD	Sub-surface damage
RAP	Reactive atom plasma machining
APPP	Atmospheric pressure plasma polishing
PSD	Power spectral density
HER	High etching rate
LER	Low etching rate
RF	Radio-frequency
HF	Hydrofluoric acid
TRP	Total internal reflecting prism

DI	De-ionized
MFC	Mass flow controller
SIMS	Secondary ion mass spectroscopy
SCCM	Standard cubic centimeter per minute
CF_4	Carbon tetrafluoride
SF_6	Sulfur hexafluoride
CRF	Capacitive radio-frequency
Psi	Porous silicon
PCVM	Plasma chemical vaporization machining
RAPT	Reactive atomic plasma technology
SiO_2	Fused silica
HRG	Hemi spherical resonator gyro
MEMS	Micro-electron-mechanical systems
UV	Ultra-violet
RLG	Ring laser gyroscopes
SiF_4	Silicon tetrafluoride
OES	Optical emission spectroscopy
IAPPM	Ion-enhanced atmosphere pressure plasma machining
CCHC	Capacitive coupled hollow cathode
WCE	Wet chemical etching

Chapter 1 Introduction and Literature Survey

1.1 Introduction

Over the past many decades, researchers have consistently improved their surface finishing ability to the order of a few nanometers (*nm*) and currently a few orders of an angstrom (*Å*). As the human race develops, surface quality transforms from decorative to an essential function for specific applications such as telescopes. Modern measurements on 17th-century telescope lenses were of superb quality for that time. Optical materials and silicon polishing in the nanometer range have been the key of interest over the last twenty years due to the necessity to manufacture super-finished lenses and integrated circuit chips. The majority of the polishing, however, still lies in the realm of glass and glass ceramic substrates, which are used in different applications for optics in lithographic machines, laser systems, and an array of microstructures in aerospace sensors. The functional requirement of the components and safety and aesthetic compulsion makes it necessary to improve the surface characteristics before putting it into useful applications. Therefore, achieving a superior surface finish close to dimensional precision is crucial. Also, 3D complex components are being found to be more valuable in today's industries, leading to an increased demand for nano-finishing. Traditional finishing methods are comparatively less valuable in the case of complex 3D surface finishing due to the lack of better controllable finishing forces and constraints in tool movement.

Advanced processing technology promises enhanced functional performance and improved product quality. The components' quality and reliability mainly depend on removing the material mechanism during fabrication. Surface integrity has a critical role in most engineering components. The quality of the surface is defined as surface integrity. In engineering terms, surface integrity is defined as a set of properties (both superficial and in-depth) of an engineering surface that affects this surface's performance in service [1]. These properties primarily include surface finish, surface texture and profile, fatigue corrosion, wear resistance, adhesion, and diffusion properties. Other properties that also affect the surface's performance during service are absorptivity, bonding capability, emissivity, flatness, frictional resistance, strength, stain resistance, surface temperature, surface tension, thermal emissivity, washability, wettability, and biological and chemical properties. Various advanced materials, such as silicon carbide, fused silica, zerodur, and aluminium oxide, have many applications in engineering components. Polishing these advanced materials is the most

critical and expensive global production process. Surface roughness affects the operational efficiency of the components. Freeform surfaces are defined as the skin of 3D complex geometrical elements. Regular surfaces, like planes, conics, cylinders, etc., differ from freeform surfaces. It does not have a rigid dimension. This type of surface consists of non-planar surfaces. In product design, not only functionality but also aesthetics are considered. So, the use of freeform surfaces is increasing in many industrial applications. Many freeform surface components are widely used in aerospace, automobile, consumer products, die and mold, and medicine industries. Various components of advanced engineering materials such as fused silica, silicon carbide, and aluminum oxide with low surface roughness value and high form accuracy are vital in advanced engineering industries, especially in ultra-precision manufacturing industries [2]. These advanced materials and super alloys, such as titanium, ceramics, glasses, and nickel-based super alloys, are being used due to their high strength-to-weight ratio, resistance to heat, wear, corrosion, and good toughness. These materials are vital in various manufacturing sectors such as aerospace, automotive, semiconductor, etc. These materials are complex to machine by conventional manufacturing methods. Finishing these advanced engineering materials' operations is the most critical and expensive global production process. Fine abrasive processes have been used for finishing purposes for a long time. Abrasive finishing is mainly used to realize components with high-quality surface topography and integrity. The finishing operation is employed as a last operation on high-value-added engineering components. Finishing fused silica using conventional methods based on fine abrasive processes are grinding, chemical mechanical polishing (CMP), magnetorheological finishing (MRF), etc. Traditional techniques usually leave some defects on the processed surface of the substrate. Residual stress is generated on the polished surface of the optical materials while finishing using traditional methods. Although traditional techniques can obtain the desired products, the efficiency of the processes is very low. For instance, the required surface roughness for a laser gyroscope is about 2Å (R_q), which will take approximately seven to eight days using conventional methods because of their particular characteristics.

Glass optical components are manufactured using conventional mechanical processes, such as lapping, grinding, buffing, etc. However, such mechanical processes cause plastic deformation and brittle fractures to the surfaces of components, which result in the deterioration of optical properties [3]. In recent years, many applications in science and technology have demanded ultra-smooth optical components. Micro-electron-mechanical

systems (MEMS), synchrotron beamlines, the semiconductor industry, astronomical telescopes, and defense equipment all use ultraprecision optical components [4,5]. Surface roughness (R_a < 10 nm) and machining accuracy (0.1–100 nm) are achieved using ultra-precision machining technology. However, the meaning of "ultra-precision" is constantly restructured from time to time as new scientific and technological advances are implemented to enhance form accuracy and surface quality. The term "ultra-precision" refers to the precise indexes of profile accuracy and surface consistency and the challenges involved in achieving a particular objective at a defined range. The flaw is a severe problem for brittle materials such as glass, ceramics, and crystals. The mechanical and structural damage on the surface of fused silica is shown in Fig. 1.1.

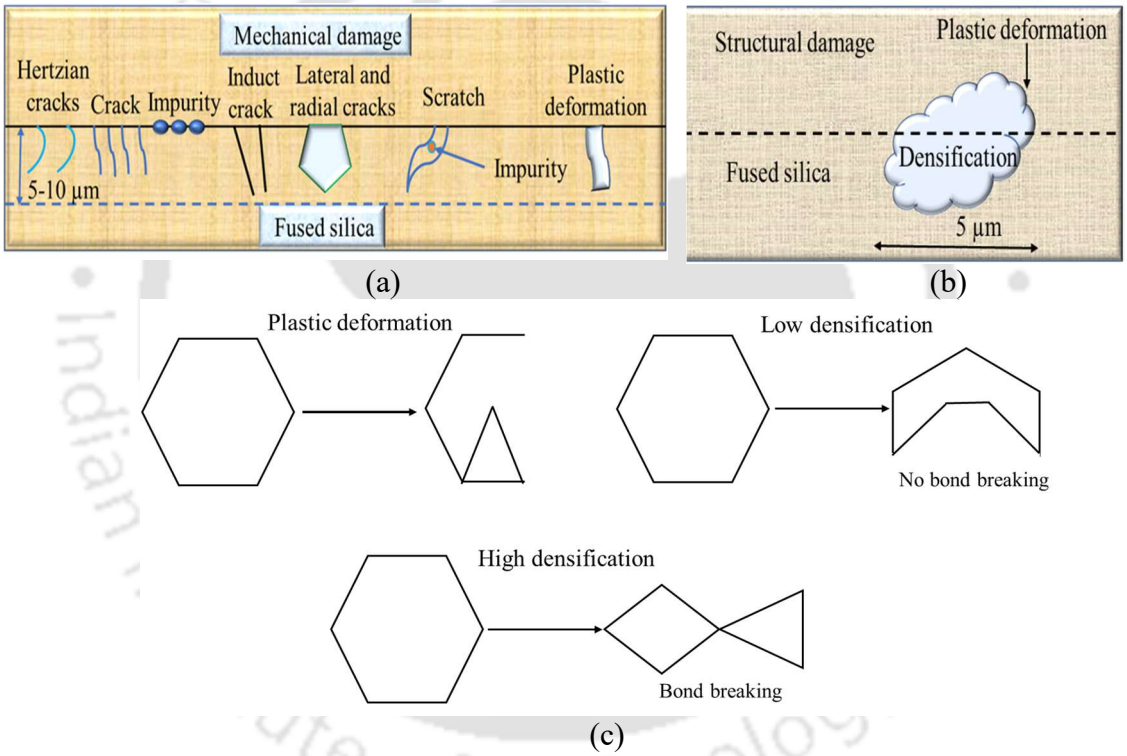

Fig. 1.1 Typical structure of fused silica (a) mechanical damage, (b) structural damage, and (c) ring deformation [6]

In recent years, nano-finishing through non-conventional processes has become the key technology for processing optical materials [7]. Nano-finished products are widely used in space applications, electronics, aviation, biomedical, optics, and communications industries [8,9]. This is due to the realization that enhanced surface polish frequently results in enhanced functionality and longer machine life [10]. Improving the surface topography of the finished product is one of the most excellent and effective ways to establish superior properties [11]. Over the years, researchers have consistently improved their surface finishing

ability to achieve a nano-level surface finish [12]. Recent advances in optics fabricating technologies permit optical engineers to implement freeform surfaces in optical devices, providing new applications in imaging and illumination, yielding minimal optical surface damage, and forming highly compacted device systems [13]. These complex free-formed optical components include non-standard aspheres, cylinders, convex or concave-shaped optics, etc. This poses new challenges for manufacturing and measuring methods [14]. At the microscopic level, atoms and their electronic configurations in the material interact with electromagnetic radiation (photons) to determine their macroscopic optical properties, such as transmission and refraction [15]. A machined surface's surface integrity is becoming increasingly important to satisfy the increasing demands of sophisticated component performance, longevity, and reliability [16]. Engineers face difficulty when it comes to the machining of quartz and glass materials with great dimensional accuracy [17]. The fine surface finish or surface texture improves machine functioning, lubrication, resistance to wear, and load-carrying capacity. Surface roughness is a critical parameter for predicting a component's performance in the natural environment [18]. For different purposes, a diverse surface roughness range is required. Surface roughness affects the operational efficiency of the components [19]. Modern sensor technology demands a 'zero defect' surface for functional performance and reliability. Subsurface damage and nano-stress-induced effects dominate the performance degradation as the size of the microstructures shrinks further. As this method is purely chemical-based, subsurface and surface defects commonly appear in the traditional machining process and are absent in the atmospheric pressure plasma polishing (APPP) process [20]. The unique advantages of the plasma polishing process are low cost, no waste, no contamination, and especially excellent surface quality, which is difficult to obtain by other processes.

Plasma polishing has been investigated since the early 1980s. Material processing with different gases (i.e., sulfur hexafluoride (SF_6), carbon tetrafluoride (CF_4), etc.) can remove atomic-level material from the substrate [21]. The electrical characteristics (like current density and voltage) at moderate pressure are investigated for capacitive radio-frequency (CRF) discharge [22]. Harb et al. [23] proposed the laser-assisted method to study the electrical conductance and photoluminescence of porous silicon (Psi) films formed on n-type Si wafers. The results show that the structural characteristics of the Psi substrate are improved by changing the input current density. Plasma chemical vaporization machining (PCVM), established by Jin et al. [24] at Osaka University, attains ultra-smooth surface

roughness up to the nanometer level, and the research area is mainly focused on the processing of silica optics. Reactive atomic plasma technology (RAPT) is established by RAPT industries while working on polishing optical components. It is stated that surface atoms react with fluorine radicals at atmospheric pressure and can achieve effective removal [25]. Fluorine radicals react with the substrate to form volatile compounds. Plasma polishing is also applicable to remove defects on metal surfaces. Surface finishing processes are frequently used in the medical, pharmaceutical, food, and chemical sectors [26]. Plasma polishing has become a versatile and reliable method for finishing fused silica [27]. It is also used for etching, cleaning, and deposition [28].

Geometrical accuracy, surface integrity, and surface finishing of the optical components and inertial sensors (such as accelerometers and gyros) are required in navigation grade [6]. For aerospace sensors, surface integrity demands ultra-low surface finishes with no surface or subsurface defects. The microstructures mostly have either complex surfaces or freeform surfaces, which are usually made of brittle and rigid materials, such as Safire, fused silica (SiO_2), zerodur, silicon carbide (SiC), etc. [29]. This demands atomic-level fabrication and surface finishing of these microstructures to increase the surface integrity. With increased complexity in optical materials, conventional and non-traditional processes cannot meet the demand with the advent of advanced materials. Because most relevant materials are brittle, the integrity of the surface lattice is always a serious concern when it comes to functional requirements [30]. Hence, an advanced polishing technique can improve the optical substrate surface without damaging its sub-surface layer [31].

1.2 Different Types of Glasses

Fused silica: Fused silica is the purest form of silicon dioxide (SiO_2). This glass has superior UV and IR spectra transmission, a very low dielectric coefficient, and excellent properties where fluorescence or solarization is an issue. Unlike Safire (a crystalline structure, not amorphous), fused silica can be shaped into different forms and produce extremely high-grade (pure) fused silica glasses that exhibit excellent ultraviolet and infrared performance [32]. Where purity, a non-reactive, durable substrate, and homogeneity between melts (uniform optical properties) are needed, this high-quality material is the likely choice.

Bk 7: Bk 7 is a barium borosilicate glass known for its high transmission and clear appearance. It is the most common material for many optical glass applications because it

offers good optical properties and a reasonable price. It is often used as a standard of comparison for other glass materials [33].

Borofloat: Borofloat is a special borosilicate glass. It is characterized by excellent flatness and better heat resistance. These characteristics make boro-float more costly than float glass. However, borosilicates retain shape and handle thermal shock better than other less expensive glasses [34].

B270 or Crown glass: B270 or Crown glass has a sound optical transmission and appears crystal clear due to fewer impurities. It can be polished and readily accepts all types of coating [35].

GE 124 and NSG OZ: GE 124 and NSG OZ are fused quartz glasses. Fused quartz is used in applications where sound ultraviolet light transmission, excellent thermal stability, and chemical inertness (resistance to stains) are required. Fused quartz is more challenging to polish than borosilicate [36]. Hence, the cost is high. Fused quartz is an appropriate choice for applications where prolonged or periodic temperatures are more extreme or there is a need for higher purity.

Float glass: Float glass is a common, inexpensive substrate. Float glass is a sheet of glass made by floating molten glass on a bed of molten tin. This method gives the sheet uniform thickness and very flat surfaces. The oldest glass float can appear with a slight greenish or blue tint, depending upon the amount of iron and other elements. It is quickly tempered to increase strength [37].

Zerodur: Zerodur is a glass ceramic made by Schott AG. It has both an amorphous (vitreous) component and a crystalline component. It is mainly used in many optical devices such as telescopes and laser gyro cavities, requiring a substrate material with a nearzero coefficient of thermal expansion (~0.02×10^{-6}/K at 0–50 ^{o}C) and excellent thermal shock resistance [38].

1.3 Application of Glasses

Among the various glass materials, fused quartz glass enjoys a premium class when manufacturing high-tech products. Its fundamental unique properties are given as follows [39]: (1) High chemical purity and resistance; (2) High softening temperature and thermal resistance; (3) Low thermal expansion with high resistance to thermal shocks; (4) High transparency from the ultraviolet to the infrared spectral range; (5) High radiation resistance. Because of these properties, fused silica finds application in various fields:

Aerospace and astronomy: It has endurance in a hostile environment, shock resistance, low weight, and, most importantly, reliability with a long lifetime. Astronomy telescopes use fused silica lenses due to their excellent chemical homogeneity, physical inclusion, and bubble-free [6].

High energy and high power lasers: They have low absorption at ultraviolet (UV) to visible and an excellent optical index of homogeneity from surface to bulk [40].

Laser material processing: Light must be transferred from the laser source to the intended working point. An optical path needs to be created. This path comprises fiber optics, lenses, prisms, mirrors, windows, and optical components. Hence, these optical components should have lower absorption, higher temperature stability, and high damage resistance; fused silica is the material of choice for this purpose [41].

Spectroscopy: Fused silica is used as a window or lens due to its excellent transmission from ultraviolet-visible near-infrared (U V-Vis-NIR) (180 nm to 3500 nm) [42].

Aerospace sensors: For aerospace space applications, the material should tolerate a hostile environment, have shock resistance, and be reliable for a long lifetime. Aerospace sensors generally use various sensors for detection and tracking applications. Most of the applications need radiation-hard fused silica glass [43]. Another prominent application of fused silica is inertial sensor applications, where critical elements such as sensing and corner optics need fused silica material.

Ultra-smooth and high surface integrity of Ring Laser Gyro: Inertial sensors like Ring Laser Gyro (RLG) need corner refractive optics for the laser to sustain. Fused silica serves the purpose very efficiently as a total internal reflecting optics due to its excellent 3D homogeneity. A laser can travel through the optics without loss. Because of UV and visible light transference of fused silica, no reduction in laser intensity occurs during the performance [44]. Due to its high laser damage threshold, fused silica is also responsible for long sustained life. A low thermal expansion coefficient also added an advantage for the performance of the gyroscope under thermal conditions.

3D freeform surfaces for hemispherical resonators: Freeform surfaces can be defined as surfaces with no areas of rotational variance (within or beyond the part). The freeform surface may appear to have an arbitrary shape and regular or irregular surface structures. Freeform optics or microstructures offer designers of precision sensors opportunities and challenges for manufacturing and surface finishing [6]. Freeform optical surfaces simplify system structure with lower mass, lower cost, smaller package size, and enhanced performance. Hemispherical shells can be considered a particular case of freeform optics with

an area of rotational invariants. Advanced gyroscopes like Hemi Spherical Resonator Gyro (HRG) also utilize fused silica as a sensing structure due to its high mechanical quality factor (Q), chemical homogeneity, and absence of any physical inclusions [45].

1.4 Surface Finishing Processes

Different complex surface finishing processes are described in the present section. Surface finish is a combination of three factors on which it is dependent: surface roughness, surface waviness, and lay. The schematic of surface roughness, waviness, and lay is shown in Fig. 1.2.

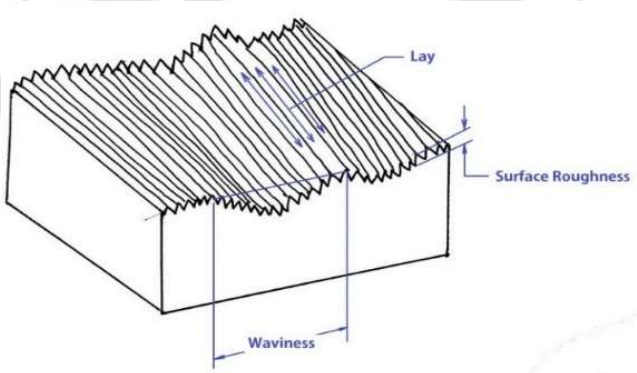

Fig. 1.2 Representation of surface roughness, waviness, and lay [46]

Surface roughness is defined as surface irregularities that are fine and uniformly spaced. Roughness, waviness, and lay together are called surface texture instead of surface finish. Surface waviness is surface irregularities that are irregularly spaced. Lay is the pattern that is formed due to machining operations on the surface, like planning, shaping, grinding, etc. The products with high surface roughness will have little life span because of corrosion and wear. Nobody would have anticipated such a long lifespan from a product they paid for with their hard-earned money. To achieve a better lifespan for products, whether big or miniature, there is only one solution: the proper finishing of the products. After manufacturing processes, various surface enhancement techniques are available, including surface finishing, surface treatment, coating, etc., as illustrated in Fig. 1.3.

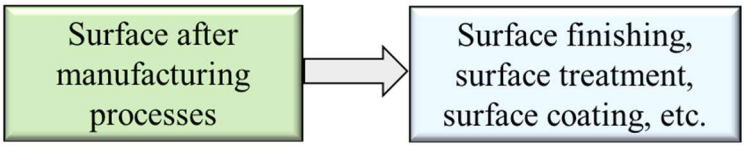

Fig. 1.3 Surface enhancement techniques after manufacturing processes

Finishing is generally termed as the reducing surface roughness of the components. The surface roughness should be as low as possible for better performance of the parts. The products with high surface roughness will have a short life span because of corrosion and wear. Proper finishing of the products is necessary to achieve a better life span of products, whether large or miniature. Machining provides the desired component shape; finishing processes remove the irregularities from the machined component's surface. Finishing processes do not change any geometry; they only reduce the surface roughness. Conventional and non-conventional approaches can perform finishing. The various classifications of machine surface finishing processes are shown in Fig. 1.4.

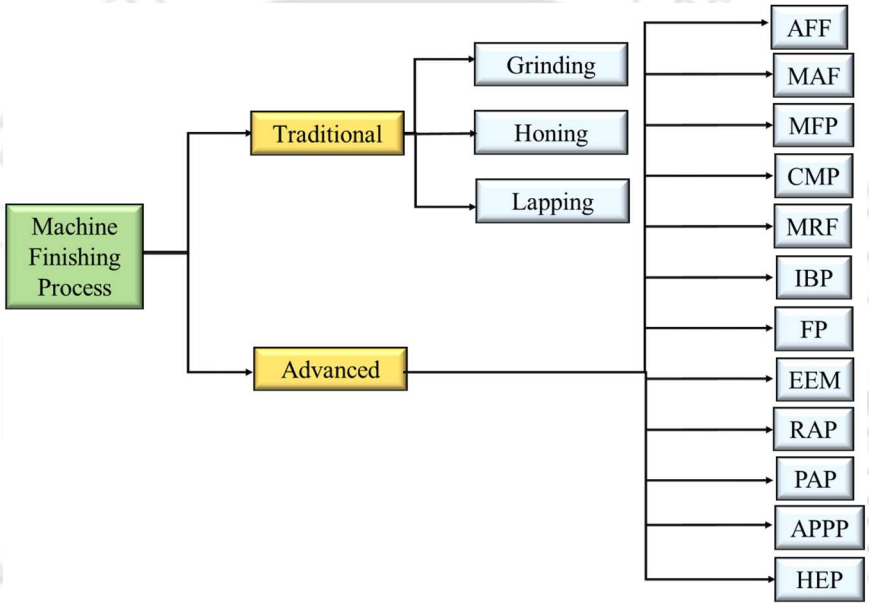

Fig. 1.4 Classification of surface finishing processes

1.4.1 Traditional Finishing Processes

In conventional finishing processes, friction between the abrasive/abrasive tool and the workpiece is responsible for material removal and producing a good surface finish with close tolerances. This process is simple and does not require immense machine knowledge. The primary conventional finishing processes are discussed below.

1.4.1.1 Grinding Process

Grinding, an abrasive finishing process, is widely used to reduce the surface roughness of the machined components. In this process, a grinding wheel bonded with abrasive particles is used to finish the surface of the workpiece. The workpiece is pressed against the grinding

wheel, so contact is constantly developed between them for proper finishing. The abrasive particles act as a single-point cutting tool to remove the material from the surface. This process gives a material removal rate compared to other traditional finishing processes. Here, abrasion is the reason for material removal. Due to the random orientation of abrasive particles, it requires the highest specific cutting energy. This process gives more material removal rate compared to other traditional finishing processes. Here, abrasion is the reason for material removal. Mizugaki et al. [47] attached an elastic grinding wheel with felt buff to the end effector of an industrial robot. It can easily follow the profile path of the complex surface due to its higher degree of freedom incorporated with the industrial robot. Huang et al. [48] reported finishing turbine-vane overhaul using a sand belt grinding wheel. Shiou et al. [49] used a spherical grinding tool to finish complex plastic injection mould steel surfaces on a CNC machining center. They developed the spherical grinding tool and its alignment components. The schematic diagram of the spherical grinding process is shown in Fig. 1.5.

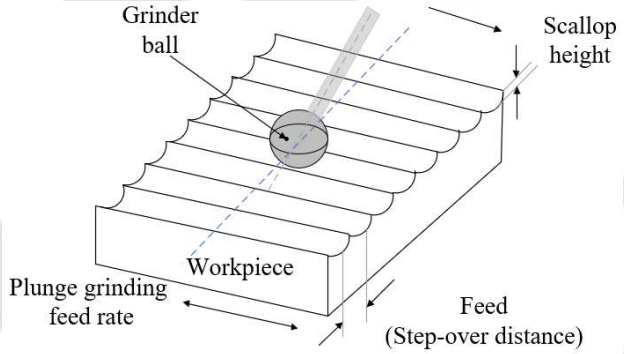

Fig. 1.5 Schematic diagram of the spherical grinding process [50]

1.4.1.2 Honing

A honing tool or stone, an abrasive stick, or a stone perform honing. The honing tool moves up and down and rotates inside the component to be finished. The honing tool abrades the workpiece surface along a predefined path with the help of cutting pressure and cutting velocity. It leaves a cross-hatched surface, which is also helpful for fuel retention in an internal combustion cylinder. This process is generally employed to finish inner cylinder surfaces. Weulu and Timmermann [51] used honing stone to finish the complex surface of dies and moulds. The honing stone is attached to the six-axis robot for better flexibility. Nowicki and Szafarczyk [52] attached abrasive sticks with two or four degrees of freedom to the machining head of an NC milling machine. The abrasive sticks rotate with the machine head, and feed is given to the workpiece in X, Y, and Z directions.

1.4.1.3 Lapping

Lapping and polishing are inherent conventional processes where the tool is larger than the substrate to fabricate optics of the desired shape, size, surface figures, and quality. The lapping process provides a high degree of surface flatness by pressing a lapping plate over the workpiece with abrasive media between them. It ensures proper match of surfaces. A conditional ring or retaining ring maintains uniform slurry distribution. The workpiece is rotated while in contact with the abrasive particles. Because of the shearing action of abrasive particles, the irregularities from the surface are removed, and an ultra-polished surface is obtained. The size and type of abrasives used for valve lapping depend upon the finishing requirements. The basic lapping process is shown in Fig. 1.6.

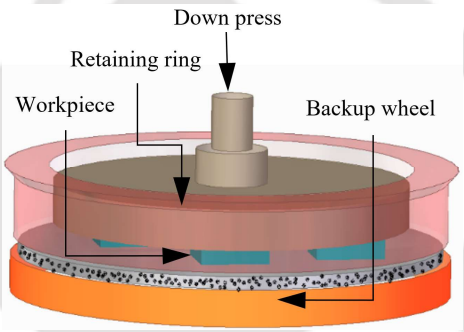

Fig. 1.6 Schematic diagram of the lapping process [53]

1.4.2 Advanced Finishing Processes

Non-conventional finishing processes are in great demand due to their capability to finish any complex shapes of miniature dimensions. The final surface roughness of the finished component is very low, even in a nanoscale. A few important non-conventional finishing processes are discussed below. Non-conventional machining does not involve direct contact between the tool and the workpiece. Due to this, negligible forces are involved during machining. Hence, the machining rate is low; however, the tolerance and surface finish of the machined components are very high. A few major non-conventional finishing processes are discussed below.

1.4.2.1 Abrasive Flow Finishing (AFF)

Abrasive flow finishing (AFF) is a process in which a small quantity of material is removed by flowing a semisolid abrasive-laden putty over the surface to be finished. The media has a high viscosity such that it can be held between fingers like a rubber ball, which deforms by

applying a little pressure. Two vertically opposed cylinders extrude abrasive media back and forth through passage(s) formed either by the workpiece and tooling or by the workpiece alone. This process is suitable for deburring, polishing, removing recast layers, producing compressive residual stresses, etc. The process can machine tens of parts simultaneously to enhance productivity. This process has high flexibility, i.e., the same machine can be used to do various jobs by changing toolings, machining parameters, media, and abrasives.

1.4.2.2 Magnetic Abrasive Finishing (MAF)

In the non-traditional AFF method, a magnetic field was introduced all over the test specimen to establish a new innovative technique called magnetically assisted AFF (MAAFF) [54]. In this process, usually, ferromagnetic particles are sintered with fine abrasive particles (Al_2O_3, ZrO_2, CeO_2, SiO_2 (silica), SiC, CBN, boron carbide (B_4C), natural diamond, synthetic diamond, or their combinations). Such particles are called ferromagnetic abrasive particles (or magnetic abrasive particles, MAPs). Under a magnetic field, a sideways pull is experienced by the abrasive media, which mainly consists of ferromagnetic particles. These particles impinged on the workpiece, causing micro-chipping phenomena [55]. The magnetic field improves MRR for non-magnetic products, though magnetic components identified insulating impact [56]. There has been no noticeable change in mean roughness (R_a) and material removal rate (MRR) post-MAAFM method relative to the AFM method. The magnetic abrasive finishing (MAF) or MAAFM process, the polishing operation uses a magnetic field throughout the working zone between the base specimen surface and the revolving magnet-poles head. The magnetic field provides rigidity and preserves ferromagnetic abrasives in the working zone [57].

1.4.2.3 Magnetic Float Polishing (MFP)

The finishing methods described in the previous sections were designed for ground structures, tubular structures, or their variants, resulting in complicated 3D shapes that do not qualify for the finishing of spherical structures. To satisfy this need, the magnetic float polishing (MFP) method was proposed [58]. The polishing technique involves mechanical brushing and chemo-mechanical cleaning. The spherical ceramic balls are polished underneath, under the control of magnetic transmutation (buoyant) force, through relative movement between balls and abrasive particles [59].

1.4.2.4 Chemo-Mechanical Polishing (CMP)

In the CMP method, chemical and mechanical processes are used together for material removal [60]. Generally, it is used to finish semiconductor material. A new soft abrasive grinding wheel (SAGW) used in chemo-mechanical grinding (CMG) was developed to machine silicon wafers. The wheel consisted of magnesia (MgO) soft abrasives, calcium carbonate ($CaCO_3$) additives, and magnesium oxychloride bonds. The grinding with the new SAGW produced a surface roughness (R_a) of about 0.5 nm and a subsurface damage layer thickness of about 10 nm. This study also revealed that the chemical reactions between MgO abrasive, $CaCO_3$ additives, and silicon material did occur during grinding, thereby generating a soft reactant layer on the ground surface. The reactant layer was easily removed during the grinding process [61]. The schematic diagram of chemical mechanical polishing is shown in Fig. 1.7.

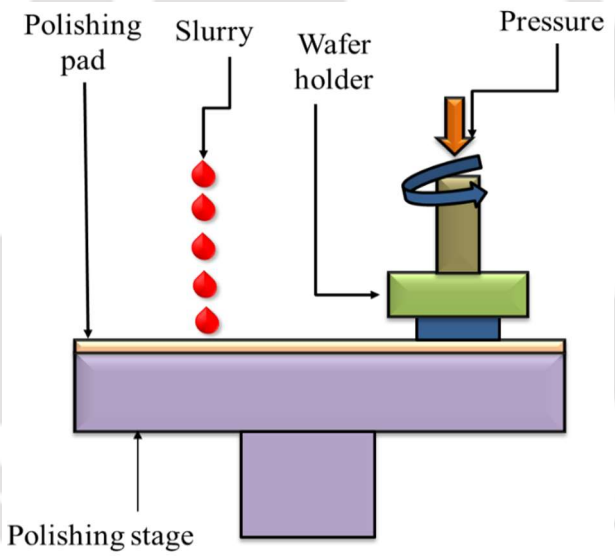

Fig. 1.7 Schematic diagram of chemo-mechanical polishing [62]

1.4.2.5 Magnetorheological Finishing (MRF)

Magnetorheological Finishing (MRF) is a non-conventional finishing technique that utilizes a smart fluid that stiffs as it comes in the vicinity of the magnetic field. Like AFF, it comprises abrasive and carbonyl iron particles (CIPs) mixed with additives. This MRF fluid and the workpiece to be polished are kept in a fixture such that magnetic lines stiffen the MRF fluid. This stiff fluid passes through the miniature component, and depending upon the magnetic strength, the stiff MR fluid removes the irregularities from the surface and provides a polished surface. The final surface roughness depends on the concentration of abrasive

particles, CIPs, magnetic strength, and polishing time. The schematic diagram of magnetorheological finishing is shown in Fig. 1.8

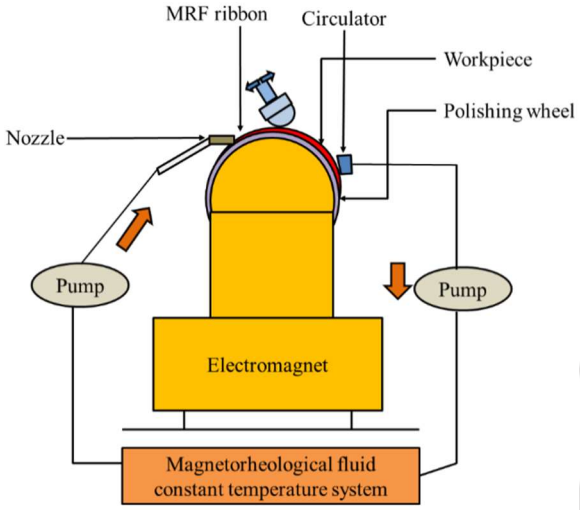

Fig. 1.8 Schematic diagram of magnetorheological finishing [63]

1.4.2.6 Ion Beam Polishing (IBP)

The ion beam polishing method is one of the non-contact types of process [64]. This type of polishing method only operates under vacuum spaces [65]. It has several ions that are used for polishing, and numerical control systems are also used to control the emission of ions from the source of ions [66]. The energy exchange happens between the surface of the polished material and the atoms due to continuous circumstances with particles, which are swallowed on the surface. It makes a deep atomic level polishing of the workpiece by creating the effect of physical sputtering when the atoms in a surface of polyester material obtain the energy, that energy of atom to break the binding of the lattice [67]. This technology is used to polish the optical component and fused quartz. The process removes the atoms on the surface by creating a heavy impact between the energetic ions and atoms in vacuum space [68]. The schematic representation of ion beam polishing is illustrated in Fig. 1.9.

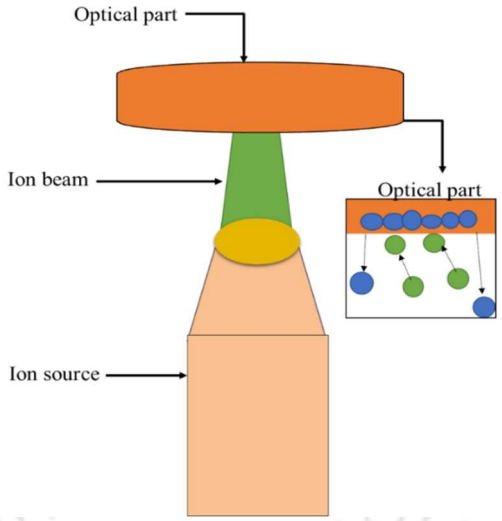

Fig. 1.9 Schematic representation of ion beam polishing [69]

1.4.2.7 Float Polishing (FP)

Namba from Oscar University introduced the float polishing method in the late 1990s. The research uses a crystal sapphire to polish using the float polishing method [70]. As a result, it got a better quality surface finish with an accuracy of the surface range from 31 to 32 nm. Further, different types of crystals are polished using the float polishing method to get an improved surface, finishing with a surface roughness in the range of 0.2 nm [71]. Then, doing further research, they developed the float polishing method with ultra-precision. The schematic representation of float polishing is illustrated in Fig. 1.10.

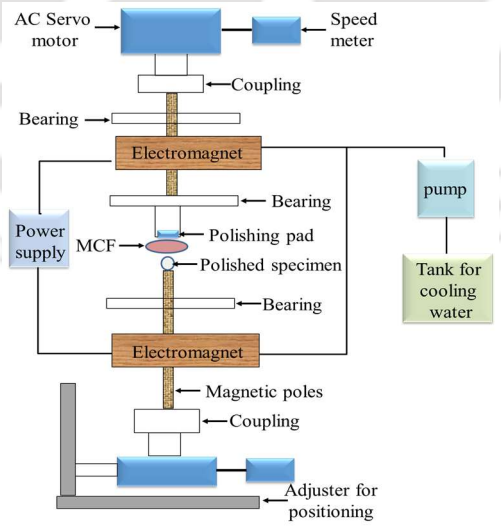

Fig. 1.10 Schematic diagram of float polishing [72]

The machining process maintains the stability between the polishing pad and the substrate while rotating [73]. The polishing liquid produces hydrodynamic pressure. Due to

hydrodynamic pressure, it develops from the liquid film as a layer between the substrate and the polishing pad [74].

1.4.2.8 Elastic Emission Machining (EEM)

Mori et al. [75] proposed finishing optical material without subsurface damage with ultra-smooth surface finishing. So, a new non-contact polishing method is called elastic emission machining. This elastic emission machining is mainly concentrated on these three factors: characteristics of chemicals, fluid characteristics, and the motion of particles [76]. It also works on the principle of hydrodynamic pressure, the same type of pressure used in the float polishing method. It also removes atomic-level material by rotating the balls made of polyurethane [77]. The polyurethane balls act as a tool to polish the material by controlling the motion of nanoparticles, which are used as a polishing abrasive [78]. Those particles achieve the atomic level material removed from the workpiece by collision. This process is used to get an ultrasmooth surface with a good quality surface without causing any damage in its subsurface and also without dislocation of the lattice and to prevent other damages [79]. Compared with other polishing technologies, it has more advantages because of the atomic-level material removal rate with minimum subsurface defects [80]. The schematic representation of elastic emission machining is illustrated in Fig. 1.11.

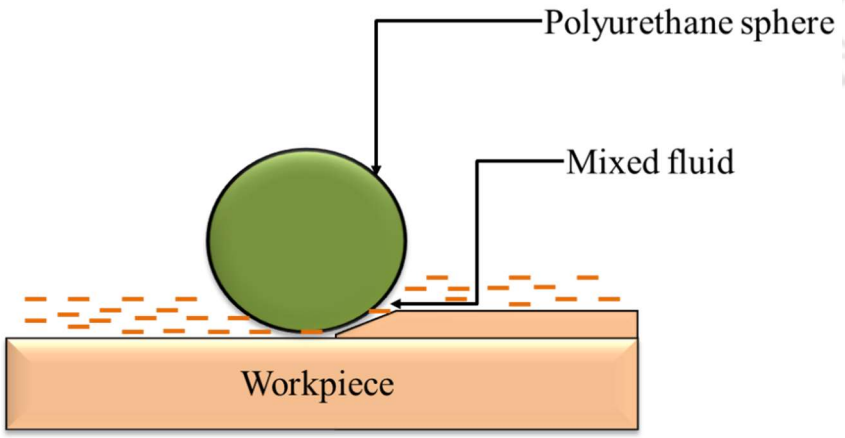

Fig. 1.11 Schematic representation of elastic emission machining [81]

1.4.2.9 Reactive Atom Plasma (RAP) Machining

Chemically reactive atom plasma machining shapes optical and semiconductor surfaces precisely. It is a dry chemical etching process. As material removal is achieved chemically, there is no subsurface damage. Computer numerical control RAP process can polish or

correct precisely complex shapes. Energy associated with this process is considerably large, approximately 1 KeV, compared to the plasma process, which is typically less than 100 eV.

1.4.2.10 Plasma-Assisted Polishing (PAP)

Yamamura et al. [82] from Osaka University developed a new polishing technology to polish the surface of very hard material [83]. Atmospheric pressure plasma jets boast a history spanning over five decades, during which their design and plasma generation mechanism has evolved and found applications across various fields [84]. The PAP technology is still relatively new; this process uses liquid vapor plasma, which consists of helium; that type of plasma creates the workpiece surface to irradiate, that irradiation makes the ions of an atom react with the atom, present on the top layer of workpiece, and it will remove the material from the surface by developing the volatile substances by using plasma-assisted polishing process. Producing exceptionally precise optical surfaces necessitates using deterministic ultra-precision machining technologies [85]. Plasma-assisted polishing has applications in various materials processing procedures [86].

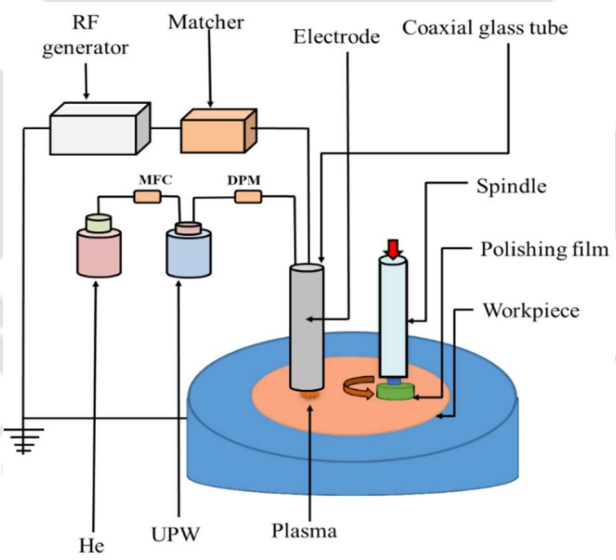

Fig. 1.12 Schematic diagram of plasma-assisted polishing [87]

Recently, there has been a rising interest in employing atmospheric pressure plasmas for materials processing due to their ability to operate without costly vacuum systems [88]. The material's surface is modified using plasma, improving roughness [89]. In addition, it doesn't create any subsurface damage and does not cause any scratches on the surface of the substrate. The substrate is ultra-smooth when using plasma-assisted polishing with abrasive

particles like CeO_2 [90]. The main advantage of plasma-assisted polishing is that it gives the materials with higher efficiency by consuming low energy [91]. The schematic representation of plasma-assisted polishing is illustrated in Fig. 1.12.

1.4.2.11 Atmospheric Pressure Plasma Polishing (APPP)

APPP utilizes chemical reactions between reactive plasma and surface atoms to remove atom–scale material. Since the process is chemical, it avoids various surface/subsurface defects that usually appear in conventional machining processes. Uniform low-temperature plasma can be generated over a large surface at a low cost and more extensive application range. Also, it quickly reacts with materials due to more active and diverse species than those generated from chemical reactions. The reaction and plasma gas with the optimum ratio is sufficiently mixed and input into the plasma chamber. It is then ionized by the radio–frequency (RF) power source. The reaction gas is excited in the plasma chamber to generate high–density and high–energy reactive radicals. The generated reactive radicals cause a chemical reaction with the surface atoms of the workpiece, which performs effective atom–scale material removal. For different materials, different combinations of plasma and reactive gas are used.

1.4.2.12 Hydrodynamic Floating Polishing (HFP)

Hydrodynamic floating polishing is one of the crucial methods developed using the principle of hydrodynamics. Watanabe et al. [92] developed hydrodynamic floating polishing to manufacture high–precision, damage–less semiconductor integrated circuit devices in 1981. Previous research articles work with monocrystalline silicon, which is polished by hydrodynamic floating polishing technology. At the end of processing, the surface quality is achieved by 1 nm by polishing the 3-inch monocrystalline silicon [93]. Ultra-smooth polishing is performed using this method by creating hydrodynamic pressure between the substrate and the polishing pad. The fluid develops pressure when the polishing pad rotates [94]. This rotation makes a small space between the substrate and the polishing pad. It makes the abrasive particles hit the surface of samples with high frequency while obtaining the required energy. It creates the shear force that collapses the attachment of the atom in the workpiece to achieve an atomic level of material removal [95]. The schematic representation of the hydrodynamic floating process is illustrated in Fig. 1.13.

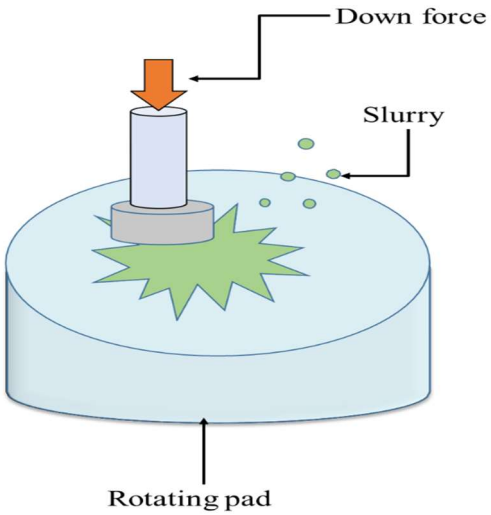

Fig. 1.13 Schematic diagram of hydrodynamic floating process [96]

1.4.3 Plasma Process: An Overview

Plasma describes a collection of partially or fully ionized gases [97] consisting of charged particles: electrons, ions, neutral atoms, and possibly molecules that exhibit effects such as conducting electrical currents and generating magnetic fields. The electrical conductivity of plasma is the leading property that differentiates it from neutral gases. As the temperature rises, the molecule becomes highly energetic and changes nature in the following order: solid, liquid, gas, and finally plasma, thereby justifying the term "fourth state of matter" [98]. Plasma is electrically conducting, interactive, and strictly sensitive to the electromagnetic field due to free electrons, electric charges, and ions. Electrically neutral ionized gases are frequently named plasma (i.e., positive ions are balanced with electron density) and hold a substantial number of electrical charge particles, enough to influence their electrical characteristics and nature. Irving Langmuir initiated the analysis of ionized gases [99] and provided this novel aspect of matter with the name plasma in 1928 when studying oscillations in ionized gases.

The process gas (He and O_2) and reactive gas (SF_6) are admitted into the process chamber with an optimum ratio during the operation. Then, it is ionized with radio-frequency (RF) power. The gases are energized in the process chamber to produce high-density, more reactive ions and radicals. It generates chemical interactions with the workpiece surface atoms (i.e., fused silica). SF_6 is used as a reactive gas, providing fluorine radicals (F*) particles that are chemically energetic and cause chemical reactions with Si atoms on the substrate surface, generating volatile products, i.e., silicon tetrafluoride (SiF_4). Helium (He) gas is used as a processing gas, which provides energy to the system, and oxygen (O_2) as a

catalyst. The interaction of radicals with the surface of fused silica is illustrated in Fig. 1.14. The chemical reactions of radicals with fused silica substrate are presented in Eqs. (1.1) and (1.2) [29].

$$SiO_2 + 4F^* \rightarrow SiF_4 \uparrow + O_2 \uparrow \quad (1.1)$$

$$Si + 4F^* \rightarrow SiF_4 \uparrow \quad (1.2)$$

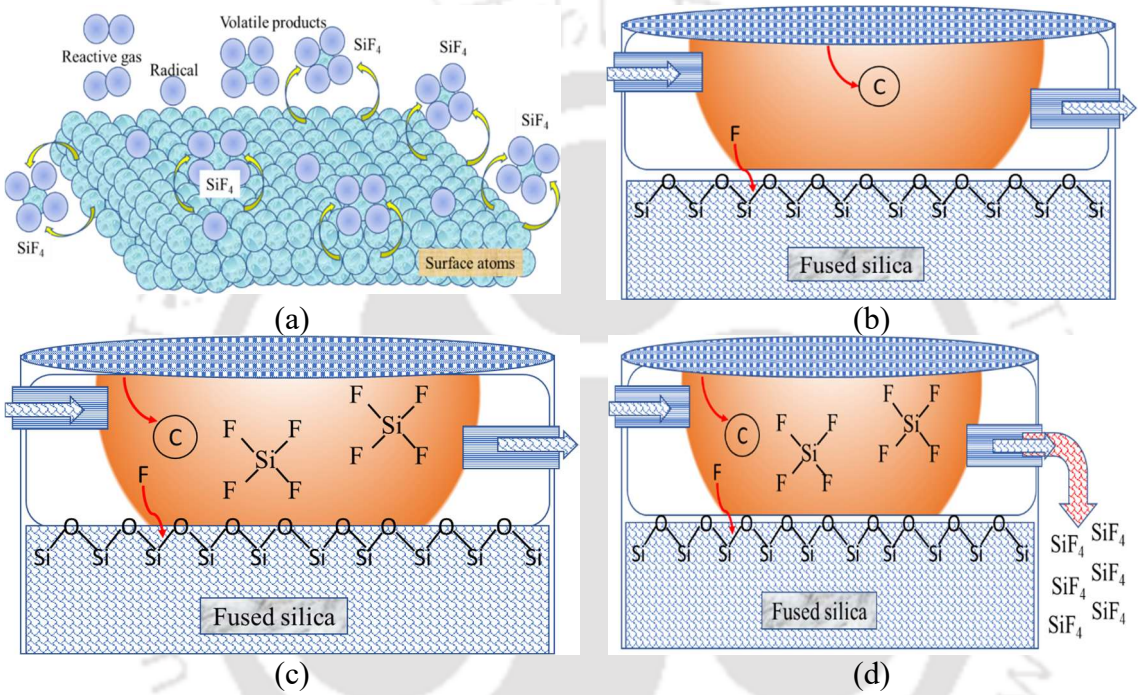

Fig. 1.14 (a) Principle of plasma polishing, (b) fluorine radicals interaction with Si-O-Si, (c) SiF_4 compound formation, and (d) removal of SiF_4 from chamber outlet

The schematic diagram of the developed experimental setup of the medium-pressure plasma process is illustrated in Fig. 1.15. The plasma chamber comprises zerodur material, and its body acts as a dielectric barrier. Three different gases (i.e., He, O_2, and SF_6) are used in this process. He and O_2, their mixture as carrying gas, and SF_6 as an active etching gas. The plasma is produced at 40.68 MHz RF power. Mass flow meters are required to control the flow rate of gases, and RF power is used to generate plasma discharge inside the process chamber. Vacuum pumps are utilized to keep the pressure constant and create a vacuum inside the plasma chamber during processing. Optical emission spectroscopy (OES) is used to measure the relative density of plasma species. Zerodur is a glass ceramic widely used in different branches of industry and science. The advantages of zerodur material are its zero thermal expansion coefficient in a wide temperature range from -40 to +100°C and excellent

mechanical properties. Chemically, zerodur comprises oxides Li_2OSiO_2-Al_2O_3 (35 to 75% SiO_2, 20 to 50% Al_2O_3, Ti, Zr, Li, and Mg oxides) [36].

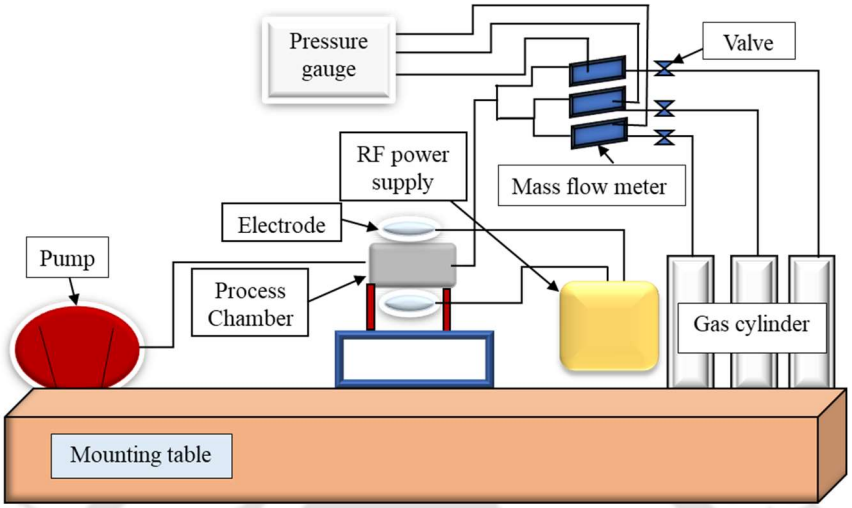

Fig. 1.15 Schematic diagram of medium-pressure plasma process (MPPP) experimental setup

The flow chart of the developed medium-pressure plasma polishing process is illustrated in Fig. 1.16. The medium-pressure plasma process is conducted in a closed chamber inside a vacuum environment, unlike the atmospheric-pressure plasma process in an open environment. The various machining stages in MPPP are presented in circular diagrams within a flow chart format. Initially, gases come out from gas cylinders and pass through mass flow meters, which control the flow of gases. The mixed gases are admitted into the plasma chamber. RF power is used to ionize the mixed gases, generating ions, radicals, and other species, which react with the fused silica surface and produce volatile compounds.

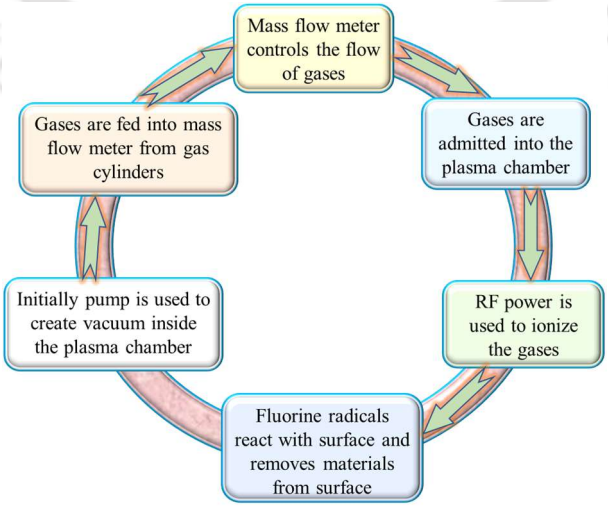

Fig. 1.16 Process flow chart of medium-pressure plasma polishing process

Previous researchers studied the significance of different input process parameters on the performance of the plasma polishing process. Plasma processing depends on various parameters such as processing time, total operating pressure, gas processing, partial pressure of each gas, applied electrical field, etc. The output response, for instance, MRR and surface finish, are influenced by the input parameters, i.e., RF power, gas composition, pressure ratio, total pressure inside the plasma chamber, and machining time. The most crucial roles of RF power are utilized to control ion-bombarding energy and plasma density [23]. The process parameters are divided into broad sets and arranged in the Ishikawa diagram, as shown in Fig. 1.17.

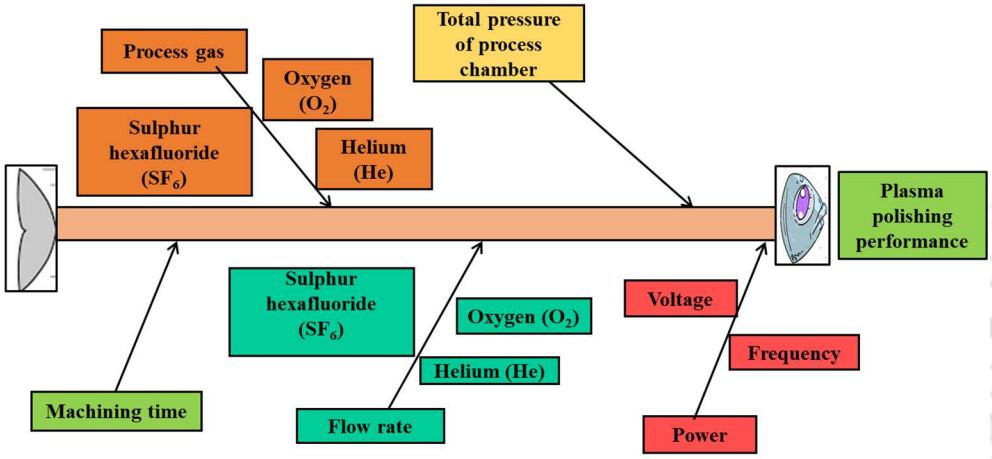

Fig. 1.17 Fishbone diagram (i.e., Ishikawa diagram) representing different process parameters of a medium-pressure plasma process (MPPP)

1.5 Literature Survey

An extensive literature survey of plasma polishing processes has been carried out in this section. The word plasma describes microscopically neutral substances containing many interacting free electrons and ionized atoms or molecules. In other words, plasma, called the fourth state of matter, is a partially ionized gas with an equal number of positive and negative particles; overall, the plasma remains electrically neutral. The plasma mainly contains free radicals, which are chemically reactive and responsible for material removal. However, depending on the total operating pressure, the plasma process is broadly classified into low-pressure, medium-pressure, and atmospheric-pressure plasma processing. At low pressure, the plasma acts as a conventional glass polishing tool where the entire substrate is treated simultaneously. At low-pressure plasma, the mean free path is higher. Hence, the physical action of the ion is a dominating factor compared to a chemical reaction. Hence, at low

pressure, plasma processing is anisotropic. Meanwhile, at atmospheric pressure, the mean free path of the partially ionized electrons is less, so the plasma acts as a non-conventional polishing sub-aperture tool. At this pressure, the chemical action is the more dominating factor; hence, primarily, the reaction is isotropic. At medium pressure, the plasma carries the advantages of both low and atmospheric pressures. At medium pressure, the plasma can be controlled such that it reacts with the substrate chemically, unlike low-pressure plasma, and simultaneously the entire substrate, unlike the atmospheric plasma process. Hence, it is the most cost-effective and reliable processing method compared to other functions. The complex 3D freeform surfaces can be polished simultaneously by optimizing the plasma parameters of medium-pressure plasma processing. The following sections describe the work reported in the area of plasma processes.

Jin et al. [100] evaluated the influence of various process parameters on zerodur substrates using APPJ processing. Also, the modification of the surface chemistry is studied in detail. Zerodur material is a multiphase-multi-chemical in nature. The effect of dwelling time (min) and O_2/SF_6 ratio on surface roughness as illustrated in Fig. 1.18(a) and (b), respectively) [100].

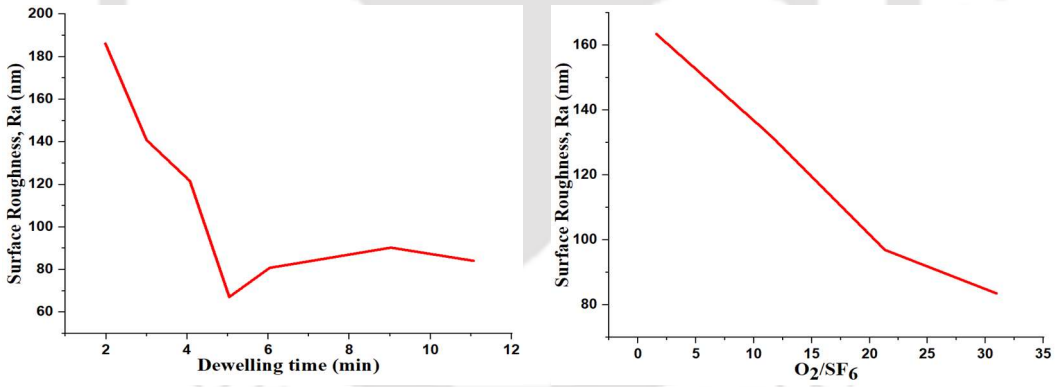

(a) (b)

Fig. 1.18 Effect of (a) dwelling time, and (b) O_2/SF_6 flow ratio on surface roughness [100]

Dev et al. [29] proposed a new non-contact type plasma-assisted freeform surface finishing method that is investigated on fused silica. This process is used to finish ultrafine surfaces without surface and sub-surface damage. He and Ne are used as processing gases with plasma, and SF_6 and O_2 are chosen as reactive gases. The pressure is maintained up to 30 mbar by using dielectric barrier capacitive coupled RF discharge. The relative density of excited species in the plasma is investigated by atomic emission spectroscopy to study the material removal mechanism. Surface roughness improvement of up to 68% was achieved

with He–O_2 plasma, while surface waviness was improved by up to 85%. Moreover, the maximum MRR achieved was 0.008 mm^3/min with the He-SF_6-O_2 gas mixture [29]. This polishing method is used to rectify the surface roughness of optical components. This method finds application in creating a smooth optical surface without sub-surface damage (SSD). Experimentally, it is observed that the RMS surface roughness decreases from 1.2 to 1.0 nm with minimum subsurface damage in the silica surface. With increased working pressure and radiofrequency power, the etching rate and the roughness of the polished surface also increase [93].

Vana et al. [26] used a stainless steel X10CrNi specimen for plasma polishing and observed the change in surface roughness and gloss level of the metal surface with the time variation from 0 to 600 seconds, as shown in Fig. 1.19. Experimentally, it is found that there was lesser surface roughness after plasma polishing with varying gloss levels during finishing, and its value depends on finishing time. After 60 seconds, the gloss level was at its maximum.

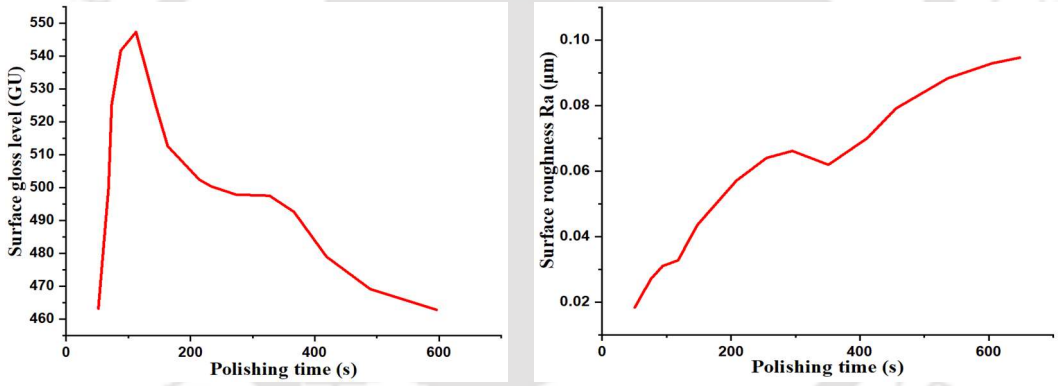

(a) (b)

Fig. 1.19 Effect of polishing time on (a) surface gloss level and (b) surface roughness [26]

Yao et al. [101] proposed the APPP process for polishing the zerodur component. The result showed the repeatability and uniformity in the distribution of the plasma jet's active chemical parts (fluorine atoms radicals) on zerodur material and the material removal mechanism using atomic emission spectroscopy. The material removal is found to be the function of work material, RF power, SF_6 flow rate, SF_6 /O_2 ratio, and working distance.

Arnold et al. [102] proposed a plasma polishing process to finish fused silica optical surfaces. The authors suggested that plasma polishing is the best-suited method for freeform surface generation with a plasma etching rate between 1–30 mm^3/min. The surface

temperature distribution affects the chemical reaction on the substrate's surface. The plasma jet source setup schematic is shown in Fig. 1.20.

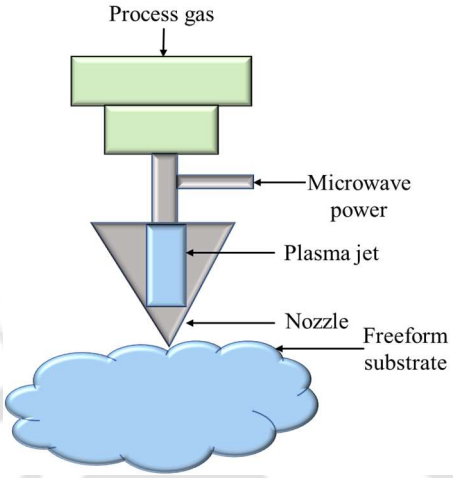

Fig. 1.20 Schematic of plasma jet source setup [102]

Wang et al. [103] proposed that a rapid and damage-free polishing process for silicon carbide (SiC) optics. The active radicals generated from CF_4 react with the optics surface of SiC to produce SiF_4 vaporization under atmospheric pressure plasma. The schematic of atmospheric pressure plasma polishing and capacitively coupled plasma (CCP) jet setup is shown in Fig. 1.21. The experimental results show that plasma discharge is stable at atmospheric pressure and sub-nanometer range surface roughness is achieved. The spectroscopic analysis shows O and He atoms in the excited states in the plasma flame. A mixture of He and O_2 gas is admitted into the plasma jet at a constant mixing ratio and velocity. Stable plasma discharge can be observed between 100 to 800 W power [103].

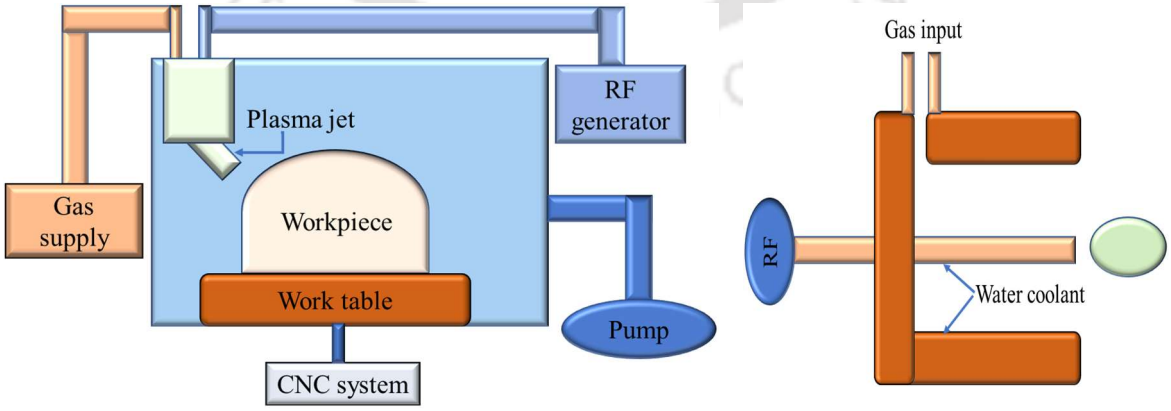

(a) (b)

Fig. 1.21 Schematic of (a) plasma polishing and (b) CCP jet setup [103]

Zhang et al. [104] investigated the machining of silicon wafer ultra-smooth surfaces using APPP. The finite element method analyzed the workpiece surface's spatial gas and temperature distributions. The result reveals a peak temperature of about 90°C at the center. The surface roughness, R_a of 0.6 nm, is measured through an atomic force microscope (AFM). X-ray photoelectron spectroscopy (XPS) investigated the finished surface's elemental composition. The experimental results showed that the APPP process could polish the optics up to the nanometer range to an ultra-smooth surface. The Si, F, O, and C elements are found on the substrate's surface using energy-dispersive X-ray spectroscopy. The elements found on the finished surface are mainly C and O from the air.

Baolu et al. [105] concluded that the processing efficiency could be improved using an ion-enhanced atmosphere pressure plasma machining (IAPPM) of silicon carbide. The reactive gas is chosen as SF_6 and is injected into the argon (Ar) plasma, where SF_6 breaks into fluorine radicals. The etching rate was 3 μm/min, and the IAPPM processed surface profile could not achieve satisfactory results. The white light interferometer is used to measure the surface profile.

Castelli et al. [106] proposed APPP to produce ultra-smooth surfaces and to enhance surface quality. The experimental results showed that after 100s, a decrease in the surface roughness (Ra) value from 4.539 to 0.93 nm is obtained. The result reveals that an improvement in surface characteristics is also achieved.

Wang et al. [107] used fused silica as a substrate and polished up to 1.4 nm by highly stable SF_6 and Ar/O_2 plasma, produced with the help of a capacitive coupled hollow cathode (CCHC) RF discharge method [107]. The process parameters considered in this experiment are gas flow rate, discharge power, and pressure. The rate of gas flow affects the material removal rate. It varies mainly by O_2 and SF_6 gas flow rate ratio. The maximum MRR is obtained when both the gases O_2 and SF_6 flow rate ratios are 1:1. Further, increasing the input plasma power increases the removal rate. Still, the surface roughness value increases when power is higher than 100 W. The effect of gas flow rate on MRR and RF power's impact on the material's surface roughness are demonstrated in Fig. 1.22(a) and (b), respectively.

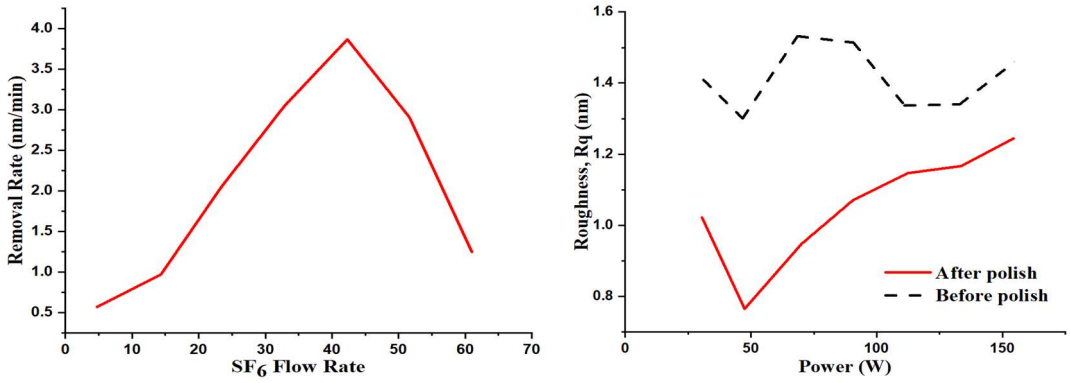

(a) (b)

Fig. 1.22 Effect of (a) gas flow rate on material removal rate and (b) RF power on surface roughness of substrate [107]

Liu et al. [108] proposed a novel plasma polishing process for finishing optical components. The study utilizes capacitive coupled hollow cathode RF excited SF_6 and Ar plasma. The gas flow rate and power influenced the plasma's characteristics. The surface finish improvement is marginal from 1.2 nm to 1.0 nm. However, surface integrity is enhanced. The experimental study used effective plasma machining on bulk fused silica under pressure lower than 0.05 mbar. The plasma energy flow pattern is shown in Fig. 1.23. Also, the plasma source is operated in two modes, i.e., low etching rate (LER) and high etching rate (HER). HER mode is used to remove surface and subsurface damaged layers, and LER mode is used to enhance the surface finish. The redistribution of polishing particles is detected in plasma processing at atmospheric pressure**.** The value of R_a improves from 1.338 to 1.361 µm because of various deep cracks that are not filled by abrasion. This result helped to understand the surface formation through the APPP process and found the application of APPP in innovative optical manufacturing.

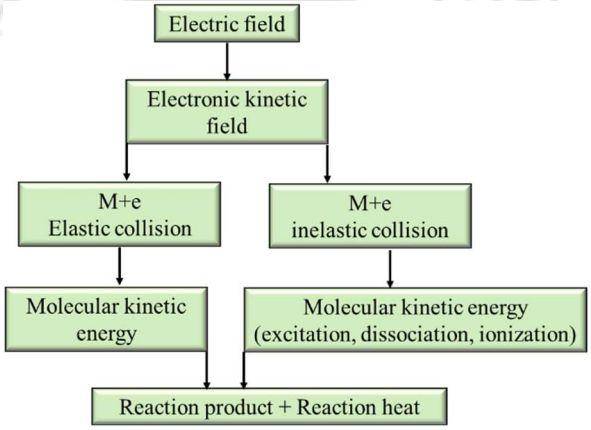

Fig. 1.23 Plasma energy flow pattern [108]

Meister et al. [109] used reactive plasma machining for optical surfaces. The material removal mechanism is chemical etching and mainly depends on the work surface temperature influenced by the jet heat flux. An enhanced three-dimensional model has been built and solved for the case of a linear motion of the plasma jet over the surface. The shape and absolute temperature distribution have been reliably predicted. Different powers, i.e., 100 and 300 W, are selected during experimentation at a constant 100 mTorr pressure. The intensity of 703.7 nm and 685.6 nm lines of atomic fluorine increased rapidly with increased oxygen to SF_6 discharge.

Hoffmeister et al. [110] used fused silica as the work material, and this process is used for the chemical reduction of a substrate by low-temperature APPP. A layer of silicon sub-oxide is produced, and hydrogen is embedded in the parent material. The changes at the workpiece surfaces, like hydrogen concentration, and the optical transmission are investigated. In the case of plasma-treated substrates, the ablation threshold is remarkably decreased. The value of the ablated spot roughness showed a notably reduced peak-to-valley height by an amount of 2.3 nm [110].

Kolpakova et al. [111] proposed a novel method to investigate the electron density at atmospheric pressure argon discharge, like neon, nitrogen, air, and helium. Plasma jet machining is based on plasma-assisted material removal. It is a cost-effective and flexible process for small pieces or small batch production, with the component's diameter varying between 5–150 mm. Spectrum analyzer software is used to depict the emission of spectra and identification of the spectrum line. The spectral range varies between 300–600 nm during the transition between the metal particle emission to discharge modes sputtered from the cathode material [111].

Ray et al. [112] proposed oxygen plasma in the RF generator below 10 mTorr is used. The formation of oxygen rate is studied as a function of the conductivity type, substrate temperature, resistivity, oxygen pressure, and generator output power. The results obtained on the masked substrate, using the silicon-mask interface as a marker, confirmed that the experimental error is within the limit, and the formation of oxide is deposited on the substrate surface. The deposition rate rises as power increases, pressure decreases, and the distance between the wafer and the plasma generating zone decreases. Excellent homogeneity is achieved with a 56 mm wafer diameter. At 600°C and above temperature, the deposited oxide properties are slightly inferior to thermal oxide grown at 1000°C [112].

Engelhardt et al. [113] proposed a local-focused plasma jet-assisted polishing process for high-accuracy crystalline silicon manufacturing. The process parameters considered in plasma jet polishing were working distance, gas composition, RF power, and scan velocity. Surface roughness value is characterized after etching using white light interferometry and AFM [113].

Dev et al. [6,114] investigated a non-contact plasma technology that eliminates the atomic-level defects in fine-finished TIR optics. Raman microscopy is used to understand the chemical structure of fused silica. A novel process is introduced to investigate the cracks on the optics' surface through in situ laser illumination. Fused silica observes an 80% reduction in higher spatial wavelength using power spectral density after plasma polishing. The model of the plasma chamber is shown in Fig. 1.24.

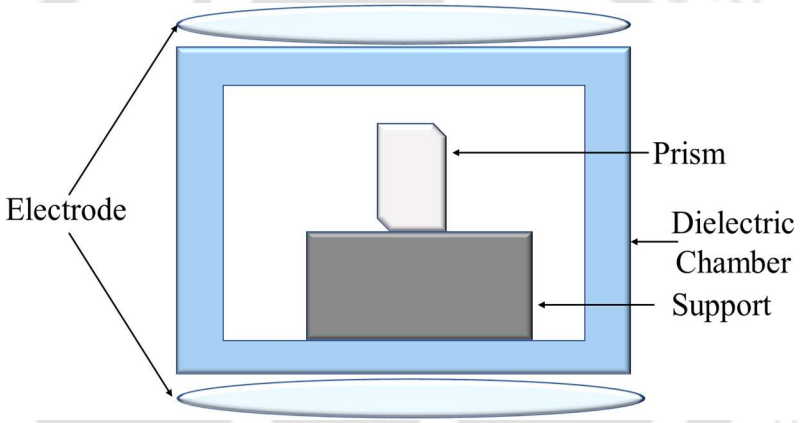

Fig. 1.24 Plasma chamber model [6]

1.6 Motivation Behind Present Research Work

From the state-of-the-art inertial sensors such as gyroscopes and accelerometers for aerospace applications, the sensing microstructure demands excellent surface integrity in terms of sub-nanometer surface finish, lower surface/sub-surface damage, nanoscale surface residual stress, and minimal surface losses. Also, the components are not simple planar or aspheric surfaces. These are complex and freeform surfaces, usually made of hard, brittle materials such as fused silica, Saffire, Zerodur, and silicon carbide. Conventional methods, such as magnetorheological and chemo-mechanical polishing, can achieve the sub-nanometer surface finish. However, it is not very deterministic when it comes to zero defect surface/subsurface damage potential. Plasma polishing has been developed as an effective deterministic process to meet zero-defect surfaces. However, its application is limited to the planar or simple surface, with minimal treatable area. The optical wedge and prism are presented in Fig. 1.25.

The component shown in Fig. 1.25 displays the fused silica surfaces that must be polished to the sub-nanometer range while maintaining very high surface integrity levels concerning surface damage, residual stress, surface topography, and geometrical tolerance. Hence, a low-power medium-pressure plasma polishing process is conceived to concurrently achieve isotropic polishing of complex 3D surfaces, including inside surfaces where no tool or beam can reach.

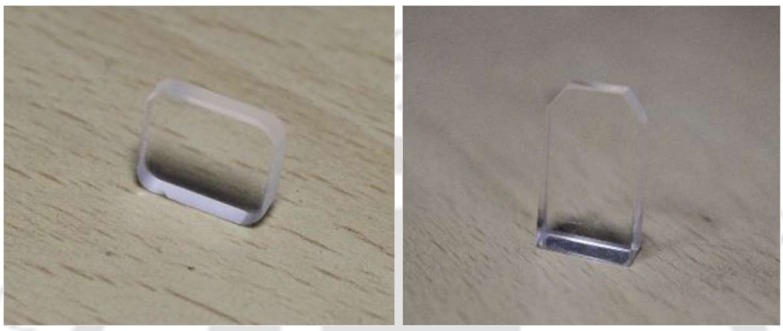

(a) (b)

Fig. 1.25 Gyro components (a) optical wedge and (b) prism

1.7 Objectives of Present Thesis

The proposed research plans to utilize and understand the plasma polishing process in detail and apply it to machining complex and freeform optical surfaces. The work focuses on developing an experimental setup for investigating fused silica, influencing process parameters, and machining complex geometry using an atom-by-atom removal mechanism approach. From this perspective, considering various requirements of the plasma polishing process for complex substrates, the following objectives are planned for the present research:

- Design and development of plasma polishing experimental setup and optimization of plasma chamber to finish fused silica substrate at medium pressure using preliminary experiments.
- Surface characterization of fused silica before and after plasma processing using FESEM, EDX, AFM, XRD, and Raman spectroscopy analysis.
- Experimental investigations on the influence of workpiece dimensions for better surface finish and higher material removal rate.
- Parametric optimization (RF power, pressure ratio, machining time, and total pressure) of medium-pressure plasma polishing process using statistical design of experiments.

- Investigation on variation in surface roughness with a material removal depth of 30 µm at two different substrate surface conditions, i.e., coarse machined and lapped fused silica.
- Surface finishing evolution of freeform fused silica (i.e., prism) by He:(SF_6/O_2) based medium-pressure plasma process and comparing with wet chemical etching.

1.8 Organization of the Thesis

The thesis is organized into seven chapters with references. The introduction to the various finishing/polishing processes describes the brief literature survey of available glass and glass-ceramic materials fabrication methodologies. Plasma processing has distinct advantages over various non-contact methods. The fundamentals of plasma and the material removal mechanism are also examined on optical materials with different properties. An extensive literature review was carried out to fabricate optical components with varying machining processes, also discussed in **Chapter 1**.

The design and development of the medium-pressure plasma process experimental setup for finishing optical material are discussed. It comprises various equipment, i.e., gas cylinder (SF_6, O_2, and He), mass flow meter, plasma chamber, vacuum gauge, gas dosing valve, RF power, and vacuum pump. Moreover, the CAD diagram of each component is also presented. The initial preliminary experiments are carried out to determine the range of process parameters. The plasma chamber's optimization for fused silica fabrication using preliminary experiments and surface characterization of fused silica before and after plasma processing using FESEM, EDX, and AFM is also discussed in **Chapter 2**.

Chapter 3 describes the experimental investigations of process parameters and the influence of workpiece dimensions of fused silica substrates on surface finish and material removal rate. The XPS analysis is also carried out in this chapter.

Chapter 4 describes the investigations of the parametric optimization (RF power, pressure ratio, machining time, and total pressure) of the medium-pressure plasma polishing process using the statistical design of experiments.

Chapter 5 investigates the variation of surface roughness with a material removal depth of 30 µm for two conditions of the surface, i.e., coarse machine and lapped fused silica. It also includes the experimental study of wet chemical etching compared to plasma polishing for fused silica optics. This chapter shows the advantages of medium-pressure plasma processing over hazardous wet chemical etching.

Chapter 6 describes the surface finishing evolution of freeform and complex fused silica (i.e., prism) by He:(SF_6/O_2) based medium-pressure plasma process and compares it with wet chemical etching. A discussion of the conclusions and critical findings of the present study with the future scope is presented in **Chapter 7**.

Chapter 2 Design and Development of MPPP Setup and Preliminary Investigations

2.1 Introduction

The word plasma describes microscopically neutral substances containing many interacting free electrons and ionized atoms or molecules. In other words, plasma, called the fourth state of matter, is a partially ionized gas with an equal number of positive and negative particles; overall, the plasma remains electrically neutral. The plasma mainly contains free radicals, which are chemically reactive and responsible for material removal. Previous research shows that uniform finishing is challenging while finishing complex and freeform optical surfaces. A non-contact medium-pressure plasma process (MPPP) setup is designed and developed to address these issues for finishing optical material. The required specification of the plasma processing setup is that it should be capable of atom-by-atom material removal without heating up the surface or initiating micro-cracks, resulting in no surface/sub-surface damage. The process should be deterministic for complex and freeform surfaces. Plasma-based polishing is an emerging technology. It utilizes the physical and chemical properties of ions/radicals for polishing fused silica without inducing any damage to the fused silica materials.

2.2 Design and Development of MPPP Setup

The increasing demand for precise optical components leads to the development of MPPP setup. An isotropic dielectric barrier cavity-based plasma, operating at a medium pressure of 1 mbar to 100 mbar, is conceived. Dielectric barrier RF excitation is chosen to minimize electron heating while allowing chemical interaction of free radicals with surface atoms of the workpiece. Typical plasma contains millions of times more radicals than ions or electrons. Radicals form more easily, and their lifetime is much longer. Ions don't etch, while radicals do. Ions affect the process by energetic (physical) bombarding of the surface, influencing chemical processes of etching. Radicals are responsible for the dry etching process. These are chemically active and react with the surfaces to produce volatile products. The plasma chamber is designed to polish components with 5 to 45 mm diameters. Uniform generation of reactive gases is considered to enable isotropic plasma while designing the chamber. Zerodur material is used to fabricate the plasma chamber. The chamber is sealed with a lid plate, which is optically transparent for 300 to 1200 nm

wavelengths. Vacuum pump is used to create the vacuum initially at the start of the experiment. Medium pressure is considered to avoid ion impingement and to enable a true non-contact process. Also, to minimize electron heating, dielectric barrier RF excitation is selected to permit chemical interaction by the reactive free radicals with the component's surface atoms. The excitation RF frequency is selected as 40.68 MHz to minimize the bombardment of ions. In the present system, three mass flow meters control the flow rate (standard cubic centimeter per minute, sccm) of gases (SF_6, O_2, and He) supplied from three gas cylinders. The system contains three distinct gas sources: He and O_2, as carrying gas, and SF_6 as an etching gas. The plasma is produced at 40.68 MHz RF power; it is chosen to reduce electron heating during the interaction of the surface atom with F^* radicals. The schematic diagram and actual photograph of the developed medium-pressure plasma process setup are illustrated in Fig. 2.1(a) and (b).

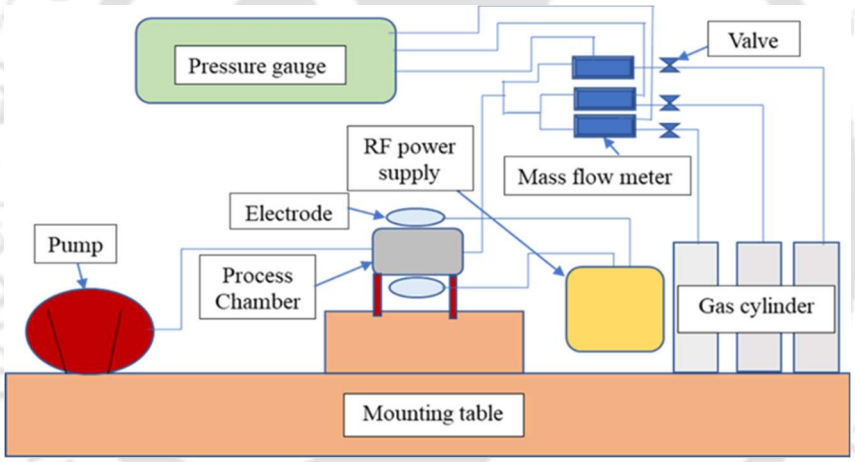

(a)

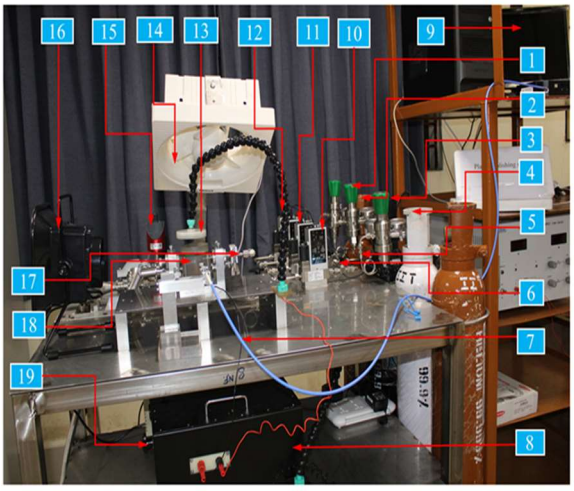

Part number- Part name

1 – Gas regulator
2 – Helium (He) gas cylinder
3 – Oxygen (O_2) gas cylinder
4 – Sulfur hexafluoride (SF_6) gas cylinder
5 – Gas flow pipe
6 – Inlet valve of mass flow meter (MFM)
7 – Optical emission spectrometer (O.E.S)
8 – RF power
9 – Desktop connected to O.E.S
10 – MFM connected to SF_6
11 – MFM connected to O_2
12 – MFM connected to He
13 – Electrode
14 – Fan
15 – Gauge
16 – Smoke absorber
17 – Inlet to plasma chamber
18 – Plasma chamber
19 – Tuning of RF power

(b)

Fig. 2.1 (a) Schematic diagram and (b) actual photograph of developed MPPP experimental setup

Plasma is the fourth state of matter and is more or less an ionized gas. It comprises electrons and ions and remains neutral in fundamental and excited states. Plasma is electrically neutral from a macroscopic view. However, it is electrically conductive and includes free-charge carriers [39]. Atomic emission microscopes are used to analyze the relative densities of plasma species in an excited state and the material removal mechanism. The actual photograph (during processing) and schematic diagram of the process chamber are illustrated in Fig. 2.2(a) and (b), respectively. The CAD model of the developed experimental setup is presented in Fig. 2.3.

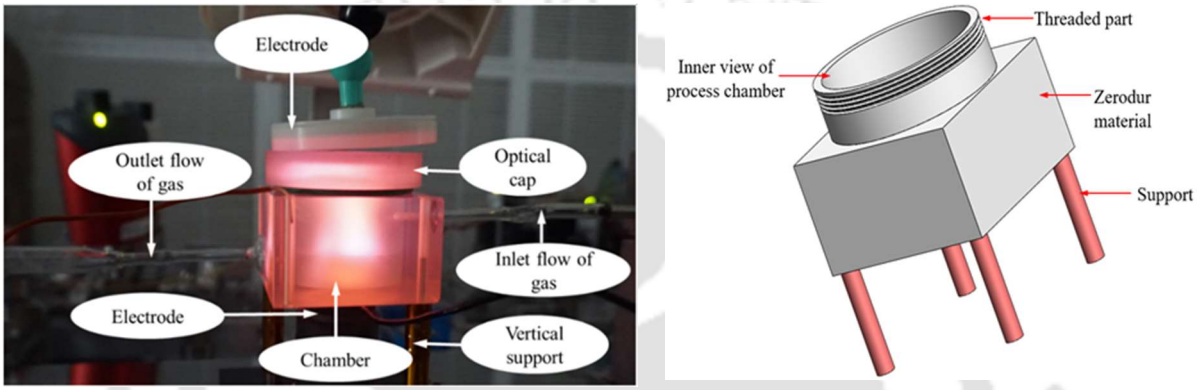

(a) (b)

Fig. 2.2 (a) Actual photograph and (b) CAD model of plasma chamber

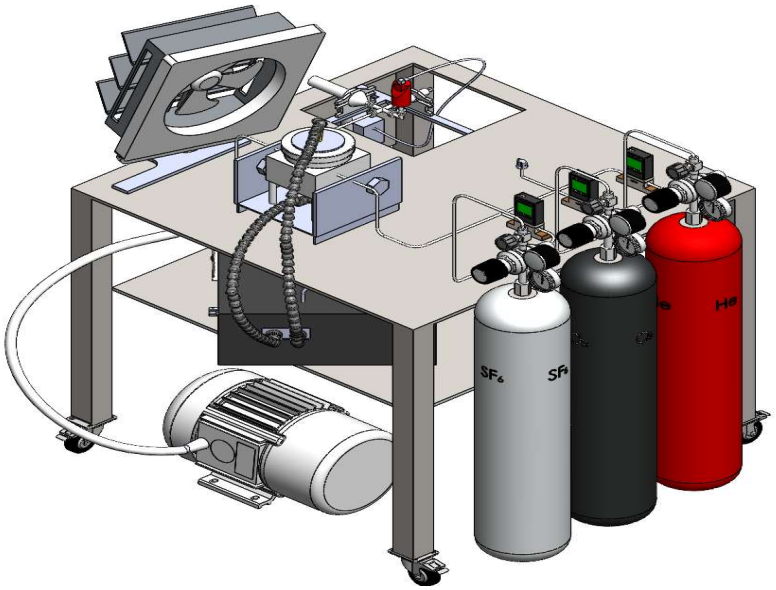

Fig. 2.3 Developed medium pressure-plasma experimental setup

The plasma polishing setup consists of three gas cylinders (He, O_2, and SF_6), mass flow meters, a process chamber, a gauge, RF power, and a vacuum pump. Plasma is generated using three different gases: He, O_2, and SF_6, as shown in Fig. 2.4(a).

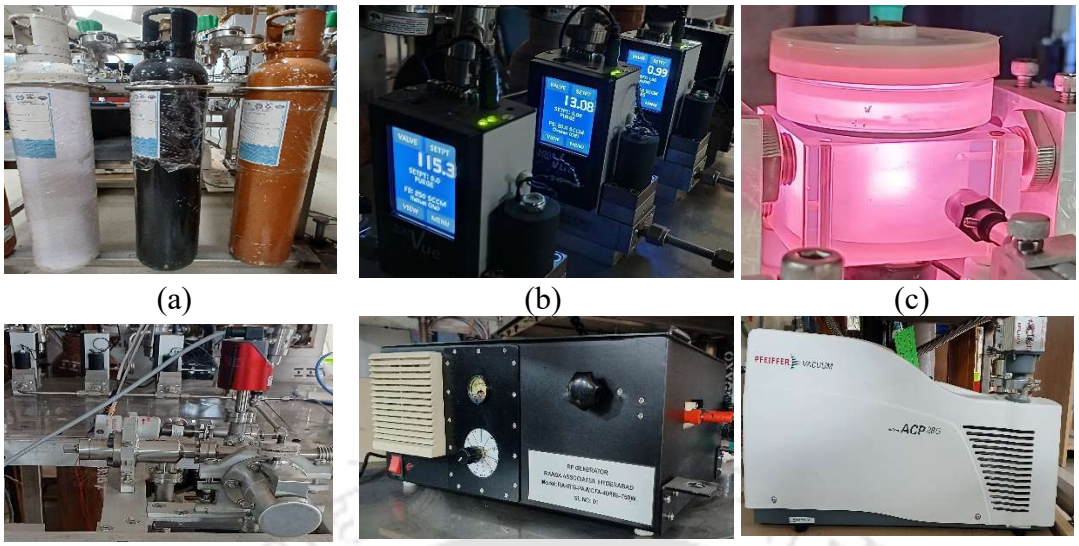

Fig. 2.4 Actual photograph of plasma process setup components (a) gas cylinders, (b) mass flow meters, (c) plasma chamber, (d) gas dosing valve and vacuum gauge, (e) RF power, and (f) pump

In the initial stage of the experiment, the gases are admitted into the chamber one by one at different flow rates and pressure. The other gases pass through these separate mass flow meters (MFM) (Fig. 2.4 (b)), and MFM controls the flow rate of gases. A mass flow meter regulates the flow of gases (SF_6, O_2, He, etc.) from the gas cylinder and provides the required flow rate for the plasma processing. The plasma chamber (Fig. 2.4 (c)) is fabricated using a zerodur material. The plasma chamber is sealed with an optically transparent cap of 300–1200 nm wavelength. The body of the plasma chamber acts as a dielectric barrier for the exciting electrodes. The plasma chamber is connected to the vacuum system and three gas feed lines. The fiber optic probe head of atomic emission is used to measure the relative spectroscopy densities of plasma species in the excited electronic states, which is very useful for interpreting the mechanism of material processing under plasma. The gas dosing valve and vacuum gauge (Fig. 2.4 (d)) are connected to the process chamber to adjust the pressure inside the plasma chamber. It is also used to evacuate the contamination and ejection of the substrate after the process. The RF power source (Fig. 2.4 (e)) is used to ionize the gases inside the plasma chamber with a frequency of 40.68 MHz. RF power and a matching box provide the discharge voltage. The circular copper electrode is attached to the +ve and -ve terminal with the RF power and placed at the top and bottom of the plasma chamber. The exhaust pumping system (Fig. 2.4(f)) is used to create a vacuum inside the plasma chamber just before the start of the experiment and also to remove the waste gases generated during

plasma processing. The actual photograph of plasma process setup components is demonstrated in Fig. 2.4.

2.3 Preliminary Experiments

Preliminary experiments are carried out using He plasma to investigate the amount of plasma discharge inside the plasma chamber. The experiments are performed at different pressures and RF power to compare the discharge inside the plasma chamber. Higher discharge directly affects the plasma polishing process. Complete discharge leads to uniform material removal from the substrate. Further, the discharge quantity decreases with increased pressure in the plasma chamber. It is because of the total pressure inside the plasma chamber, i.e., at higher pressure, electrons have less chance to gain enough energy between collisions to perform excitation and ionization. When the total pressure rises inside the plasma chamber, the intensity of atoms decreases due to the reduced mean free path of the ions since the electrons have less chance to gain enough energy between collision to perform excitation and ionization. The qualitative measurement of plasma discharge at different pressures and RF power is mentioned in Table 2.1.

Table 2.1 Qualitative discharge percentage at various pressures and power

Pressure (mbar)	20 W	30 W	40 W	80 W
5	100%	100%	100%	100%
10	100%	100%	100%	100%
20	75-80%	100%	100%	100%
30	60-70%	80%	85%	90%
40	30%	50%	55%	60%
50	20%	35%	45%	50%
60	<20%	25%	30%	40%
62	<10%	10-12%	15%	20%

Further, the experiments are carried out with SF_6, O_2, and He gases. The intensity of excited atoms' emission spectrum reaches its maximum value at wavelengths 685.6 nm, 667.8 nm, 844.6 nm, and 780.0 nm for fluorine (F), helium (He), oxygen (O), and silicon (Si), respectively as measured from optical emission spectroscopy (OES). The experiments were conducted at different chamber pressure, pressure ratios (SF_6/O_2), gas compositions ($He:(SF_6+O_2)$), and RF power, as shown in Table 2.2.

Table 2.2 Process parameters and their range

Parameters	Unit	Value
Total pressure	mbar	5, 10, 20, 30
Gas composition (He: SF_6+O_2)	%	50:50, 70:30, 90:10
Pressure ratio (SF_6/O_2)	–	1:2, 1:1, 2:1, 3:1
RF power	W	20, 40, 80
Machining time	minutes	60
O_2 gas flow	sccm	0.20–20
SF_6 gas flow	sccm	0.50–50
He gas flow	sccm	2.5–250

Initially, the experiments are conducted at process parameters, gas composition of 50:50, 70:30, 90:10 and pressure ratio of 1:2, 1:1, 2:1, 3:1 with constant machining time of 60 minutes, total pressure of 5 mbar and RF power of 80 W. The results show that a higher value of plasma discharge intensity is observed with gas composition of 90:10 and pressure ratio of 1:1 for all F, He, O, and Si atoms due to the higher concentration of He gas. It increases plasma density as the collision of atoms inside the plasma chamber increases. At gas compositions of 70:30 and 50:50, the mixture's He atom content decreases, reducing plasma discharge intensity. Therefore, the gas composition of 90:10 has been chosen for further experimentation as higher plasma discharge has been obtained at each pressure and also achieved higher plasma discharge intensity compared to other gas compositions, i.e., 50:50 and 70:30. In some cases, there is no discharge because of insufficient collision of atoms, probably due to the reduced mean free path of atoms/ions, i.e., less chance to gain sufficient energy. It is clear that the discharge plasma density is higher around the 1:1 pressure ratio compared to others, as demonstrated in Fig. 2.5. Further experiments are performed at the remaining total pressure of 10, 20, 30, and 40 mbar and RF power of 20 and 40 W and the results follows the similar pattern. Jin et al. [100] observed that higher intensity leads to a higher material removal rate. Also, Dev et al. [29] experimentally found that radicals, i.e., fluorine, are responsible for sustained material removal. The other two gases, SF_6 and O_2 are bulky compared to He. The optimum concentration of O_2 aids the complete dissociation of SF_6 into F* and sulfur pentafluoride (SF_5), which prevents the recombination of SF_5 with F*.

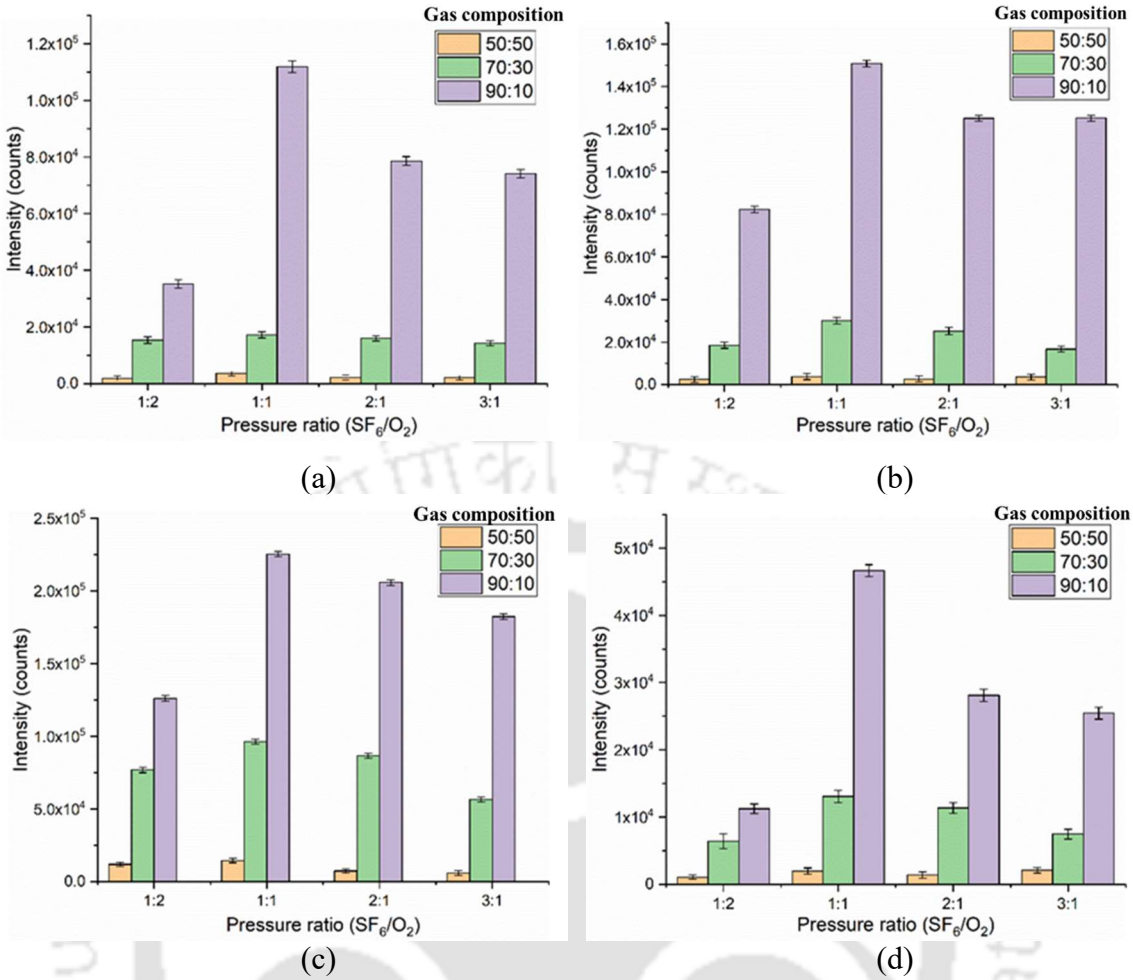

Fig. 2.5 Variation of plasma discharge intensity with pressure ratio (SF_6/O_2) for (a) F, (b) He, (c) O, and (d) Si atom at 5 mbar total pressure and 80 W RF power

Further, the experiments are conducted at different RF power and total pressure inside the plasma chamber to optimize these two parameters for a fixed gas composition (90:10), and pressure ratio (1:1). The discharges are observed for 5, 10, 20, and 30 mbar total pressures. The experimental results in Fig. 2.6 show higher discharge intensity at 5 and 10 mbar total pressure than 20 and 30 mbar. The plasma intensity at 5 and 10 mbar is higher as the atomic mean free path is higher, i.e., the collision energy is more inside the plasma chamber.

Further experiments are carried out at optimum parametric conditions, i.e., gas composition (He:(SF_6+O_2)) of 90:10, pressure ratio (SF_6+O_2) of 1:1 with different total pressure inside the plasma chamber of 5 and 10 mbar. At 5 mbar total pressure, MRR of 0.1, 0.04, and 0.2 mm^3/min are obtained at 80 W, 40 W, and 20 W RF power, respectively. Further, at a total pressure of 10 mbar, MRR of 0.08, 0.03, and 0.02 mm^3/min are achieved at 80 W, 40 W, and 20 W RF power, respectively. As seen in Fig. 2.7, MRR decreases for both

5 and 10 mbar total pressures with reduced RF power. However, it has been observed that higher MRR is associated with 5 mbar total pressure as compared to 10 mbar. Dev et al. [29] previously achieved a maximum MRR of 0.008 mm^3/min using similar plasma processing gases. Hence, MRR is improved with the optimized process parameters. Material removal rate (mm^3/min) in plasma processing is calculated using Eq. (2.1).

$$\text{Material removal rate (MRR)} = \frac{\text{Change in weight } (\Delta w)}{\text{Density}(\rho) \times \text{Machining time (t)}} \quad (2.1)$$

Where Δw is the change in weight (mg), ρ is the density of fused silica (mg/mm^3), and t is machining time (min).

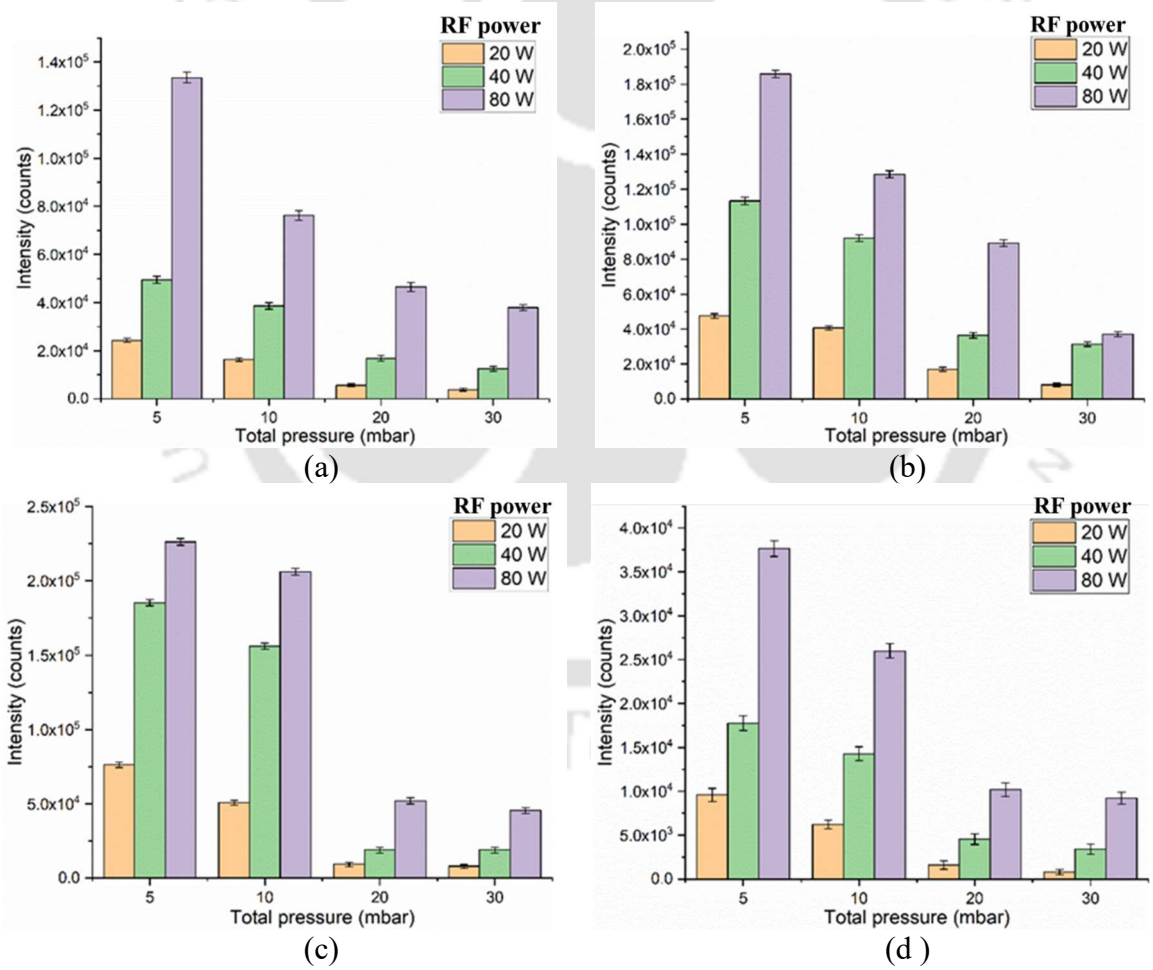

Fig. 2.6 Variation of plasma discharge intensity with total pressure for (a) F, (b) He, (c) O, and (d) Si atom at gas composition of (90:10) and pressure ratio of (1:1)

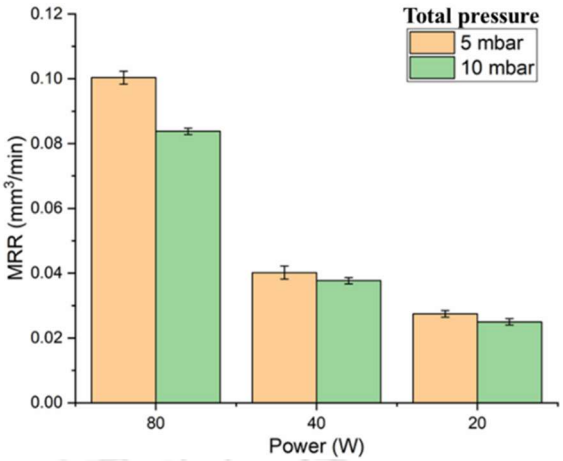

Fig. 2.7 MRR at different power

2.4 Raman Microscopy

Raman microscopy reveals broad bands representing fused silica network-linked vibration modes. The chemical structural integrity of fused silica is investigated using Raman microscopy. Characteristic Raman peak (ω1) in the silica network concentrated at 490 cm^{-1} is linked with Si-O-Si bond angle; also, its breadth represents the distribution of Si-O-Si bond angle. SiO_2 network should preferably have six members. However, because of mechanical tensions created during contact polishing of initial samples, forming 3 and 4-member structures on SiO_2 surfaces is relatively prevalent. Two bands concentrated at 490 cm^{-1} and 605 cm^{-1} (D1) are created by the breathing movement of O atoms in puckered 4 and 3-member ring configurations. The ratio of area under 440 cm^{-1} to 605 cm^{-1} peaks before and after plasma polishing of fused silica are presented in Fig. 2.8.

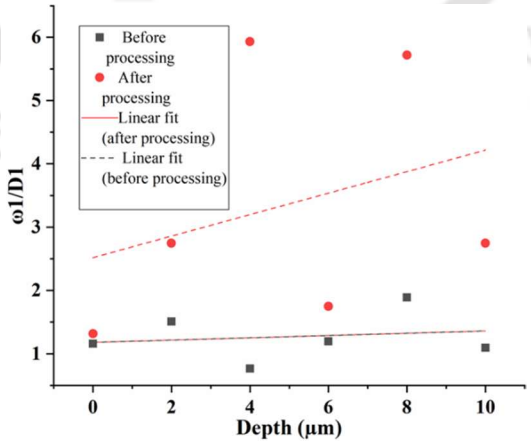

Fig. 2.8 Raman spectra comparison in ratio of area under 440 cm^{-1} to 605 cm^{-1} peaks of substrate surface before and after plasma processing

The average ratio ω1/D1 (at different depths) improves from 1.88 before processing to 2.12 after plasma processing, which affirms that the substrate surface's chemical bond structure is like bulk material. Also, the surface and sub-surface atomic-level flaws are significantly reduced.

2.5 Summary

The developed experimental setup details for finishing optical components have been discussed. The developed setup includes gas cylinders, a mass flow meter, a plasma chamber, a gas dosing valve and vacuum gauge, RF power, and a vacuum pump. Further, a preliminary experimental investigation on the atomistic material removal rate over fused silica surfaces using the medium-pressure plasma process is carried out. The plasma polishing optimized parameters, i.e., gas composition of 90:10, pressure ratio of 1:1, total pressure of 5, and RF power of 80 W, are selected based on the preliminary experiments. A series of experiments have been conducted for each optimized parameter. It is found that the material removal rate is significantly affected by the total pressure and gas composition. The material removal rate is improved up to 0.10036 mm^3/min at the optimized parameters. Furthermore, Raman's analysis results show that the average ratio ω1/D1 (at different depths) improves from 1.88 before processing to 2.12 after plasma processing, enhancing a 13% reduction in damaged and strained layers on the substrate surface after plasma processing.

Chapter 3 Effect of Substrate Dimensions on MRR and Surface Roughness

3.1 Introduction

Medium-pressure plasma polishing process has been proposed as a non-contact type plasma-assisted atom-by-atom material removal technique for finishing optical materials. It is a complex phenomenon, and MRR and surface roughness depend on factors like RF power, time of operation, chamber condition, total pressure, flow rate, etc. Any fabrication process optimized by knowing MRR. MRR can be obtained by analyzing the processed end product, but it is time-consuming, and real-time controlling is impossible. Sometimes it may not be possible to achieve the desired end product. Real-time Material removal rate analysis is essential for monitoring and controlling the process. The qualitative analysis of the plasma and atom emission spectrum explores the plasma generation and scattering of the activated fluorine (F*) radicals inside the plasma chamber. The material removal rate and surface roughness variation are analyzed at different RF power with varying substrate dimensions. Material removal rate and surface roughness variations have been investigated at different total pressures between 5–30 mbar and substrate dimensions (i.e., varying length between 5–45 mm with fixed width and thickness of 5 and 2 mm) at fixed process parameters, i.e., radio-frequency power of 80W, pressure ratio of 1:1, and gas composition of 90:10. The microstructure, chemical composition, and surface topography are also analyzed before and after plasma processing.

3.2 Substrate Position inside Plasma Chamber

Fused silica workpieces are initially prepared by grinding and lapping to investigate MRR, surface roughness variation, and substrate surface characteristics after plasma processing. Initially, the samples are ultrasonically cleaned with acetone and alcohol and dried with nitrogen gas. Further, the substrate is washed and cleaned in an ultrasonic bath using deionized water and then dried at room temperature. The plasma chamber comprises zerodur material. The outer portion of the plasma chamber acts as a dielectric barrier for the exciting electrodes. The plasma chamber is associated with the vacuum pump and three gas lines connected to the mass flow meters. An optical emission spectrometer is used to measure the relative densities of plasma species in the excited electronic states, which is very useful for interpreting the mechanism of material processing during plasma processing. The width and

thickness of the substrate are constant, i.e., 5 mm and 2 mm, whereas the substrate length varies (i.e., 5−45 mm). The individual substrate is kept inside the plasma chamber at the same location for all the experiments. The 3D schematic of the plasma chamber with different substrate dimensions placed at various locations within the plasma chamber is illustrated in Fig. 3.1.

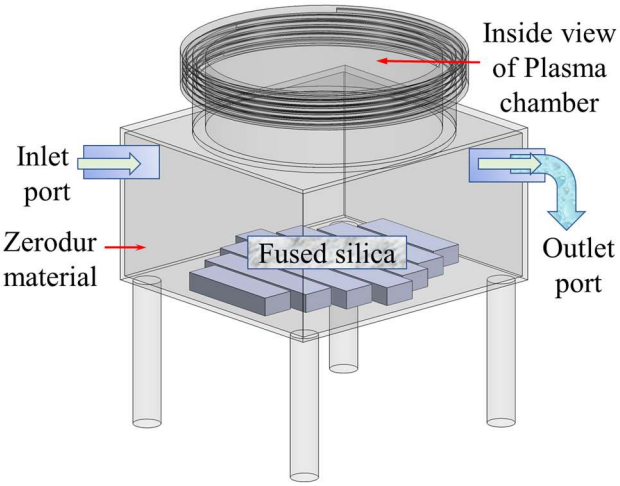

Fig. 3.1 3D view of plasma chamber with substrate inside plasma chamber

3.3 Results and Discussion

The following section discusses the MRR and variation in surface roughness with substrate dimensions at different total pressures.

3.3.1 Plasma Discharge During Processing

The experiments are carried out using process gas, i.e., He, O_2, and reactive gas, i.e., sulfur hexafluoride (SF_6), for polishing fused silica. At first, the experiments are performed to analyze the correlation between the flow rate of gases and the plasma chamber pressure (mbar). The gases are filled one by one into the plasma chamber, which is controlled by the mass flow meters of individual gases. Initially, experiments are carried out to get a discharge with He gas inside the plasma chamber. The maximum flow rate can reach up to 262 sccm for the He mass flow meter. The gauge is connected to the plasma chamber and gives the corresponding pressure inside the plasma chamber. It can be observed that the pressure follows an approximately linear pattern with the flow rate of the He gas, as illustrated in Fig. 3.2. The initial experiments are performed to get the range of process parameters for plasma discharge inside the plasma chamber.

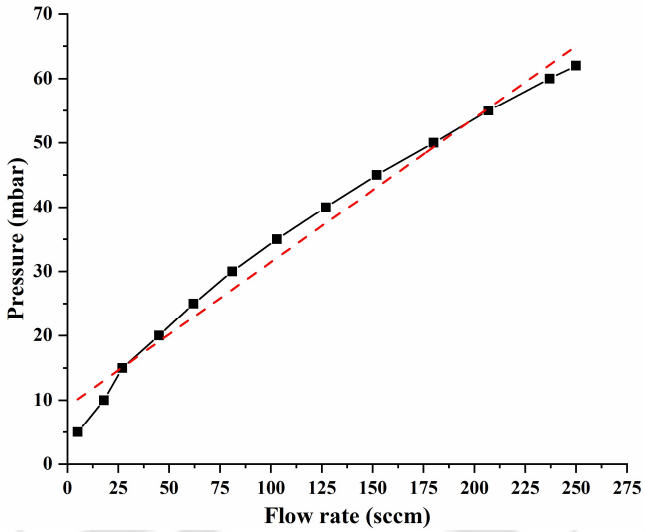

Fig. 3.2 Variation of plasma chamber pressure with He gas flow rate

Experiments are carried out to determine the qualitative measurement of plasma generation inside the plasma chamber at various pressures (5−30 mbar). Qualitative measurement of plasma generation refers to the assessment and description of the characteristics and properties of a plasma, typically without relying on precise numerical values or quantitative data. The discharge percentage is measured by (1) observing the color and appearance of the plasma, which can provide information about its discharge percentage, (2) using spectroscopy to analyze the spectral lines and emission spectra of the plasma, (3) examining the visual patterns or shapes of the plasma. Initially, the He gas is filled into the plasma chamber at different pressures, i.e., 5, 10, 15, 20, 25, and 30 mbar. Then, the gas is excited by RF power inside the plasma chamber. The discharge of gas at different chamber pressures inside the plasma chamber affects the removal of material. Qualitative discharge percentages at different pressures are analyzed and presented in Fig. 3.3. It clearly shows that the discharge intensity remains constant up to 20 mbar, and then decreases. It is caused by the mean free path of electrons and ions inside the plasma chamber at high pressure.

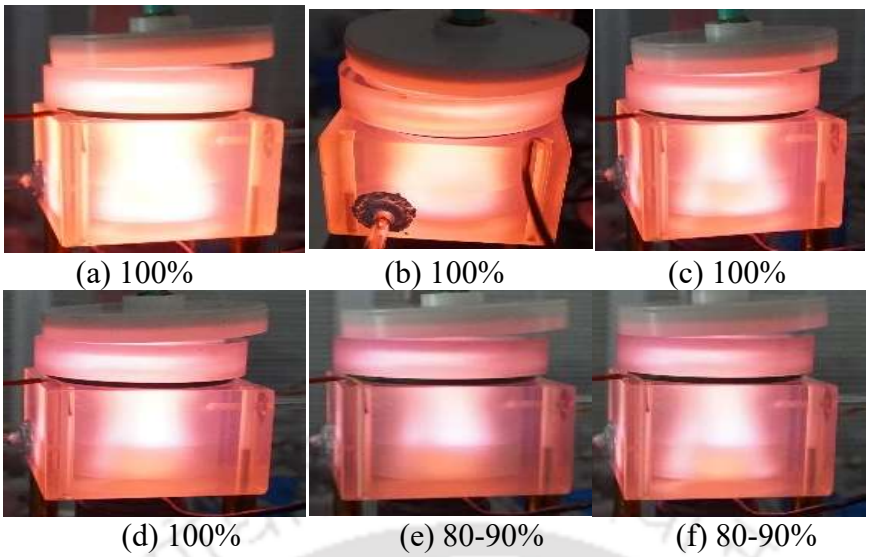

(a) 100% (b) 100% (c) 100%

(d) 100% (e) 80-90% (f) 80-90%

Fig. 3.3 Qualitative measurement of plasma generation at various pressures (a) 5, (b) 10, (c) 15, (d) 20, (e) 25, and (f) 30 mbar

3.3.2 Characterization of Plasma

The spatial distribution and uniformity of chemically reactive radicals within the plasma chamber significantly affect surface roughness and material removal. The plasma is monitored at specific wavelengths using an optical emission spectrometer. During plasma polishing, a non-invasive spectroscopic method is employed for real-time examination. Fig. 3.4 presented the intensity of active F* atoms in the plasma chamber at different wavelengths and total pressure. Fluorine atoms at different wavelengths are essential in material removal from the surface. The intensity increases when the ratio of SF_6 /O_2 reaches 1:1, and further reduction is observed, particularly in the spectral line of the F* atom at a different wavelength. This is attributed to the presence of oxygen, which enables the dissociation of SF_6 into SF_5 and F*. Further increase in oxygen causes the fused silica surface to react with O and form aggregates of SiO=SiO, which reduces atom intensity [107]. With an increase in total pressure, the intensity of F* atom consistency diminishes, especially at wavelengths of about 685.60 nm. Accordingly, MRR will be more significant with the wavelength of the F* atom at 685.60 nm from the machined surface. Atoms at the wavelength of 685.60 nm demonstrate the most powerful function in finishing the fused silica materials.

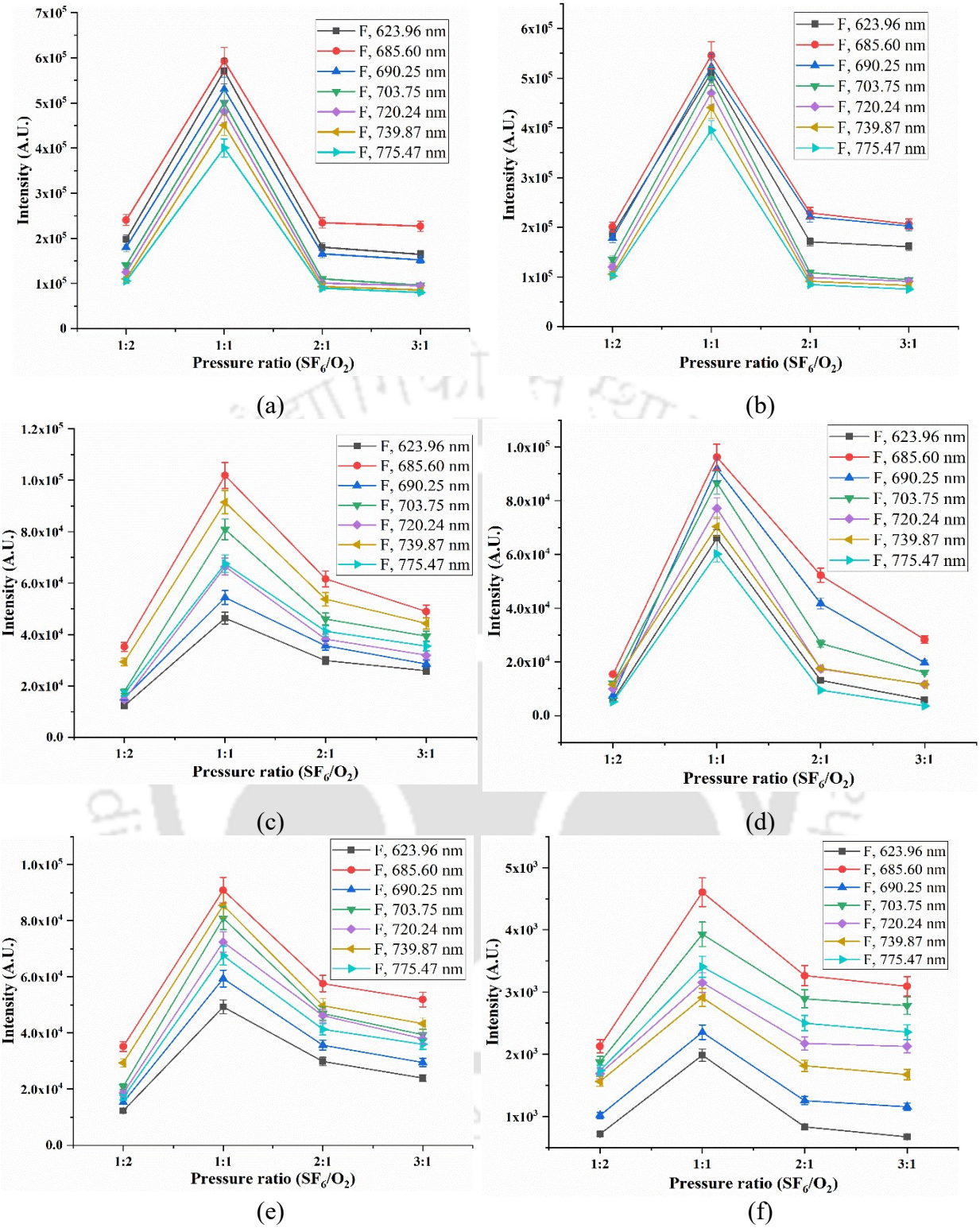

Fig. 3.4 Consistency and spatial distribution of F* atoms at various total pressures (a) 5, (b) 10, (c) 15, (d) 20, (e) 25, and (f) 30 mbar

3.3.3 Variation of Intensity with Pressure

The experiments are performed to determine the intensities at various RF power (i.e., 20, 40, 60, and 80 W) and total pressure (i.e., 5, 10, 15, 20, 25, and 30 mbar). Fluorine and silicon

atoms play significant roles in removing materials from the surface. These two atoms are the most effective while finishing fused silica [30]. Fig. 3.5 presents the intensity of F (685.60 nm wavelength) and Si atoms with different RF powers and total pressures at 1:1 pressure ratio (SF_6/O_2). The intensity of atoms is observed at its highest value for 80 W RF power due to the increased electron density in the discharge [115]. With increased RF power, plasma emission intensity increases [36]. The electric field near the electrodes increases as the driving power increases, thus ensuring a larger current proportional to $\partial E/\partial t$ (where E denotes the electric field). The increased electric field E/N (where N is gas mixture density) close to the electrodes causes increased excitation and ionization rates and, consequently, the spectral intensity [37].

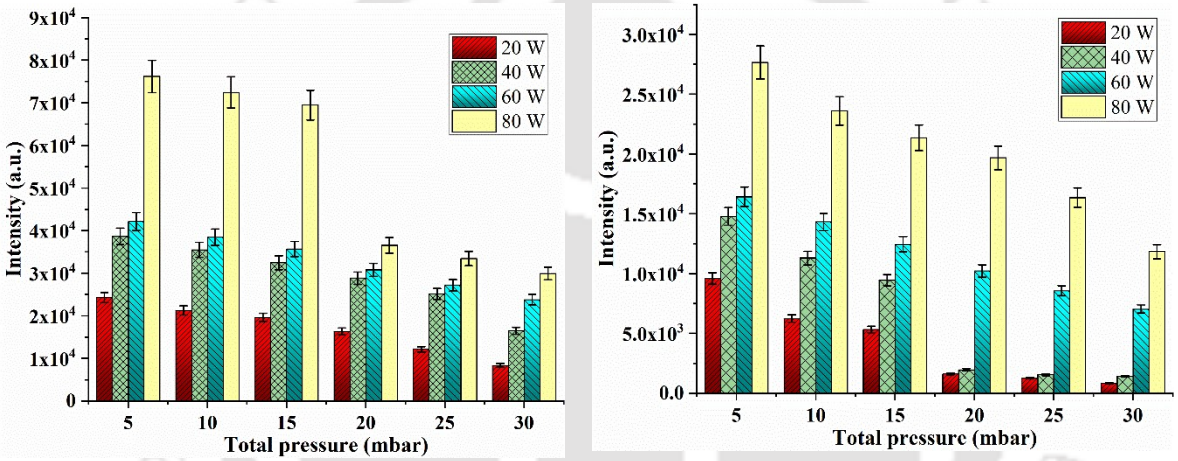

(a) (b)

Fig. 3.5 Intensity variation at different pressures (a) F atom and (b) Si atom

3.3.4 Variations of MRR with Substrate Dimensions

In the plasma polishing process, the material removal mechanism of fused silica is based on the chemical reaction between F* radicals (i.e., dissociated from SF_6) and the fused silica substrate surface. Based on the preliminary and previous literature studies, the experiments are performed at optimum values of fixed parameters, i.e., SF_6/O_2 of 1:1, 80 W RF power, and He:(SF_6+O_2) of 90:10. The experiments are performed at various process parameters mentioned in Table 3.1.

During plasma polishing experiments, the fused silica substrate dimensions vary between 5−45 mm, whereas the width and thickness of the substrates are kept constant, i.e., 5 mm and 2 mm, respectively. All seven samples are placed inside the plasma chamber, keeping individual substrate's (having the same dimension) locations fixed while performing

the experiments at different chamber pressures. Material removal rate strongly depends on the plasma chamber pressure and substrates' surface area/dimensions during processing, as shown in Fig. 3.6(a−f). The experimental results reveal that when the chamber total pressure is increased to 30 mbar and the substrate dimension is reduced to its smallest size/length, i.e., 5×5×2 mm, MRR is observed at its lowest value of 0.0061 mm^3/min. However, when the chamber total pressure is decreased to 5 mbar, and the substrate dimension is increased to a larger size/length, i.e., 45×5×2 mm, MRR is found to be at its highest value of 0.039 mm^3/min. A higher surface roughness value is observed at lower pressure because of the increased excitation and ionization rate due to more contact between the fluorine and surface atoms. Moreover, at constant pressure, MRR increases with increased substrate dimension. At lower pressure, there has been an increased MRR at higher substrate dimensions. According to the findings, when the total pressure is increased, there is a decrease in the discharge within the plasma chamber compared to the lower pressure. This decrease in discharge leads to a reduction in material removal. The material removal rate remains relatively constant between 25 to 30 mbar total pressure due to the lower discharge generation within the plasma chamber. Hawat and Akel [22] reported that the intensity of atoms decreases with increasing pressure in the bulk plasma or the discharge's central part. Meister et al. [116] studied and analyzed the etching rate of optical material using plasma-assisted chemical etching. The experiments are repeated three times for each set of process parameters, and subsequently, an average MRR is computed out of these three measurement values.

Table 3.1 Range of process parameters and their values

Parameters	unit	Values
Total pressure	mbar	5−30
O_2 flow rate	sccm	1−20
He flow rate	sccm	1−262
SF_6 flow rate	sccm	1−50
RF power	W	80
He:(SF_6+O_2)	−	90:10
SF_6/O_2	−	1:1

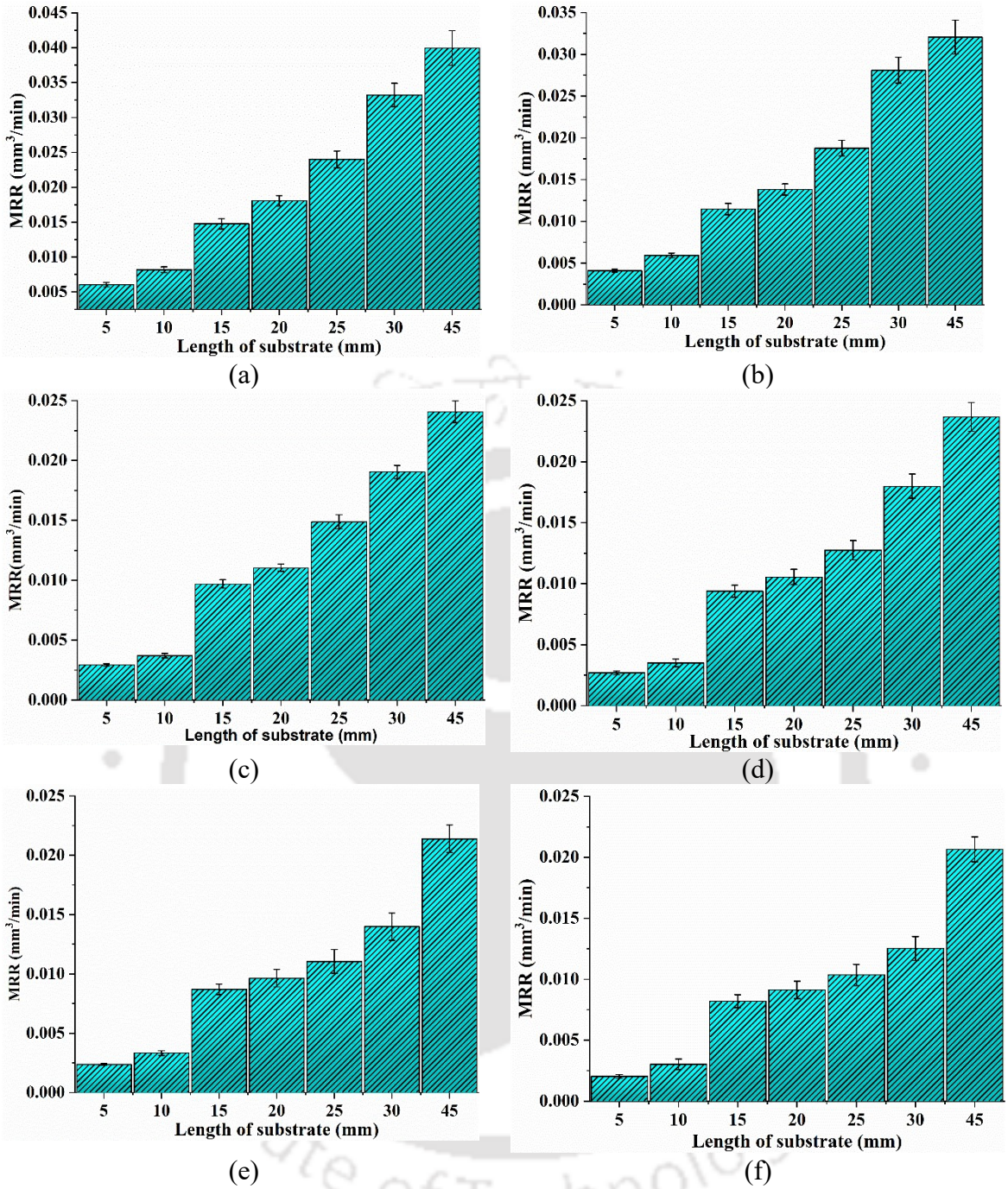

Fig. 3.6 Material removal rate with substrates having different lengths at various total pressures (a) 5, (b) 10, (c) 15, (d) 20, (e) 25, and (f) 30 mbar for 80W RF power

3.3.5 Variations of Surface Roughness with Substrate Dimensions

Surface roughness is investigated before and after plasma processing at 5, 10, 15, 20, 25, and 30 mbar total pressures with constant process parameters, i.e., 80 W RF power, He:(SF_6+O_2) of 90:10 and SF_6/O_2 of 1:1. The initial surface roughness of the fused silica substrates varies between 0.13−0.16 µm. Maintaining a very high precision in the initial surface roughness value of the tested samples is very difficult for optical materials. Therefore, a slight deviation

between the initial surface roughness values is observed for the tested samples. Fig. 3.7 demonstrates the variation in surface roughness of fused silica with different pressures and sample dimensions.

After plasma processing at different parameters, the results in Fig. 3.7 show that the substrate surface is marginally degraded because of subsurface cracks, holes and fracture openings. The findings demonstrated that the inherent isotropic etching of plasma causes variations in the pits' depth created by microcracks at a lower pressure, leading to an increased MRR and more surface deterioration. It can be realized from Fig. 3.7 that at lower total pressures (i.e., 5 and 10 mbar), the surface roughness drastically increases for smaller substrates of 5 and 10 mm lengths, and the % change in surface roughness (%ΔR_a) decreases for a substrate having a higher length at the same pressure. The highest and lowest percentage change in surface roughness observed are 86.4% and 17.1% at 5 mbar and 30 mbar for substrates with 5 and 45 mm lengths, respectively. The width and thickness of the substrates are assumed to be unchanged because of their smaller size and smaller contact area with the reactive radicals. The initial surface roughness values on SiO_2 substrates after the initial stage of plasma polishing are relatively smoother. After removing a thin layer of material, the plasma opens cracks, causing isolated etched pits to form up to a certain depth; the reduction in surface roughness (ΔR_a) is observed. Xin et al. [117] reported that the roughness evolves with the etching depth for plasma processing while polishing on the initial surface, and the roughness evolution is a single-peaked curve. This curve results from opening and coalescing surface cracks and fractures on a polished fused silica surface. With further material removal from the workpiece surface, the surface cracks got polished, and the surface became smoother with reduced surface roughness. The pits slightly increase the surface roughness, as illustrated in Fig. 3.7(a−f). The isolated pits continue to grow and start to coalesce as more material is wiped off [118]. The surface roughness becomes almost constant at higher pressure, as shown in Fig. 3.7(e and f). The sharp edges are removed during the etching of the plasma processed samples; all the major and minor pits disappear, and the surface deterioration/degradation becomes comparatively lower. The surface roughness variations become less between 15−30 mbar pressure with more than 15 mm substrate length. Also, the effective polished surface has been achieved up to 30 mm substrate length. During processing, it was observed that there was more plasma generation in the central region of the plasma chamber. In the case of a higher-dimension substrate, the plasma is not processed in the whole substrate chamber. Moreover, less deviation at higher pressure happened because the discharge quantity decreased with increased pressure in the plasma chamber.

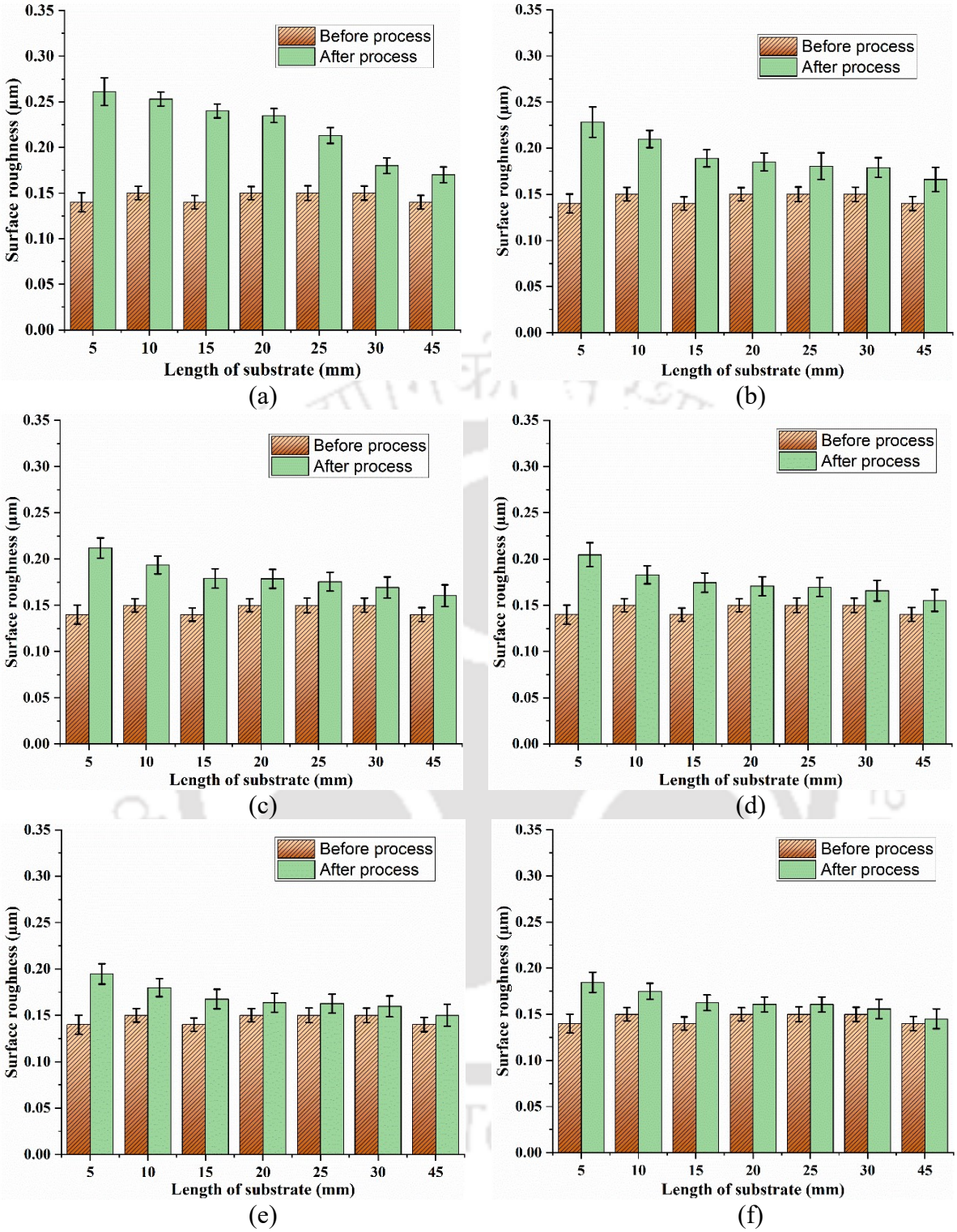

Fig. 3.7 Measured surface roughness values on substrates having different lengths before and after plasma processing at (a) 5, (b) 10, (c)15, (d) 20, (e) 25, and (f) 30 mbar total pressures

3.3.6 Surface Morphology Analysis

Field emission scanning electron microscopy (FESEM) is used for surface morphology analysis of substrate surfaces. FESEM images of the surface and cross-sectional view of

fused silica substrates without processing and after the plasma process are provided in Fig. 3.8. Fig. 3.8(i)(a) presents the surface morphology of the initial SiO_2 substrate, revealing irregular microstructure and a few cracks observed on the initial substrates' surface. Those cracks and irregular surfaces are reduced after plasma processing at 30 mbar total pressure and 80 W RF power on a 30×5×2 mm^3 substrate, as shown in Fig. 3.8(ii)(a). Fig. 3.8(i)(b) illustrates the cross-sectional view of FESEM images of SiO_2 before and after the process, as shown in Fig. 3.8(ii)(b). During the reaction of radicals with substrate surfaces at the start of the finishing process, many etching spots are randomly created on the substrate. These etching locations experience isotropic etching, which produces hemispherical etch pits on the substrate surfaces. The size of the etch pits increases as the etching time and material removal depth increases, causing the nearby pits to coincide and eventually combine into the larger etch pits, which reduces surface roughness.

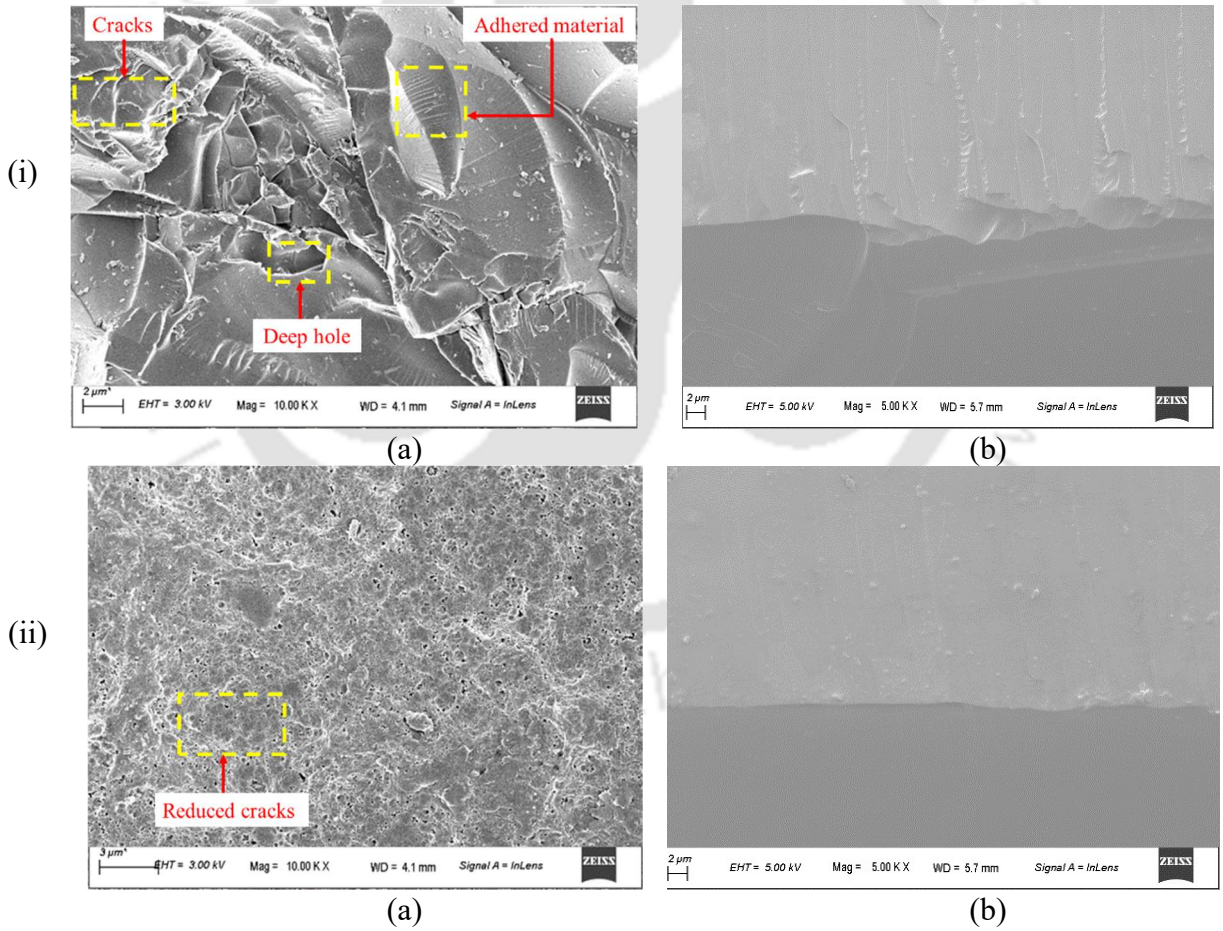

Fig. 3.8 FESEM images of SiO_2 (a) surface, and (b) cross-sectional view (i) without and (ii) after plasma processing

Further energy dispersive X−rays (EDX) are also performed on the substrate surfaces, as shown in Fig. 3.9(a−g).

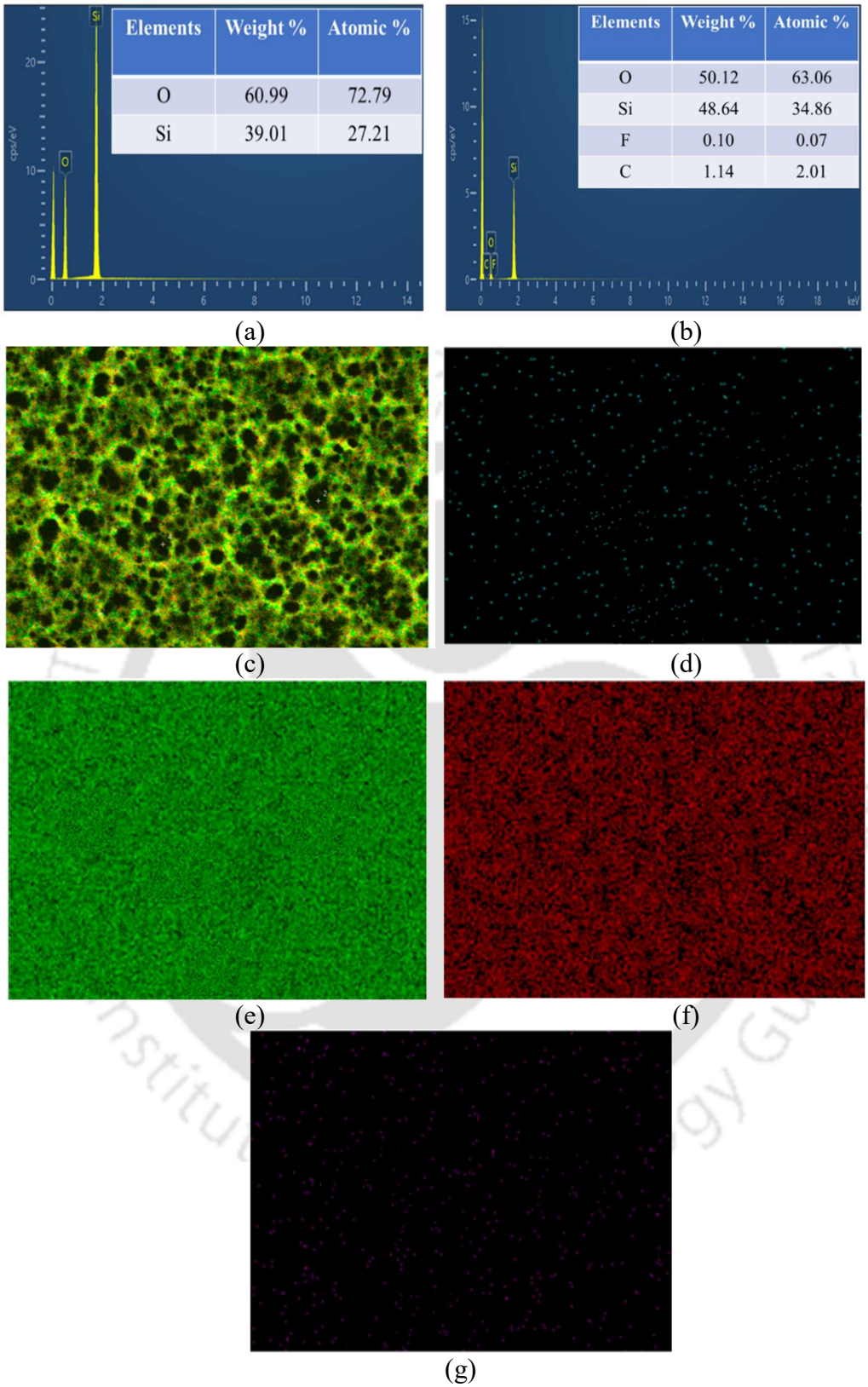

Fig. 3.9 EDX analysis of SiO_2 (a) before and (b) after plasma process; elemental mapping of plasma processed surface constituting various elements (c) combined elements F, C, O, and Si, (d) F, (e) Si, (f) O, and (g) C

Fig. 3.9(a) and (b) present the elemental peaks corresponding to elements before and after plasma processing. After MPPP, the Si, O, C, and F elements are observed on the SiO_2 substrate. The presence of the F element indicates the occurrence of plasma etching during the process. Elemental mapping is performed through EDX to verify all the constituent elements on the processed surface. The EDX area mapping results, illustrated in Fig. 3.9 confirm the uniform distribution of Si, O, F, and C elements on the fused silica substrate surface after plasma processing. It is observed that the elemental distribution of combined elements, namely F, C, O, and Si, is uniformly distributed on the surfaces, as illustrated in Fig. 3.9(c). The uniform distribution of individual elements on the plasma processed surface of F, Si, O, and C are illustrated in Fig. 3.9(d−g), respectively.

3.3.7 X-ray Photoelectron Spectroscopy Analysis

The term "binding energy" is a commonly employed concept in XPS analyses, making it essential to provide a detailed explanation of its implications [119]. XPS is a surface analysis method used to evaluate materials' elemental composition and chemical state. XPS provides information about the binding energy (BE) of photoelectrons. The BE of a photoelectron is characteristic of the element, and it comes from a chemical state. In the early stages of XPS development, a method was suggested that involves analyzing the C 1s spectra of an unintentional carbon layer, which can be found on all surfaces exposed to air [120]. Al Kα is the excitation source, the electron emission angle is 45 degrees, the analyzed area is 10 μm, and no sputter-etched prior to analyses. The base pressure is 1.6×10^{-6} pascal, and charge neutralization is used. The energy difference between the X-ray and the kinetic energy of the emitted photoelectron determines the binding energy. XPS spectra are achieved at O 1s, Si 2p, F 1s, and C 1s during the processing of fused silica. Further, curve fitting of O 1s, Si 2p, F 1s, and C 1s peaks is carried out. The XPS survey spectra of SiO_2 before and after the plasma process are shown in Fig. 3.10(a) and (b), respectively. The XPS results reveal that the additional F 1s electrons have been observed on the processed surface. This implies the reactions occurring on the substrate surface; no other impurities have been produced, a peak corresponding to carbon (C 1s) is also detected; it is attributed to contamination from the surrounding atmospheric air or may be coming from the O ring used in the lid on the top of the plasma chamber. The XPS analysis focuses on core levels, specifically Si 2p, O 1s, C 1s, and F 1s [121].

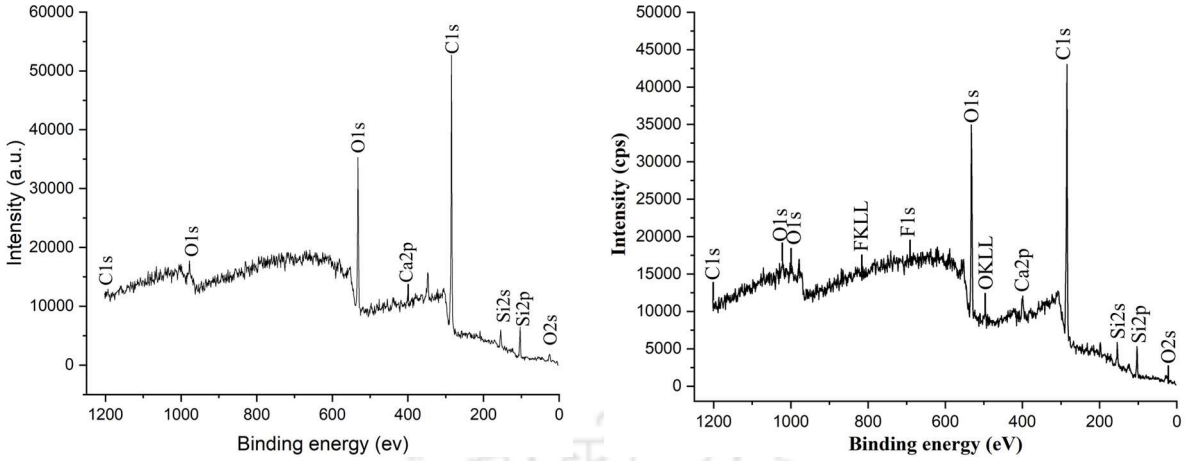

(a) (b)

Fig. 3.10 XPS survey spectra of SiO_2 (a) before and (b) after plasma processing

Fig. 3.11(a−c) reveals the presence of core levels, i.e., carbon (C1s), silicon (Si 2p), and oxygen (O 1s), on the initial and final substrate surface after plasma processing. Moreover, the additional presence of core level, i.e., fluorine (F 1s), on the processed surface after plasma processing is illustrated in Fig. 3.11(d). The best approach is to set the BE of the C 1s peak at 289.58 - Φ_{SA} eV and to align all other core levels accordingly [122]. All the high-resolution XPS spectra are referenced with charge referencing based on the sample work function determined by UPS, as shown in Fig. 3.11.

The work function of the SiO_2 sample is Φ_{SA} = 0.93 eV and 1.46 eV, before and after the plasma process, respectively. The peak position of C 1s after correction is E_B = 289.58–0.93= 288.65 eV and E_B = 289.58–1.46 = 288.12 eV [122], before and after the plasma process (as shown in Fig. 3.11(a)) for the SiO_2 sample respectively. Similarly, all other core levels have aligned accordingly. The XPS spectra of Si 2p peak are fitted (after correction) and centered at a binding energy of 102.6 eV before and 101.8 eV after the plasma process are illustrated in Fig. 3.11(b). Also, Si-containing groups are associated with two O atoms. Furthermore, the O 1s peak is observed (after correction) at a binding energy of 531.7 eV before and 531.0 eV after the plasma process, as shown in Fig. 3.11(c), which is attributed to oxygen bonded to silicon. The peak fittings indicate that the Si 2p and O 1s components are associated with O−Si−O bonds, which are characteristic of SiO_2 material composition. Fig. 3.11(d) shows the F 1s spectra centered (after correction) at 685.8 eV, signifying that F is adsorbed on the SiO_2 surface during plasma processing.

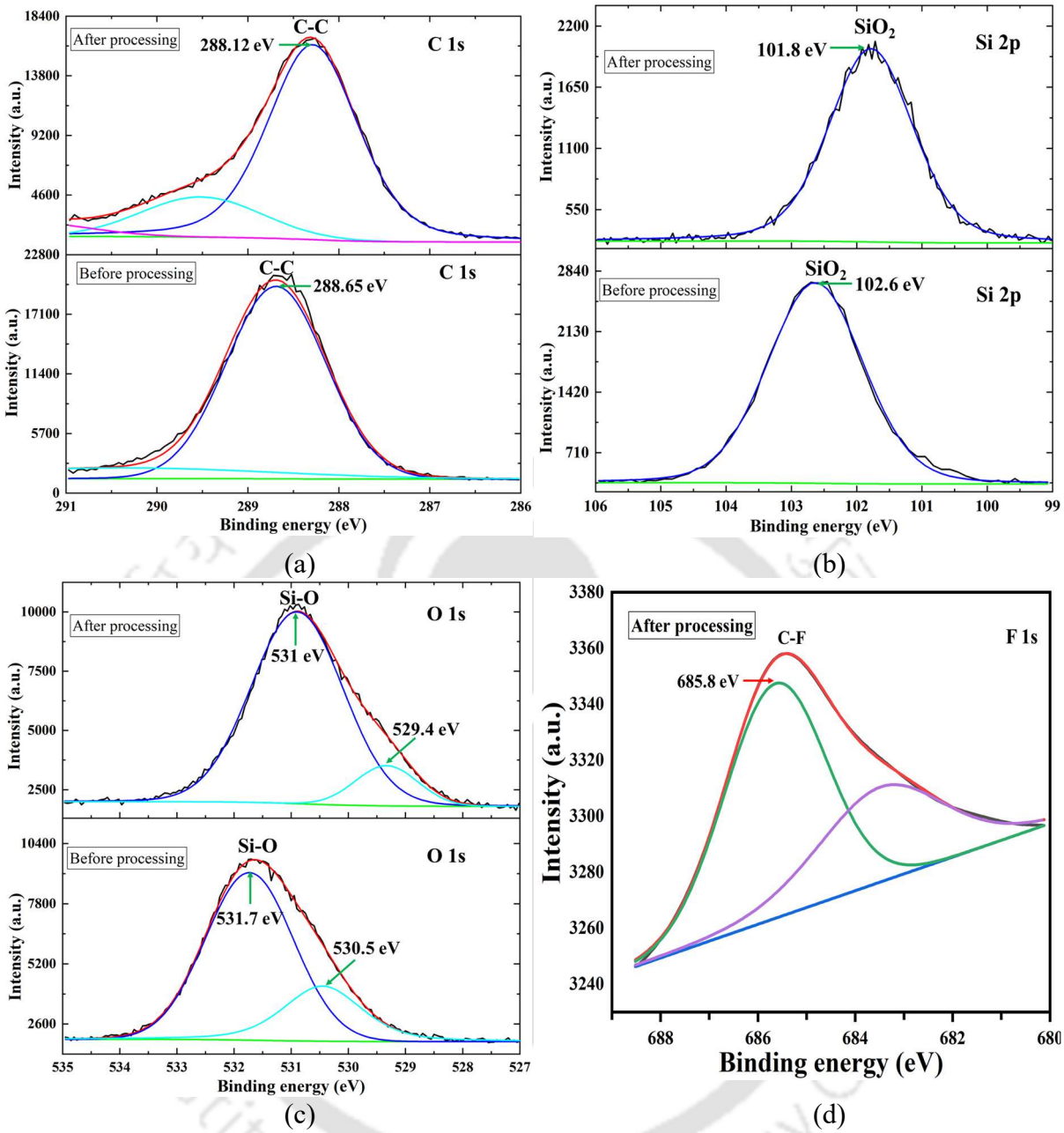

Fig. 3.11 XPS spectra of SiO_2 before and after plasma processing (a) Si 2p, (b) O 1s, (c) C 1s; (d) F 1s after plasma processing

3.4 Summary

Material removal rate and surface roughness variation at different total plasma pressures with varying substrate dimensions/lengths have been investigated and analyzed. Qualitative discharge percentages at various pressures show that the discharge intensity remains constant up to 20 mbar and then decreases. With an increase in total pressure, the intensity of F* atom consistency diminishes, especially at wavelengths of about 685.60 nm. Accordingly, MRR will be more significant with the wavelength of the F* atom at 685.60 nm. Atoms at the

wavelength of 685.60 nm demonstrate the most powerful function in finishing the fused silica materials. Material removal rate increases with increased substrate dimension/length at higher total pressure. Also, MRR decreases with increased plasma chamber pressure for smaller substrate dimensions/lengths. The highest and lowest MRR achieved at 5 mbar and 30 mbar pressure are 0.039 mm^3/min and 0.0061 mm^3/min for substrate dimensions/lengths of 45×5×2 mm^3 and 5×5×2 mm^3. The dimension of the smallest substrate (5×5×2 mm^3) shows the highest change in surface roughness because of more radicals surrounding the substrate. The microstructure and chemical composition of the elements are analyzed before and after plasma processing. The work function of the SiO_2 sample is Φ_{SA} = 0.93 eV and 1.46 eV before and after the plasma process, respectively.

Chapter 4 Statistical Design of Experiments and Optimization Process Parameters

4.1 Introduction

The medium-pressure plasma process has been proposed as a non-contact type plasma-assisted atom-by-atom material removal technique for an optical material, i.e., fused silica. These studies are focused on the variation of MRR and % ΔR_a with input process parameters. During the polishing of the fused silica substrate, the process parameters, namely radio-frequency (RF) power, pressure ratio (SF_6/O_2), machining time, and total pressure of the plasma chamber are investigated and optimized for MRR and % ΔR_a using response surface methodology. The process parameters, i.e., pressure ratio (SF_6/O_2) of 1:1 and gas composition (He: (SF_6+O_2)) of 90:10, have been kept constant during all experiments.

4.2 Experimental Design and Analytical Determination

Three different levels (–1, 0, and +1) of process parameters, such as RF power, pressure ratio (SF_6/O_2), and total pressure of the process chamber, have been chosen via a comprehensive review of the literature and by conducting preliminary tests to determine the impact of input parameters. A statistical design of experiments (DOE) is formulated using the RSM technique's central composite rotatable design (CCRD) to investigate the effect of process parameters and interactions with output responses. The process parameters and their levels are illustrated in Table 4.1.

Table 4.1 Process parameters with range and fixed parameters

		Levels		
Symbol	**Process Parameter**	-1	0	+1
A	RF Power (W)	40	50	60
B	Pressure ratio (SF_6/O_2)	2	2.5	3
C	Total pressure (mbar)	10	12.5	15
Constant parameters				
Processing time			50 min	
Gas composition (He: (SF_6+O_2))			90:10	

Table 4.2 shows the experimental runs for the experiments, which have been designed using a three-level factorial design. The experiments are repeated three times for every set of process parameters, and the average value of these three measurements is calculated to get the

responses, i.e., MRR and % ΔR_a. The material removal rate (mm^3/min) and percentage change in surface roughness (% ΔR_a) are computed using Eqs. (4.1) and (4.2), respectively.

Table 4.2 Experimental values of responses with experimental runs as per DOE

	Input parameters				**Responses**			
No. of Exp.	Power (W)	Pressure ratio (SF_6/O_2)	Total pressure (mbar)		Avg. MRR (mm^3/min)	Avg. % ΔR_a	Standard deviation (σ)	
							MRR	% ΔR_a
1	50	2.5	12.5		0.0090	11.199	0.00032	1.020
2	50	2.5	5		0.0069	13.733	0.00065	1.730
3	50	2.5	12.5		0.0074	9.086	0.00073	1.224
4	40	3	10		0.0085	12.308	0.00057	1.608
5	50	2.5	20		0.0031	-1.3271	0.00195	0.416
6	50	4	12.5		0.0139	-0.322	0.00408	0.195
7	40	3	15		0.0063	14.786	0.00244	1.510
8	60	3	15		0.0122	4.828	0.00326	1.061
9	50	2.5	12.5		0.0074	9.515	0.00163	1.428
10	40	2	15		0.0029	-4.848	0.00122	1.004
11	60	2	10		0.0074	21.362	0.00163	2.816
12	50	2.5	12.5		0.0085	11.158	0.00081	1.363
13	20	2.5	12.5		0.0052	1.765	0.00367	0.416
14	60	2	15		0.0087	14.677	0.00155	1.886
15	50	2.5	12.5		0.0078	9.167	0.00236	1.020
16	50	1	12.5		0.0059	6.835	0.00375	1.477
17	50	2.5	12.5		0.0083	8.997	0.00285	1.649
18	40	2	10		0.0075	7.141	0.00204	1.192
19	80	2.5	12.5		0.0139	10.457	0.00734	1.110
20	60	3	10		0.0104	1.242	0.00653	0.367

$$\text{MRR} = \frac{\text{Change in weight } (\Delta w)}{\text{Density}(\rho) \times \text{Machining time } (t)} \tag{4.1}$$

$$\%\ \Delta R_a = \left(\frac{\text{Final } R_a - \text{Initial } R_a}{\text{Initial } R_a}\right) \times 100 \tag{4.2}$$

Where the change in weight of the substrate (Δw) is in gram, ρ is the density of the substrate in g/mm^3, and machining time (t) is in minutes. The machining time (50 min) and gas composition (He:(SF_6+O_2) = 90:10) are kept constant for each experiment. The initial and final surface roughness values are measured using a 3D optical profilometer at different positions on the fused silica surface. The area (844.56×706.56) µm, pixel size: 0.69 µm/pixel, topography: 1224 x 1024 px, and three profiles are used to measure each sample's initial and final surface roughness values. After that, an average value of % ΔR_a is calculated. Based on

these three experimental measurements, the standard deviation ($\sigma = \sqrt{\frac{\Sigma(x_i-\mu)^2}{N}}$, x_i= observed data points, μ = mean, N = number of observations) analysis is calculated, as presented in Table 4.2.

4.3 Results and Discussion

The present section discusses the optimized MRR and percentage change in surface roughness at the optimized process parameter.

4.3.1 Statistical Analysis of Developed Model

Twenty sets of experiments (3 levels for 3 parameters) have been conducted to study the influence of RF power, pressure ratio, and total pressure of the process chamber on output responses, i.e., MRR and %ΔR_a. The data is analyzed statistically, and a quadratic model is selected for MRR and %ΔR_a based on model summary statistics, as illustrated in Table 4.3 and Table 4.4, respectively. The cubic relationship is aliased for both responses.

Table 4.3 Model fit summary for MRR

Source	Sq* p-value	LoF* p-value	Adj* R^2	Pred* R^2	Remarks
Linear	0.0001	0.0111	0.6561	0.3466	
2FI	0.1888	0.0135	0.7032	0.4552	
Quadratic	**< 0.0001**	**0.8183**	**0.9643**	**0.9331**	**Suggested**
Cubic	0.6923	0.7276	0.9570	0.7913	Aliased

*Sq– Sequential, *Adj– Adjusted, *Pred– Predicted, *LoF– Lack of Fit

Table 4.4 Model fit summary for %ΔR_a

Source	Sq* p-value	LoF* p-value	Adj* R^2	Pred* R^2	Remarks
Linear	0.1479	0.0003	0.1417	-0.1352	
2FI	< 0.0001	0.0087	0.8098	0.6618	
Quadratic	**0.0003**	**0.2376**	**0.9603**	**0.8406**	**Suggested**
Cubic	0.2455	0.2462	0.9701	-0.3056	Aliased

*Sq– Sequential, *Adj– Adjusted, *Pred– Predicted, *LoF– Lack of Fit

The statistical parameters assessment of the empirical models is accomplished using analysis of variance (ANOVA). The outcomes from the ANOVA test for MRR and % ΔR_a are illustrated in Table 4.5 and Table 4.6, respectively. As per Table 4.5 and Table 4.6, the models are statistically significant as the associated p-value < 0.05 (α = 0.05 for a 95% confidence level). The analysis also tests the significance of the achieved models, lack-of-fit,

and coefficient of determination (R^2). The F-value from the test is considered to determine the model's significance. A higher F-value has more significance in the model. The p-value describes the model's significance at a 95% confidence level. The lack-of-fit term has been obtained as insignificant, which is required for a model. The R^2 value is greater than 97%, demonstrating the suitability of the model and the higher correlation between the input process parameters and the responses. Some interaction terms are insignificant.

Table 4.5 ANOVA for MRR

Source	SS*	DF*	MS*	F-value	P-value
Model	0.0002	9	0.0000	58.07	< 0.0001*
A-RF Power	0.0001	1	0.0001	198.62	< 0.0001*
B-Pressure ratio	0.0000	1	0.0000	150.97	< 0.0001*
C-Total pressure	8.850×10^{-6}	1	8.850×10^{-6}	28.79	0.0003*
AB	5.450×10^{-7}	1	5.450×10^{-7}	1.77	0.2126**
AC	0.0000	1	0.0000	40.92	< 0.0001*
BC	1.033×10^{-6}	1	1.033×10^{-6}	3.36	0.0966**
A^2	3.668×10^{-6}	1	3.668×10^{-6}	11.93	0.0062*
B^2	5.331×10^{-6}	1	5.331×10^{-6}	17.34	0.0019*
C^2	0.0000	1	0.0000	46.07	< 0.0001*
Lack of Fit	9.097×10^{-7}	5	1.819×10^{-7}	0.4204	0.8183**

*SS– Sum of Squares, *DF– Degree of freedom, R^2– Coefficient of determination = 0.9812, *MS– Mean square, *Significant (p-value < 0.05), ** Not Significant (p-value > 0.05)

Table 4.6 ANOVA for $\%\Delta R_a$

Source	SS*	DF*	MS*	F-value	P-value
Model	754.46	9	83.83	52.12	< 0.0001*
A-Power	57.90	1	57.90	36.00	0.0001*
B-Pressure ratio	27.28	1	27.28	16.96	0.0021*
C-Total pressure	128.45	1	128.45	79.86	< 0.0001*
AB	374.96	1	374.96	233.12	< 0.0001*
AC	5.14	1	5.14	3.19	0.1042**
BC	76.50	1	76.50	47.56	< 0.0001*
A^2	23.38	1	23.38	14.53	0.0034*
B^2	70.04	1	70.04	43.54	< 0.0001*
C^2	22.29	1	22.29	13.86	0.0040*
Lack of Fit	10.67	5	2.13	1.97	0.2376**

*SS– Sum of Squares, *DF– Degree of freedom, *MS– Mean square, R^2–Coefficient of determination = 0.9791, *Significant (p-value < 0.05), ** Not Significant (p-value > 0.05)

Table 4.5 and Table 4.6, provide the developed statistical model, including the significant parameters and model adequacy. ANOVA measures the % contribution of every independent variable. It represents the relative effect that a process parameter has on the response. The highest contribution towards the MRR (Table 4.5) can be seen as RF power (A), followed by

pressure ratio (SF_6/O_2). The contributions of these two parameters are 39.8% and 30.1%, respectively. Similarly, the highest contribution towards the $\%\Delta R_a$ (Table 4.6) can be seen as the interaction of RF power and pressure ratio (AB), followed by total pressure (C). The contributions of these two parameters are 48.5% and 17.9%, respectively.

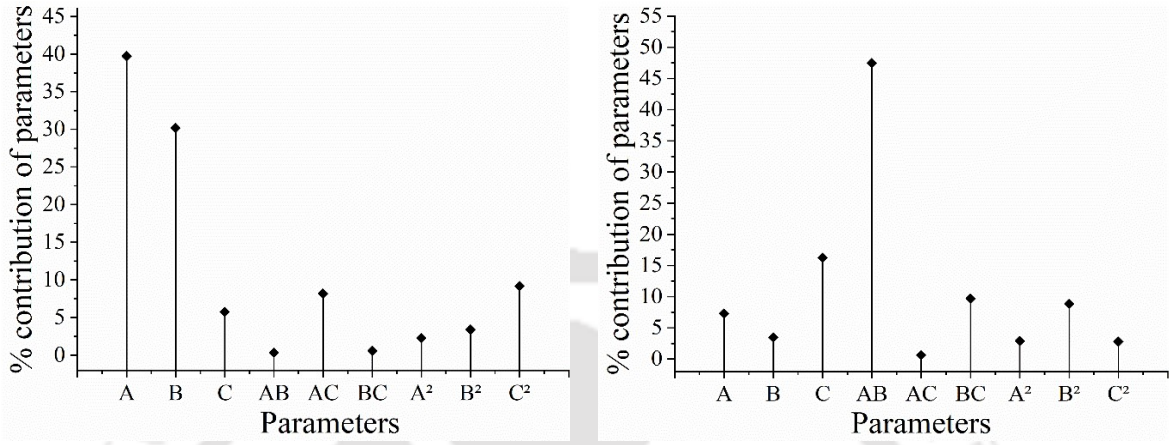

Fig. 4.1 Percentage contribution of process parameters on (a) MRR and (b) % ΔR_a

Furthermore, the percentage of significance for individual parameters and their combined effects are calculated from the F-test values for both responses, illustrated in Fig. 4.1(a) and (b), respectively. The percentage contribution of parameters is evaluated using the F/ΣF values for each factor [123]. The parameters such as RF power (A) and combined effect of RF power and pressure ratio (AB) have the highest contribution to MRR and $\%\Delta R_a$, respectively. Regression analysis is carried out to establish a relationship between process parameters and the responses. ANOVA results from Table 4.5 and Table 4.6 revealed that the empirical models are significant. The regression equations for MRR and % ΔR_a have been derived using the quadratic approximation as per the model adequacy test and are presented in Eqs. (4.1) and (4.2), respectively.

$$\begin{aligned}\text{MRR} = {} & 0.00800621 + 0.00153237\,\text{A} + 0.001336\,\text{B} - 0.000583421\,\text{C} \\ & + 0.000261012\,\text{AB} + 0.00125391\,\text{AC} + 0.000359399\,\text{BC} \\ & + 0.000171902\,\text{A}^2 + 0.000207223\,\text{B}^2 - 0.000337736\,\text{C}^2\end{aligned} \tag{4.1}$$

$$\begin{aligned}\%\Delta R_a = {} & 10.1793 + 1.49235\,\text{A} - 1.02441\,\text{B} - 2.22272\,\text{C} - 6.84621\,\text{AB} + \\ & 0.801429\,\text{AC} + 3.0923\,\text{BC} - 0.433938\,\text{A}^2 - 0.751118\,\text{B}^2 - 0.423729\,\text{C}^2\end{aligned} \tag{4.2}$$

Where A, B, and C represent RF power, pressure ratio, and total pressure, respectively. The coefficient of determination (R^2) values indicate the model accuracy, 98.12% and 97.91% for MRR and %ΔR_a, respectively. The experiment and prediction outcomes for MRR and %ΔR_a are very close, as illustrated in Fig. 4.2(a) and (b), respectively. Prediction outcomes are based on the range and level defined in Table 4.1.

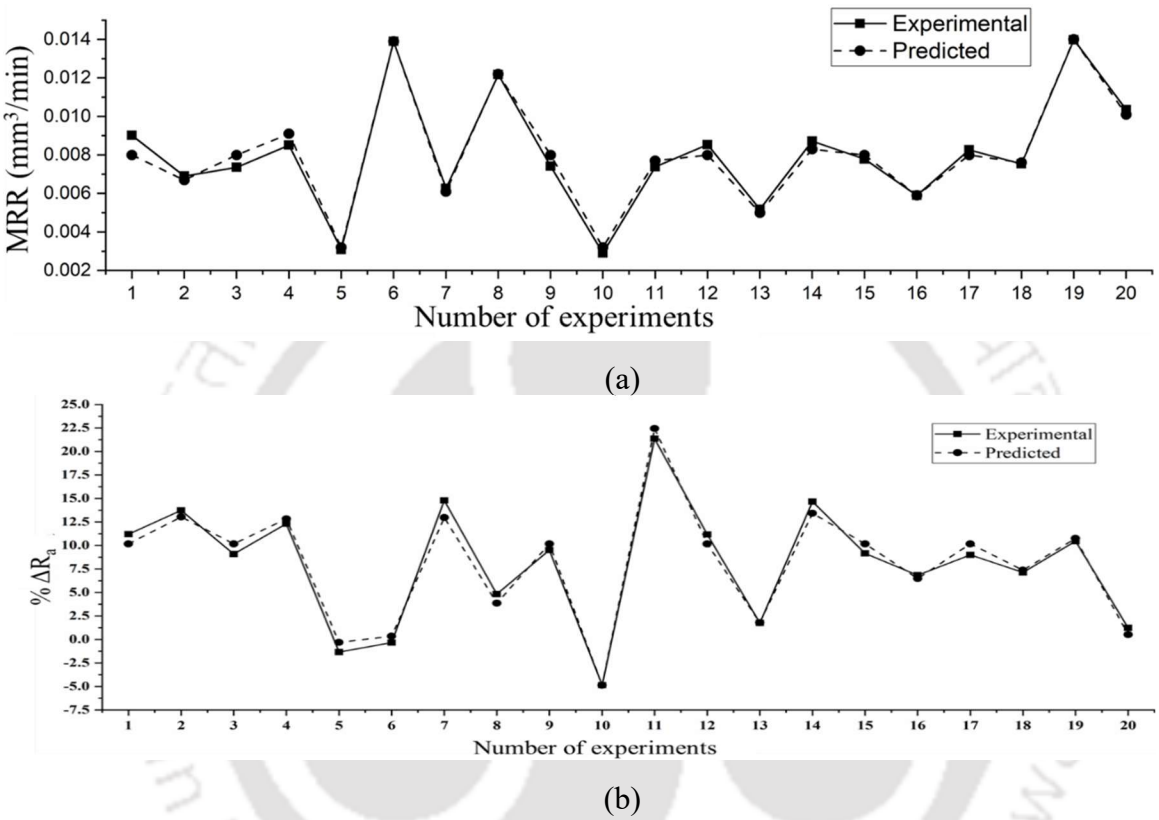

Fig. 4.2 Comparison between experimental and predicted values of (a) MRR and (b) % ΔR_a

4.3.2 Parametric Analysis

This section explains the individual and combined effect of variables such as RF power, pressure ratio, total pressure on MRR, and % ΔR_a using 2D and 3D plots.

4.3.2.1 Individual Effect of Process Parameters

It is required to analyze the effect of each parameter simultaneously on outcomes and obtain the best possible solution to achieve the desired output responses. The plasma intensity increases with RF power, which can be thought of as an increase in the electron density of the discharge. Changes in plasma discharge mode affect plasma temperature, resulting in visible changes in plasma dynamics [26]. Yao et al.[15] also reported that the depth and width are

increased using an atmospheric pressure plasma jet (APPJ) machining with the increased RF power. When the power exceeds 360 W, abrupt changes in depth are obtained, caused by increased plasma temperature. Thus, RF power has a significant impact on the removal function. Fig. 4.3(a) and (d) show the variation of MRR and % ΔR_a with the increased RF power.

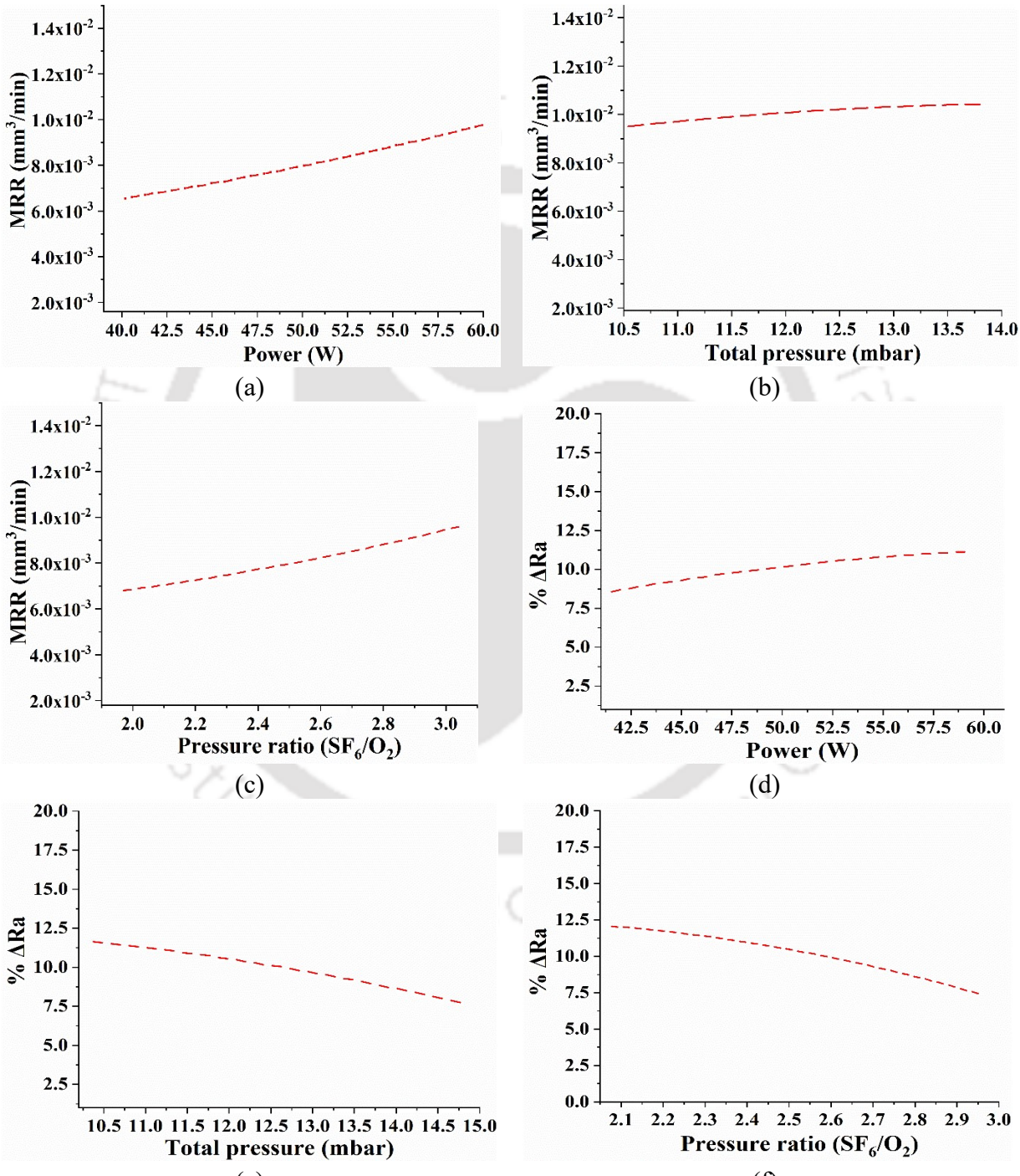

Fig. 4.3 MRR and % ΔR_a variation with power (a, d), total pressure of the chamber (b, e), and pressure ratio of SF_6/O_2 (c, f), respectively

The increasing trend of MRR has been found with the variation of pressure ratio between 2 to 3, as shown in Fig. 4.3(c). This could be because more atoms are produced with the increase in SF_6 gas, which leads to more materials being removed from the surface. The occurrence of oxygen will endorse the separation of SF_6 into SF_5 and F*. Moreover, adding the process oxygen with SF_6 gas can help increment the reactive radicals' intensity and further higher MRR. Fig. 4.3(f) shows the variation of $\%\Delta R_a$ where its value decreases with increased SF_6/O_2 pressure ratio. It occurs due to chemical machining, which increases the speed of chemical reactions at a higher pressure ratio. As the pressure ratio increases, the presence of O will promote the dissociation of SF_6 into SF_5 and F*, and O will associate with SF_5 and prevent the recombination of F* and SF_5. Hence, it is observed that the roughness variation decreases with the increase in pressure ratio. Because of the rise of the SF_6 and O_2 flow rate, the generated O* reacts with the fused silica surface to form SiO=SiO aggregates, which will reduce the etching rate of the silica. So, surface roughness variation decreases with the increase of the pressure ratio. Fig. 4.3(b) and (e) show that MRR is slightly raised and $\% \Delta R_a$ is decreased with the total pressure. The plasma intensity increases in bulk can be expected with increasing the total pressure at constant power. It may be due to the electron's increased mean free path, as there is more chance to gain enough energy between collisions to perform ionization and excitation.

4.3.2.2 Combined Effect of Process Parameters

Statistical analysis (shown in Table 4.5 and Table 4.6) reveals that the input variables have a cumulative effect on the output responses. 3D response surface plots are required to understand combined parametric effects on output responses. The interaction of the pressure ratio and RF power, the total pressure of the plasma chamber and RF power, total pressure and pressure ratio, and their consequences over the MRR and $\% \Delta R_a$ are illustrated in Fig. 4.4(a-c) and (d-f)), respectively. From Fig. 4.4(a-b), it is realized that with increased pressure ratio and RF power, MRR increases; MRR also increases with decreased total pressure and increased RF power. MRR increases with a lower value of total pressure and a higher value of pressure ratio, as illustrated in Fig. 4.4(c). The ions/radicals density increases with the increased RF power, which leads to higher MRR. As stated earlier, a higher concentration of ions/radicals causes more etching. The particle collisions are strong enough to etch more material whenever the RF power increases. Even at reduced RF power, effective collisions become lower due to lesser particle energy, leading to smaller MRR.

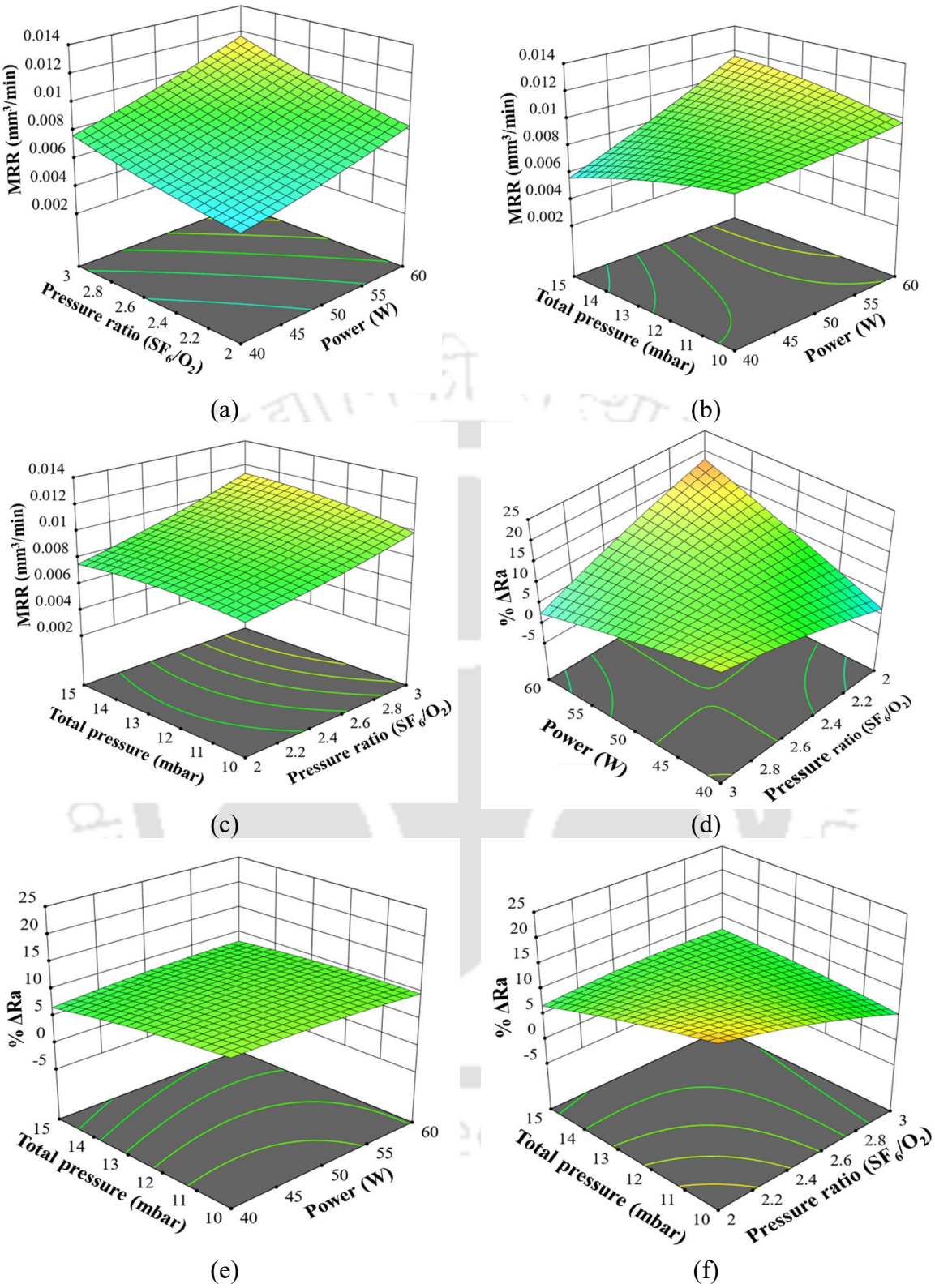

Fig. 4.4 Combined effect of power and pressure ratio (a, d), power and total pressure (b, e), and pressure ratio and total pressure (c, f) on MRR and % ΔR_a, respectively

The variation of % ΔR_a with RF power, pressure ratio, and the total pressure is emphasized using 3D plots, as shown in Fig. 4.4(d-f). At higher RF power and lower pressure ratio, %

ΔR_a becomes maximum (Fig. 4.4(d)). The combined RF power and total pressure effect on % ΔR_a are insignificant, as shown in Fig. 4.4(e). At lower total pressure and pressure ratio, the % ΔR_a is maximum (Fig. 4.4(f)) due to the higher energy of radicals and ions generated inside the plasma chamber.

A scale-free value termed desirability is created from an estimated response using the desirability function technique [124,125]. Derringer and Suich [124] proposed a particular function for the transformation of the responses (X_i) to the desirability $d_i(X_i)$. As a result, two transformations are suggested, as illustrated in Eq. (4.3).

$$d_i(X_i) = \begin{cases} 0, & X_i < l_i \\ \left(\dfrac{X_i - l_i}{t_i - l_i}\right)^s & l_i \leq X_i \leq t_i \\ \left(\dfrac{X_i - u_i}{t_i - u_i}\right)^t & t_i \leq X_i \leq u_i \\ 0, & X_i > u_i \end{cases} \tag{4.3}$$

The one-sided transformation is utilized to minimize or maximize X_i; the two-sided transformation (i.e., Eq. (4.3)) is used to acquire the objective value t_i for X_i, where u_i and l_i are the upper and lower limits of the responses. The superscripts s and t in Eq. (4.3) correspond to the weighted factors. The term s and t are the parameters that govern the shape of $d_i(X_i)$. For $s = t = 1$, the desirability function increases linearly to t_i. The overall desirability function Y in Eq. (4.4) is defined as the geometric mean of the specific desirability functions of individual responses, i.e., $d_i(X_i)$, where n is the number of responses. The optimal solutions are obtained by maximizing Y.

$$Y = \left(\prod_{i=1}^{n} d_i(X_i)\right)^{1/n} \tag{4.4}$$

Multi-response optimization using the RSM technique is used in the current study to find the optimal values of the process parameters. Here, desirability is used as a measure to optimize the responses (MRR and % ΔR_a) in the medium-pressure plasma process. During optimization, the main objective is maximizing MRR while minimizing %ΔR_a. The input variables are kept "in range" during optimization, as presented in Table 4.7. Results and plots obtained using the optimization study are displayed in Fig. 4.5. According to Fig. 4.5, it can be observed that at 60 W RF power, pressure ratio of 3, and total pressure of 14.3 mbar, the

optimized MRR and %ΔR_a values are 0.012 mm^3/min and 3.59, respectively. The maximum desirability value is 0.7490 at optimal parametric conditions.

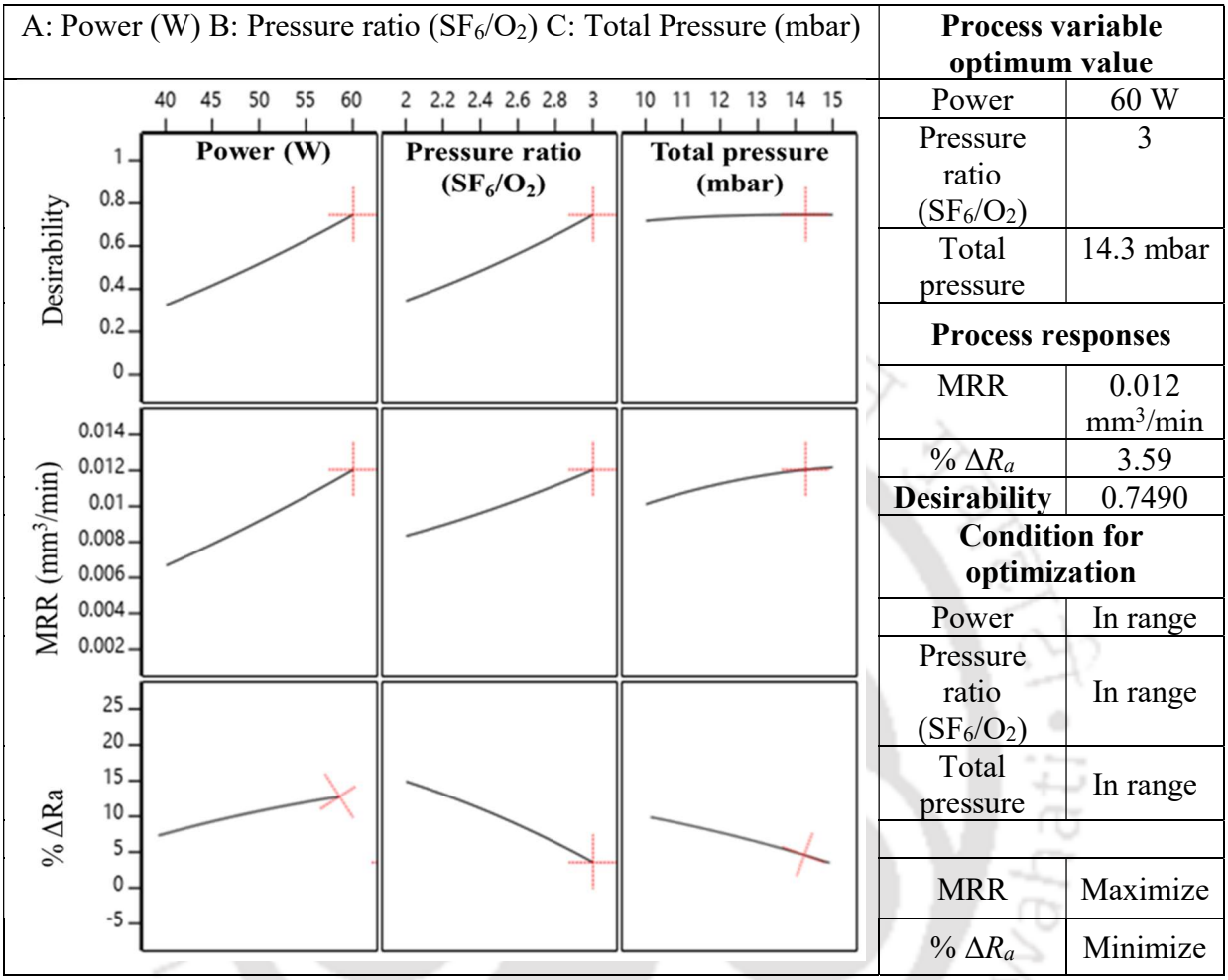

Process variable optimum value	
Power	60 W
Pressure ratio (SF_6/O_2)	3
Total pressure	14.3 mbar
Process responses	
MRR	0.012 mm^3/min
% ΔR_a	3.59
Desirability	0.7490
Condition for optimization	
Power	In range
Pressure ratio (SF_6/O_2)	In range
Total pressure	In range
MRR	Maximize
% ΔR_a	Minimize

Fig. 4.5 Optimization plots for MRR and % ΔR_a

Table 4.7 Range of process parameters for MRR and % ΔR_a

		Range	
Input Process parameters	Goal	Lower	Upper
A: RF Power (W)	in range	40 W	60 W
B: Pressure ratio (SF_6/O_2)	in range	2	3
C: Total pressure (mbar)	in range	10 mbar	15 mbar
Output parameters	**Goal**	**Weightage**	
MRR	maximize	1	
% ΔR_a	minimize	1	

A confirmatory test is carried out after determining input parameters for optimum responses. While performing the experiments, machining time and gas composition are set to a constant value of 50 min and 90:10, respectively. The experiments are conducted three times at optimum machining conditions, and the mean value of the responses is obtained, as

mentioned in Table 4.8. Based on these three measurements, the standard deviation of MRR and %ΔR_a are calculated as 0.0073 and 0.8328, respectively, as shown in Table 4.8. At the optimal parametric condition, the average MRR and %ΔR_a values are 0.0113 mm^3/min and 3.48, respectively. Table 4.8 represents the output responses with standard deviation and % error. A maximum error of 5.83% and 3.06% are observed for MRR and %ΔR_a between experimental and regression results, which are within the feasible range that proves the RSM model's validity.

Table 4.8 Experimental validation of RSM model at optimized parameter values

Process parameters		**Predicted values**		**Experimental values**		**% Error**		**Standard deviation (σ)**	
Input parameters	values	MRR (mm^3/min)	% ΔR_a	Avg. MRR (mm^3/min)	Avg. % ΔR_a	MRR	% ΔR_a	MRR	% ΔR_a
Power (W)	60								
Pressure ratio	3	0.012	3.59	0.0113	3.48	5.83	3.06	0.0073	0.8328
Total pressure (mbar)	14.3								

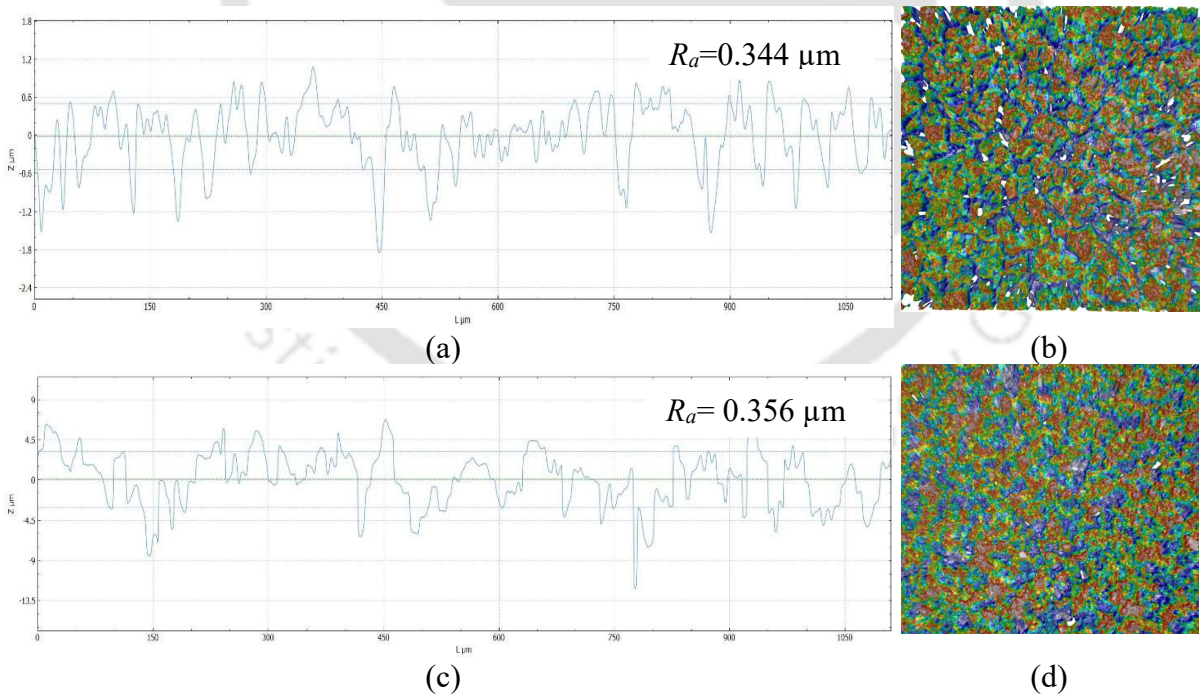

Fig. 4.6 1D surface roughness profiles (a) before and (c) after plasma processing; 2D surface roughness profiles (b) before and (d) after plasma processing

The surface roughness profiles of the substrate are measured using a 3D optical profiler before and after plasma processing at a constant processing time of 50 minutes. Fig. 4.6(a-d)

represents the surface roughness before and after post-processing using a medium-pressure plasma process under optimum conditions, i.e., RF power of 60 W, pressure ratio (SF_6/O_2) of 3, and total pressure of 14.3 mbar. The processed substrate is slightly degraded from its initial surface roughness (R_a) value of 0.344 µm to the final R_a value of 0.356 µm without any etched pits. During plasma polishing, although surface roughness increases, subsurface defects diminish. The rate of surface roughness increases with increased MRR. Hence, the plasma polishing process aims to achieve the optimum material removal rate.

Plasma polishing is a surface treatment process used to improve the quality and finish of a material's surface. During plasma polishing, machining time is an essential factor for several reasons:

- **Surface finish**: The machining time directly affects the surface finish of the material. Longer machining time often results in smoother surfaces as the plasma process has more time to remove imperfections and irregularities. Achieving the desired surface finish is crucial in applications where aesthetics, friction, or other surface properties are critical.
- **Material removal rate**: The machining time is closely related to the material removal rate, which is the amount of material removed per unit of time. Controlling the machining time allows for precise control over the amount of material being removed during plasma polishing.
- **Efficiency and cost**: Efficient use of machining time is essential for productivity and cost-effectiveness. Optimizing the process to achieve the desired surface finish in the shortest possible time helps to reduce production costs and improves overall efficiency.

In summary, machining time is crucial in plasma polishing to control the surface finish, material removal rate, uniformity, and overall process efficiency. It allows for the customization of the treatment to meet specific requirements for different materials and applications. Further, the present investigation considered the main input parameters, i.e., RF power, total pressure, and machining time, based on the previous optimization analysis.

4.4 Experimental Design

The process parameters, for instance, RF power (A), the total pressure of the process chamber (B), machining time (C), and their levels, have been chosen via a comprehensive literature review and by conducting preliminary tests to determine the impact of input parameters. A design of experiments (DOE) scheme has been formulated using the RSM technique's central composite design (CCD) to investigate process parameters' effects and

interactions with output responses. Table 4.9 displays the process parameters and their levels. Table 4.10 shows the experimental runs for the experiments, which have been designed using a three-level factorial design. Each experiment is repeated three times, and the average value is considered for analysis. The pressure ratio (SF_6/O_2) of 1:1 and gas composition (He:(SF_6+O_2)) of 90:10 have been kept constant during all experiments.

Table 4.9 Coded levels and their actual values of process parameters

		Level		
Process variable	**Symbol codes**	**–1**	**0**	**+1**
RF Power (W)	A	40	60	80
Total pressure (mbar)	B	11.6	14.95	18.3
Machining time (mins)	C	60	67.5	75

Table 4.10 3-level factorial design of experiments and responses

	Process parameters			Responses	
Exp. No.	**RF power (W)**	**Total pressure (mbar)**	**Machining time (min)**	**MRR (mm^3/min)**	**% ΔR_a**
1	40	15	67.5	0.0080	0.98
2	60	18	60	0.0079	-7.50
3	70	15	67.5	0.0200	7.39
4	60	18	75	0.0110	8.85
5	60	11.5	60	0.0218	10.30
6	80	18	60	0.0165	10.79
7	100	15	67.5	0.0175	-1.61
8	70	15	67.5	0.0170	9.94
9	70	25	67.5	0.0085	-0.10
10	70	15	90	0.0200	35.17
11	80	18	75	0.0144	14.40
12	70	15	67.5	0.0174	7.48
13	70	15	67.5	0.0170	9.21
14	70	5	67.5	0.0497	6.90
15	70	15	67.5	0.0185	7.24
16	70	15	45	0.0141	-1.52
17	80	11.5	75	0.0245	3.14
18	70	15	67.5	0.0206	10.44
19	80	11.5	60	0.0315	1.04
20	60	11.5	75	0.0300	23.10

4.5 ANOVA Study

The present section discusses the optimized MRR and percentage change in surface roughness at the optimized process parameter.

4.5.1 Model Fit Summary

Twenty sets of experiments (3 levels and 3 parameters) have been performed to study the effect of RF power, total pressure of the process chamber, and processing time on the outcomes, i.e., MRR and % ΔR_a values. The experiments are performed to choose an acceptable model that fits the outcomes, i.e., MRR and % ΔR_a, as illustrated in Table 4.11. The "Sequential model sum of squares" test and "Model summary statistics" test depict that the quadratic equation is adequate for MRR and % ΔR_a. The data is analyzed statistically, and "Model summary statistics" suggested a quadratic model for both MRR and % ΔR_a, as illustrated in Table 4.11. The cubic connection is aliased for both responses.

Table 4.11 Fit summary for MRR and %ΔR_a

Source	MRR Seq. p-value	% ΔR_a Seq. p-value	Remarks
Linear	< 0.0001	0.0071	
Two Factor Interaction	0.5167	0.0158	
Quadratic	**< 0.0001**	**< 0.0001**	**Suggested**
Cubic	0.3312	0.2731	Aliased

The model would be improved by including squared terms in addition to linear, two-factor interactions, and mean. The value of R^2 is 98.23, and the adjusted R^2 is 96.63 for MRR, as demonstrated in Table 4.12. Moreover, the R^2 and adjusted R^2 values are 98.29 and 96.75, respectively, for % ΔR_a, as illustrated in Table 4.13. Fig. 4.7(a) and (b) depict the experimental data for MRR and % ΔR_a that are fitted to the predicted investigation.

Table 4.12 ANOVA for MRR

S*	SOS*	df	MS*	F-value	p-value	Remarks
Model	0.0017	9	0.0002	61.54	< 0.0001	ST
A-RF Power	0.0001	1	0.0001	25.14	0.0005	ST
B-Total Pr	0.0013	1	0.0013	408.90	< 0.0001	ST
C-Machining time	0.0000	1	0.0000	4.91	0.0510	ST
AB	7.074×10^{-6}	1	7.074×10^{-6}	2.29	0.1614	
AC	0.0001	1	0.0001	16.93	0.0021	ST
BC	2.222×10^{-9}	1	2.222×10^{-9}	0.0007	0.9791	
A^2	0.0001	1	0.0001	16.48	0.0023	ST
B^2	0.0002	1	0.0002	55.83	< 0.0001	ST
C^2	3.202×10^{-6}	1	3.202×10^{-6}	1.04	0.3329	
LoF	0.0001	5	3.722×10^{-6}	1.51	0.3312	Not ST

MS*– Mean square, S*– Source, SOS* – Sum of squares, ST*– significant, R^2=0.9823, Adjusted R^2=0.9663, Predicted R^2=0.9105, Adeq precision=35.0993, LoF– Lack of Fit

Table 4.13 ANOVA for % ΔR_a

S*	SOS*	df	MS*	F-value	p-value	Remarks
Model	0.1613	9	0.0179	63.89	< 0.0001	ST
A-RF power	0.0005	1	0.0005	1.85	0.2033	
B-Total pressure	0.0040	1	0.0040	14.15	0.0037	ST
C-Machining time	0.0808	1	0.0808	288.23	< 0.0001	ST
AB	0.0350	1	0.0350	124.95	< 0.0001	ST
AC	0.0068	1	0.0068	24.28	0.0006	ST
BC	0.0004	1	0.0004	1.55	0.2412	
A^2	0.0122	1	0.0122	43.40	< 0.0001	ST
B^2	0.0041	1	0.0041	14.71	0.0033	ST
C^2	0.0104	1	0.0104	37.04	0.0001	ST
LoF	0.0018	5	0.0004	1.77	0.2731	Not ST

MS*– Mean square, S* – Source, SOS*– Sum of squares, ST*– significant, R^2 = 0.98, Adjusted R^2= 0.96, Predicted R^2=0.84, Adeq precision=35.13, LoF– Lack of Fit

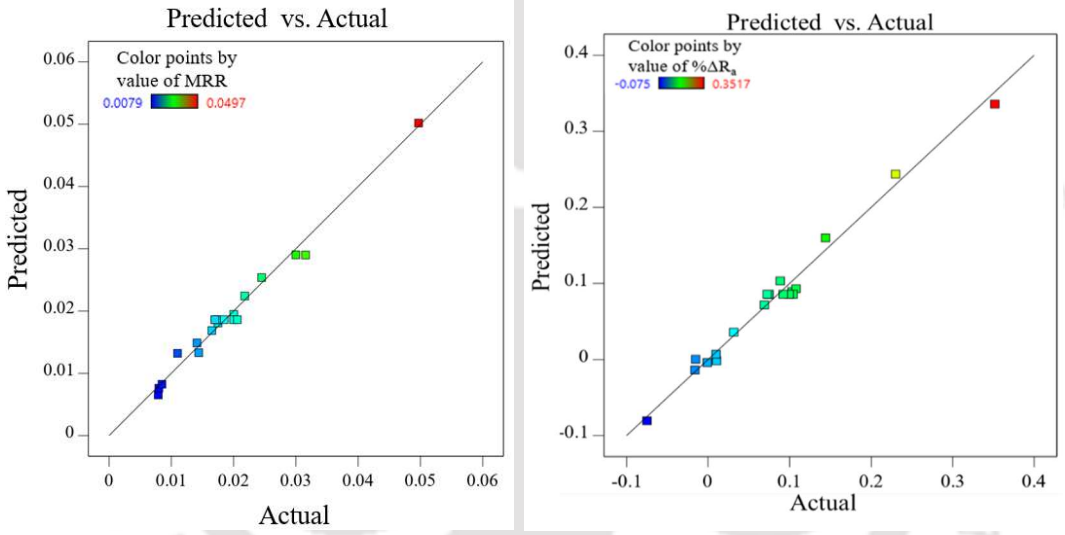

(a) (b)

Fig. 4.7 RSM design for actual Vs. predicted values of (a) MRR and (b) % ΔR_a

Fig. 4.8(a) and (b) depict the residual probability of MRR and % ΔR_a, respectively. The residual plot describes that all the experimental data are usually near a linear fashion and confirms strong affinity for both experimental and predicted values, as MRR and % ΔR_a models indicate a satisfactory fit. Furthermore, the contribution percentage for individual parameters and their combined effects are calculated from the F-test value for both responses, i.e., MRR and % ΔR_a, demonstrated in Fig. 4.9(a) and (b), respectively. The percentage contribution of parameters is evaluated using the F/ΣF value for each significant factor [126]. The parameters, such as the total pressure of plasma chamber (B) and machining time (C), have the highest contribution to MRR and % ΔR_a, respectively.

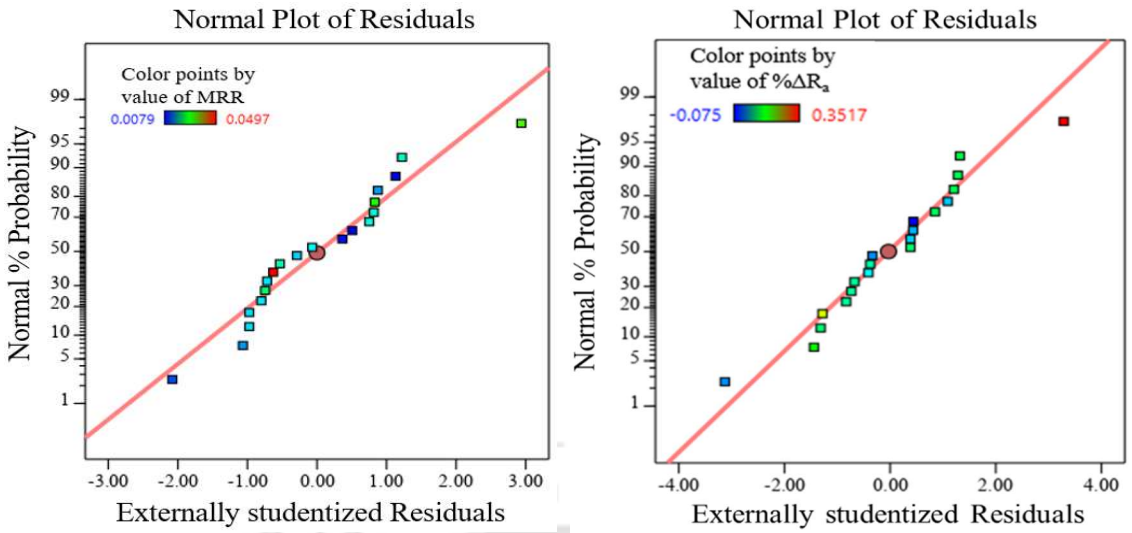

(a) (b)

Fig. 4.8 Residual normal probability plots for (a) MRR and (b) % ΔR_a

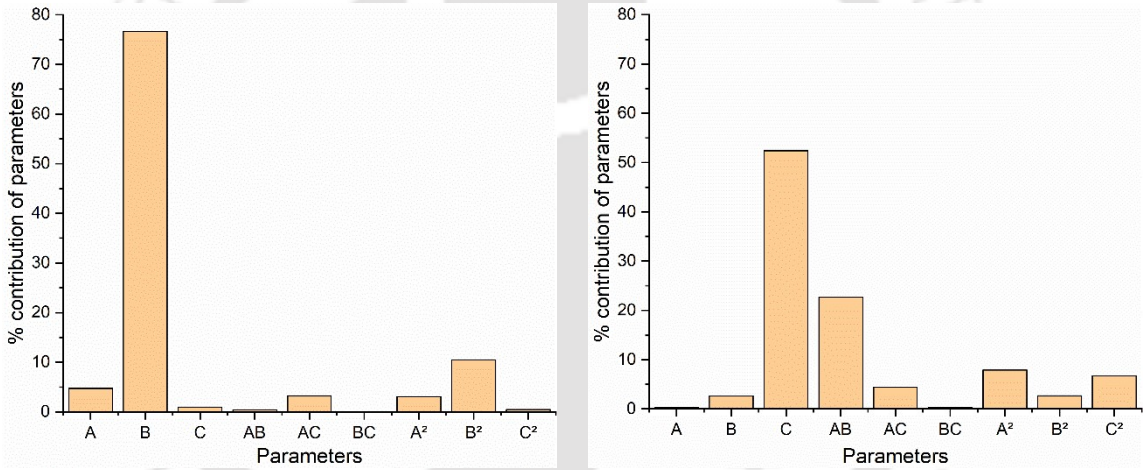

(a) (b)

Fig. 4.9 Percentage contribution of process parameters on (a) MRR and (b) % ΔR_a

4.5.2 Regression Models

The quadratic models are developed for the responses, viz., MRR and % ΔR_a. Equations (4.5) and (4.6) show the regression equations obtained from the quadratic model for MRR and % ΔR_a, respectively.

$$MRR = -0.1198 + 0.0029 \times A - 0.0073 \times B + 0.0029 \times C + 0.00003 \times AB - 0.000034 \times AC + 6.8226 \times 10^{-7} \times BC - 6.4073 \times 10^{-6} \times A^2 + 0.00011 \times B^2 - 2.8544 \times 10^{-6} \times C^2 \quad (4.5)$$

$$\%\Delta Ra = 0.4047 + 0.00928 \times A - 0.1509 \times B + 0.0082 \times C + 0.00203 \times AB - 0.00039 \times AC + 0.00030 \times BC - 0.000099 \times A^2 - 0.00052 \times B^2 + 0.00016 \times C^2 \quad (4.6)$$

Where A, B, and C represent RF power, total pressure of the plasma chamber, and machining time, respectively. The regression analysis's coefficient of determination (R^2) value indicates the model accuracy of 98.23% and 98.29% for MRR and $\%\Delta R_a$, respectively. The experiment and predicted outcomes for MRR and $\% \Delta R_a$ are very close, as illustrated in Fig. 4.10(a) and (b), respectively.

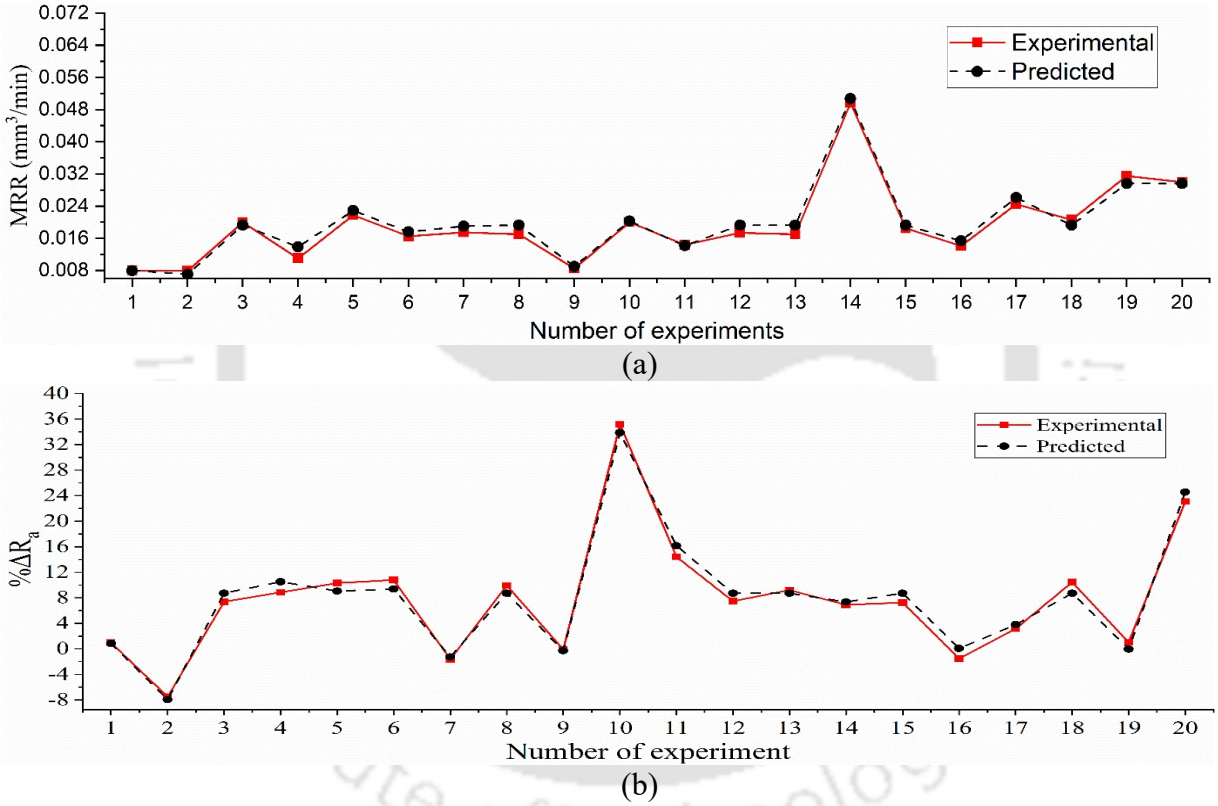

Fig. 4.10 Comparison of experimental and predicted values for (a) MRR and (b) $\% \Delta R_a$

4.5.3 Parametric Effect Analysis

This section explains the individual and combined effects of process input variables, for instance, RF power, total pressure of the plasma chamber, and machining time on MRR and $\% \Delta R_a$, using 2D plot and 3D plot groups.

4.5.3.1 Effect of input process parameters on MRR

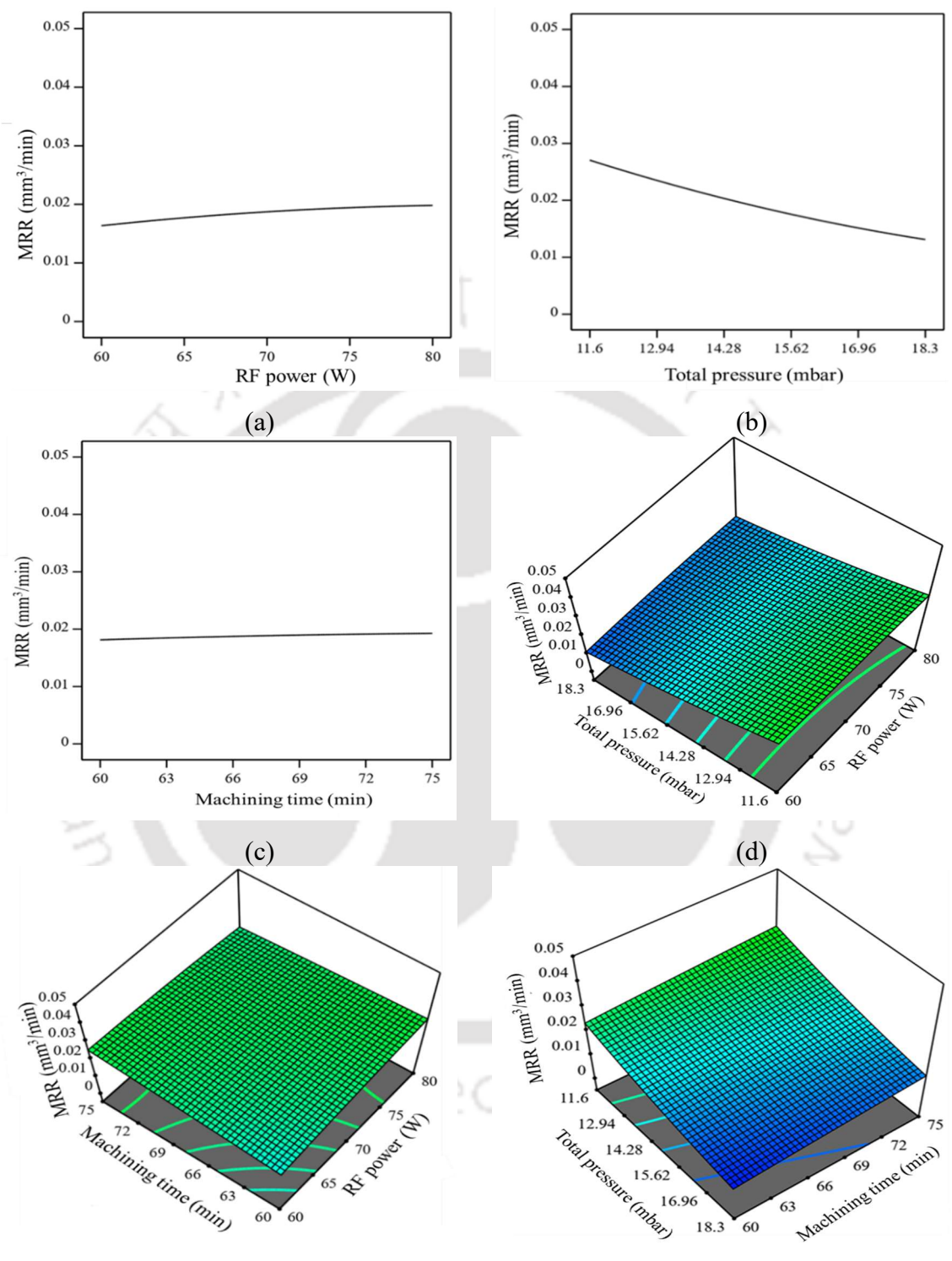

Fig. 4.11 2D plots for MRR with (a) RF power, (b) total pressure, and (c) machining time; 3D surface plots for MRR with (d) total pressure and RF power, (e) machining time and RF power, and (f) total pressure and machining time

Spatial distribution and discharge intensity of radicals in the plasma chamber directly affect the material removal rate and % ΔR_a [127]. The input RF power increases along with the plasma intensity, which can be interpreted as an increase in the discharge's electron density. Plasma temperature is affected by the changes in plasma discharge mode, resulting in visible changes in plasma dynamics [22]. Wang et al. [107] reported that higher relative etch rates are observed with increased RF power at a constant flow rate. Fig. 4.11(a) depicts that MRR increases with increased RF power caused by increased discharge intensity during processing. Fig. 4.11(b) shows that MRR decreases with an increase in the total pressure of the plasma chamber. The physics behind that is the mean free path of species, i.e., at higher pressure, the collision between ions decreases, leading to insufficient energy between two successive collisions. Fig. 4.11(c) shows that the MRR slightly increases with machining time because the species increases inside the chamber, which increases the generation of ions and radicals. Fig. 4.11(d) shows the combined effect of total pressure and RF power with MRR. It is observed that with increased RF power and total pressure, MRR increases and decreases, respectively. Fig. 4.11(e) depicts that MRR increases with the increased combined effect of RF power and machining time. Fig. 4.11(f) shows the increase in MRR with decreased total pressure and increased machining time. Fig. 4.11 shows the variation of MRR with individual and combined effect input parameters (i.e., RF power, machining time, and total pressure).

4.5.3.2 Effect of input process parameters on % ΔR_a

Yao et al. [128] reported the plasma etching of optical material at atmospheric pressure using an excited plasma jet. The results revealed that the surface roughness mainly depends on the plasma parameters, especially the machining time, RF power, and total pressure of the plasma chamber. From Fig. 4.12(a), it could be observed that the processed surface displayed an increased roughness with the increase in RF power. Wang et al. [107] reported that surface roughness increases with an increase in RF power because of increased intensity of plasma emissions. The excellent surface finish of fused silica has been achieved with processing and reactive gas, i.e., O_2, He, and SF_6, at a total pressure of 20 mbar [29]. Fig. 4.12(b) shows that surface roughness is constant initially and decreases further. The physics behind that is the chemical reaction that dominates at higher pressure over physical bombardment.

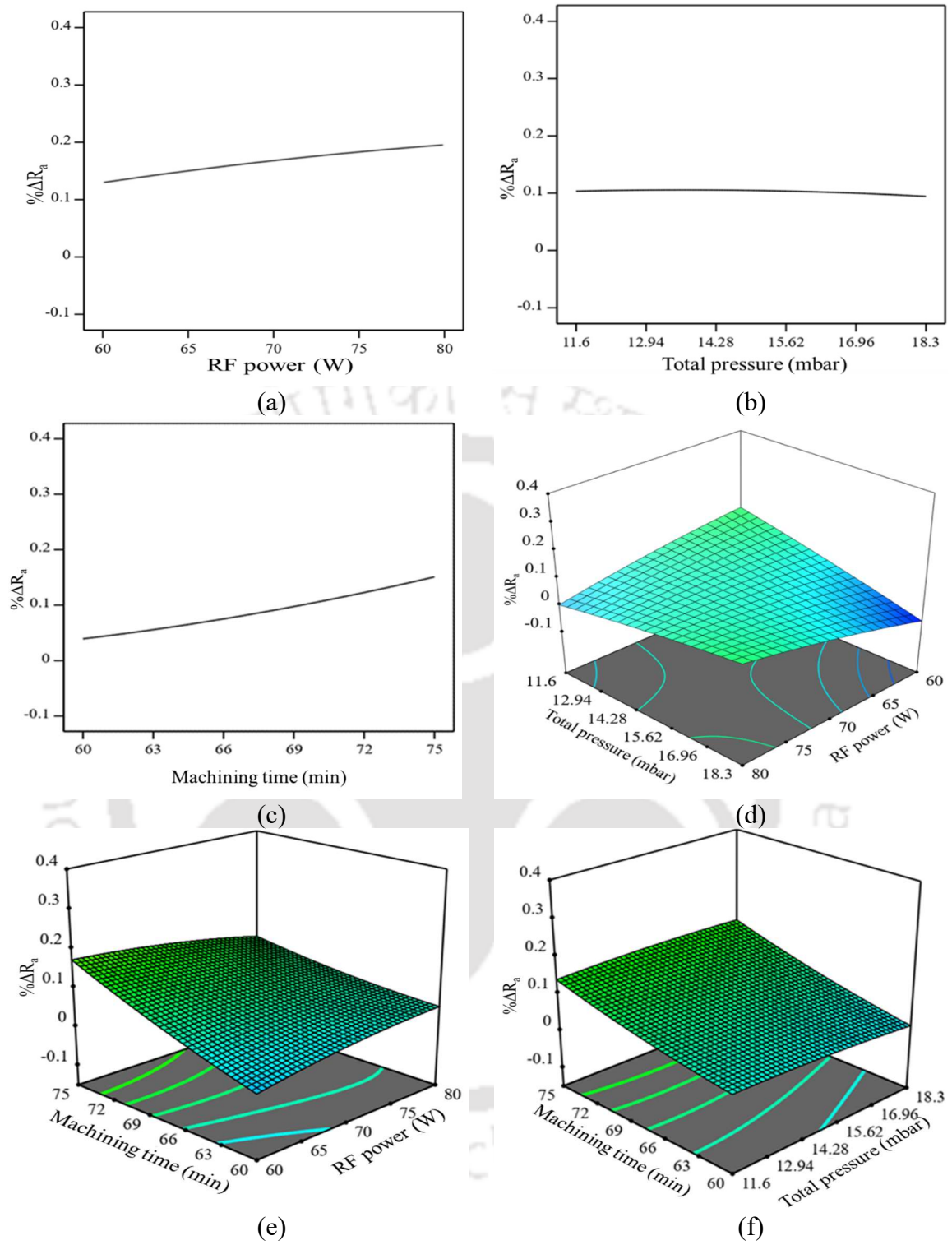

Fig. 4.12 2D plots for % ΔR_a with (a) RF power, (b) total pressure, and (c) machining time; 3D surface plots for % ΔR_a with (d) total pressure and RF power, (e) machining time and RF power, and (f) total pressure and machining time

Dev et al. [29] reported that the silicon atom state increases with the machining time, leading to an increased surface reaction with a fluorine radical. It can be seen from Fig. 4.12(c) that % ΔR_a increases with an increase in the machining time. Fig. 4.12(d) reveals that

the surface roughness dominates at higher power, and the % change is higher at higher power. It is because of the discharge intensity of radicals inside the plasma chamber. Fig. 4.12(e) depicts that the machining time dominates over RF power, and the surface roughness increases with increased machining time. Fig. 4.12(f) shows the effect of machining time and total pressure on surface roughness. It reveals that surface finishing is higher at higher machining times. Fig. 4.12 shows the variation of % ΔR_a with individual and combined effect input process parameters (i.e., RF power, machining time, and total pressure).

4.5.3.3 Optimum Condition and Validation of Model

ANOVA results in Table 4.12 and Table 4.13 show the individual and combined impact of the input variables on the responses, i.e., MRR and % ΔR_a. Multi-response optimization using the RSM technique is utilized in the present study to find out the optimum solution. In the current investigation, the aim is to maximize the MRR and minimize the % ΔR_a. The input parameters remain "in range," as illustrated in Table 4.14. Graphs and experimental results achieved using the RSM technique during optimization are demonstrated in Fig. 4.13 and Table 4.15, respectively. Fig. 4.13 shows that at input parameters, i.e., RF power of 80W, total pressure of 11.6 mbar, and machining time of 60 min, the outcomes, i.e., MRR and % ΔR_a have been achieved as 0.029 mm^3/min and 3.4%, respectively. Furthermore, the highest desirability is obtained as 89.5% at the optimum parametric condition. The experiments are carried out three times at optimum parametric conditions, and the average response value is shown in Table 4.15. While conducting the experiments, pressure ratio (SF_6/O_2) and gas composition ($He:(SF_6+O_2)$) are kept to a constant value of 1:1 and 90:10, respectively. At the optimal input parameter values, the MRR and % ΔR_a values are 0.031 mm^3/min and 3.24%, respectively.

Table 4.14 Input process parameter range for MRR and % ΔR_a

		Limits	
Input parameters	**Goal**	**Lower**	**Upper**
A: RF power	is in range	60	80
B: Total pressure	is in range	11.6	18.3
C: Machining time	is in range	60	75
Output parameters	**Goal**	**Weightage**	
Material removal rate	maximize	1	
$\%\Delta R_a$	minimize	1	

The experiments are conducted at optimum parameters, i.e., RF power of 80 W, total pressure of 11.6 mbar, and a machining time of 60 minutes. Surface roughness (R_a) values are measured three times, and their mean value is considered. The surface roughness values are measured using a 3D optical profiler. Fig. 4.14(a) and (b) presented the surface roughness before (R_a = 2.79 µm) and after (R_a = 2.82 µm) the plasma processing at optimum parametric conditions. It is observed that the surface roughness marginally changes after the plasma process.

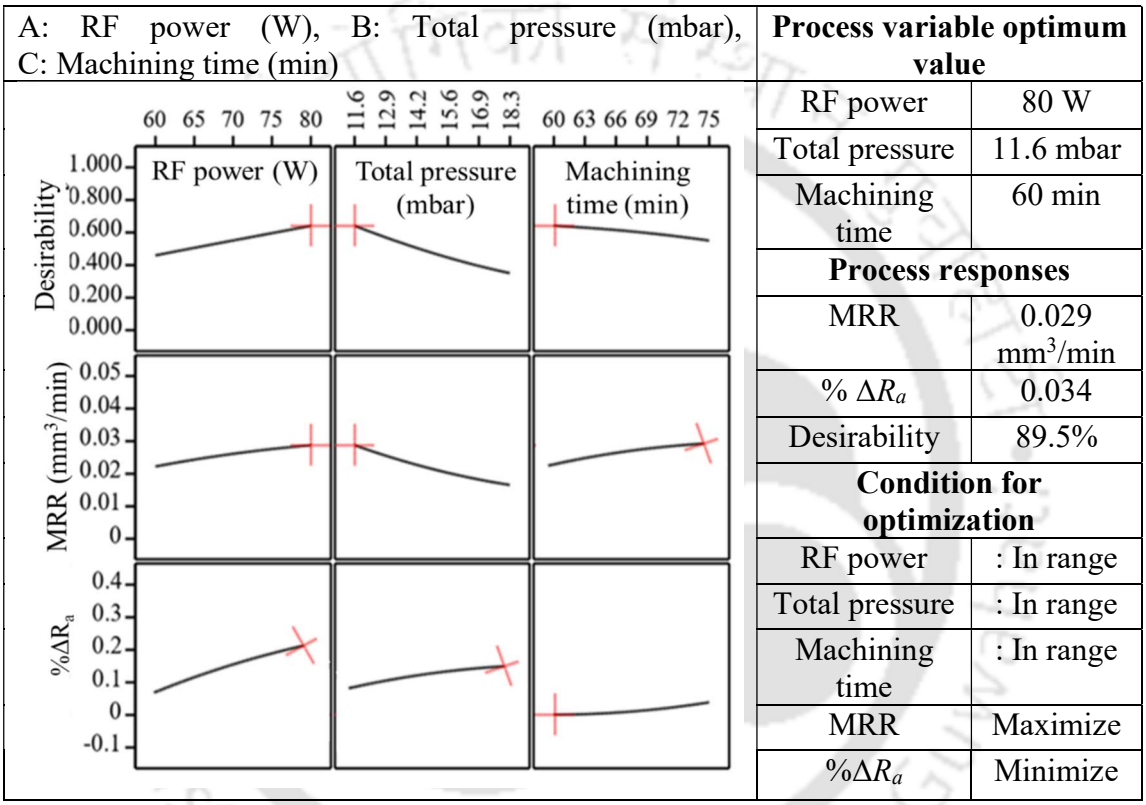

Process variable optimum value	
RF power	80 W
Total pressure	11.6 mbar
Machining time	60 min
Process responses	
MRR	0.029 mm^3/min
% ΔR_a	0.034
Desirability	89.5%
Condition for optimization	
RF power	: In range
Total pressure	: In range
Machining time	: In range
MRR	Maximize
%ΔR_a	Minimize

Fig. 4.13 Optimization plots for MRR and % ΔR_a

Table 4.15 Optimal variable values (input and output) and confirmative results

Process parameters		**Predicted**		**Experimental**		**% Error**	
Input	values	MRR (mm^3/min)	%ΔR_a	Avg. MRR (mm^3/min)	Avg. %ΔR_a	MRR	%ΔR_a
RF power (W)	80						
Total pressure	11.6	0.029	3.4%	0.031	3.24%	6.8%	4.7%
Machining time (mins)	60						

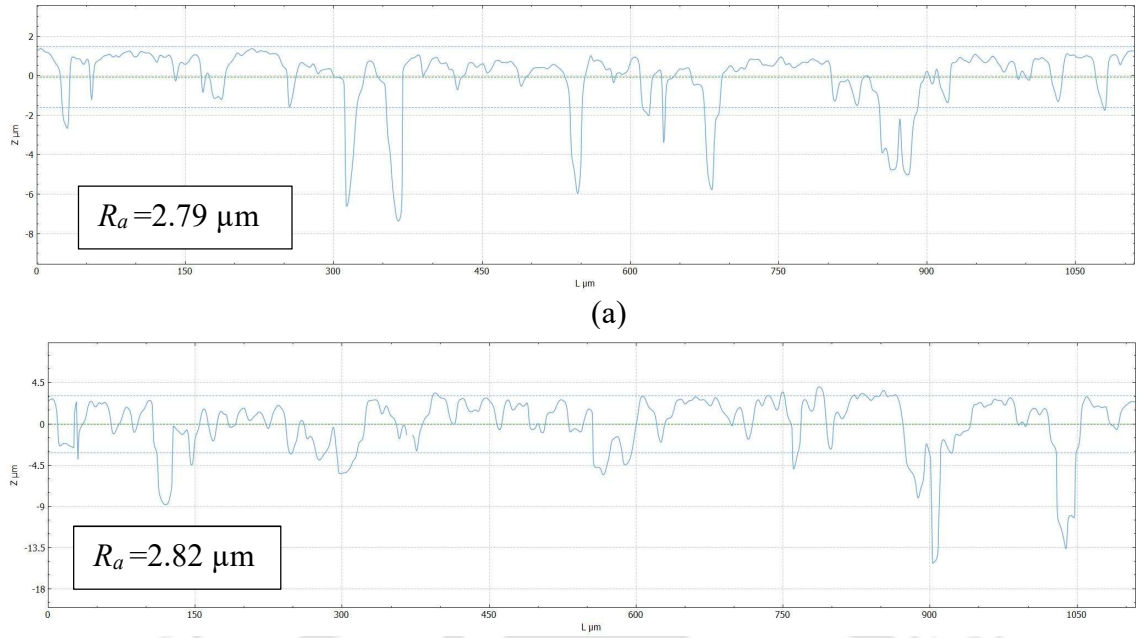

Fig. 4.14 Surface roughness of fused silica (a) before (R_a = 2.79 µm) and (b) after (R_a = 2.82 µm) plasma processing

4.6 Summary

The parametric optimization of process parameters is analyzed using RSM. Regression and statistical analysis for MRR and % ΔR_a with different RF power, pressure ratio, total pressure, and machining time are performed to find a suitable relationship between input and output parameters. A low-pressure ratio and low power with constant total pressure during the reaction resulted in lower MRR and % ΔR_a. The maximum values of MRR and % ΔR_a achieved throughout all experiments are 0.013 mm^3/min and 21.36, respectively. The values achieved after the optimization study of MRR and % ΔR_a are 0.012 mm^3/min and 3.59 for RF power, pressure ratio, and total pressure of 60 W, 3, and 14.3 mbar, respectively. The obtained desirability is 74.90%, which is acceptable. Further, the statistical analysis is carried out with the modified input parameters having different parameter ranges. The optimized values achieved for MRR and % ΔR_a are 0.29 mm^3/min and 3.4%, at RF power of 80 W, total pressure of 11.6 mbar, and processing time of 60 mins. The result depicts that surface roughness marginally changes from 2.79 to 2.82 µm after plasma processing at optimum parametric conditions. The obtained desirability is 89.7%, which is acceptable and better than the previous results.

Chapter 5 Comparative Study of Fused silica Finishing between MPPP and WCE

5.1 Introduction

Plasma is an ionized gas with free positive and negative charges in equal numbers, neutral atoms, radicals, or molecules, in addition to photons emitted from excited species. Plasma processing is a complex phenomenon, and surface finish depends on factors like RF power, time of operation, chamber condition, pressure ratio, total pressure and flow rate, etc. This chapter describes the experimental investigations of surface finish on fused silica using two processes, i.e., medium pressure plasma process (MPPP) and wet chemical etching (WCE). Initially, the experiments are carried out using MPPP and WCE using a mixed hydrofluoric and sulfuric acid solution on two different surface conditions, i.e., coarse machined and lapped surfaces. Fused silica's surface microstructure and chemical composition before and after processing is investigated using field-emission scanning electron microscopy (FESEM) and energy-dispersive X-ray analysis (EDX). Moreover, a comparative study of the plasma process and wet chemical etching for surface roughness and morphology has been discussed.

5.2 Experimental Details

The experiments are conducted on a fused silica substrate with dimensions 20 x 15 x 2 mm^3. The workpiece is kept inside the process chamber on a circular lid substrate made of sital materials of 15 mm diameter. The experiments are conducted after admitting different gases inside the process chamber while passing through the mass flow meters at different flow rates. The fused silica substrate and circular lid are shown in Fig. 5.1(a) and (b), respectively.

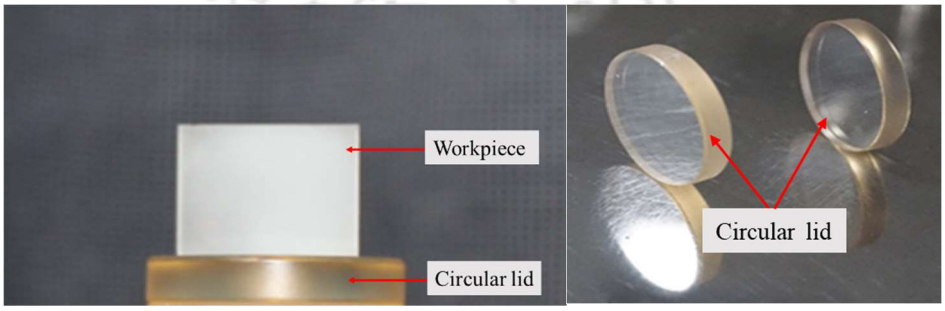

(a) (b)

Fig. 5.1 Representation of (a) fused silica sample and (b) circular lid for workpiece holding

The process parameter, i.e., gas flow rate, RF power, machining time, total pressure, and gas pressure ratio, plays a vital role in surface finish and MRR. During experiments, a set of variable process parameters are chosen, including total pressure, RF power, and machining time. Gas composition and pressure ratio are kept constant throughout the experiment. Fig. 5.2 presents the plasma input process parameters, plasma generation, and output variables. Process parameters play a crucial role in determining the outcome and performance of a plasma process.

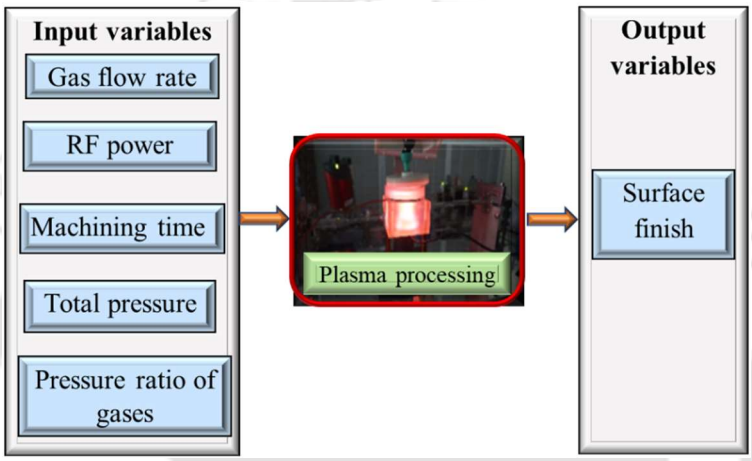

Fig. 5.2 Input parameters and output responses of plasma polishing process

The experimental work is divided into parts A and B. Part A focuses on finishing fused silica using MPPP on coarse machined and lapped surfaces. O_2 and He are used as the process gases, and SF_6 is used as a reactive gas. The occurrence of oxygen helps to dissociate SF_6 into sulfur pentafluoride (SF_5) and fluorine radicals (F*), also preventing the recombination of F* with SF_5 [107]. The higher He content in the mixture indicates increased plasma intensity, affecting the surface finish and material removal rate [115].

Further, in part B, the experiments are conducted on coarse machined and lapped surfaces using wet chemical etching with a mixed solution of hydrofluoric acid and sulfuric acid having a ratio of HF: H_2SO_4 as 2:1. Dev et al. [44] reported that wet chemical etching significantly improves the surface topography while removing micro-cracks. The parameter settings were decided based on preliminary experimental studies [129] and previously published results in the literature by other researchers [6]. The variable and constant parameters used in the experimentation are mentioned in Table 5.1 and Table 5.2. The other experimental details are illustrated in Table 5.3.

Table 5.1 Parameters values selected during experiments

Parameters	Values
Total pressure (mbar)	5, 10, 20
RF Power (W)	80
Machining time (hour)	1–3
Material removal depth (μm)	5, 10, 15, 20, 25, and 30

Table 5.2 Constant parameters selected during experiments

Parameters	Values
Gas composition (He: (SF_6+O_2))	90:10
Pressure ratio (SF_6/O_2)	1:1
HF:H_2SO_4	2:1

Table 5.3 Other experimental details

Description	Details
Number of samples	6
Sample size (mm)	20 ×15 ×2.5
Sample material	Fused silica
Abrasive powder	Al_2O_3
Size of abrasive powder (μm)	15 and 30

Three sets of experiments are carried out in part A using MPPP on the coarse machined and lapped fused silica surfaces. The experiments are conducted at total pressures 5, 10, and 20 mbar to get the variation in the surface finish until 30 μm depth from the substrate surface on coarse machined and the lapped surfaces of fused silica substrates having a dimension of 20 × 15 × 2.5 mm^3. Initial samples are prepared on a lapping machine with surface roughness (R_a) varying between 2.49–2.51 μm for the coarse machined surface. A certain initial surface finish of the substrate is required for plasma polishing before processing on the lapped surface. Lapping is performed to achieve the required surface roughness, followed by plasma polishing. The lapped surface, whose initial surface roughness is 0.13 μm, is generally prepared with 30 and 15-sized abrasive powders on a lapping machine for 5 and 2-minute polishing times, respectively. Moreover, the substrate is cleaned with acetone and ethyl alcohol, followed by the ultrasonic cleaner. In the present study, a planar specimen is kept inside the plasma chamber, and the constant parameters, i.e., gas composition (He:(SF_6+O_2)), of 90:10, pressure ratio (SF_6/O_2) of 1:1, fixed RF power of 80 W are selected to conduct the experiments.

Further, in part B, experiments are conducted on coarse machined and lapped fused silica substrate using wet chemical etching to remove material up to 30 μm depth from the

substrate surface. Initial samples are prepared on a lapping machine with surface roughness (R_a) of 2.52 µm and 0.13 µm for the coarse and lapped surfaces, respectively. The substrate is cleaned with acetone and ethyl alcohol, followed by ultrasonic cleaning. The solution of $HF:H_2SO_4$ is used to remove the material from the substrate.

5.3 Results and Discussion

This section discusses the surface finish of fused silica substrate in parts A and B are analyzed with two different processes, i.e., medium-pressure plasma and wet chemical etching.

5.3.1 Part A: Effect of Plasma Polishing on Fused silica

5.3.1.1 Coarse Machined Surface

Fig. 5.3 shows the surface topography of fused silica at various material removal depths and total pressure. The result depicts that surface roughness linearly increases with the material removal depth, i.e., between 5–30 µm at a total pressure of 5 mbar. The experiments are conducted on similar surfaces (2.49–2.51 µm) at three different plasma chamber pressures to get the variation in the surface roughness with varying material removal depth. The surface roughness achieved after the plasma processing shows a minor increase from the initial roughness value with a material removal depth up to 30 µm. During plasma processing, the fluorine radicals react with the substrate surface. The fluorine radicals react with the sidewalls of the micro-cracks. Thus, the micro-cracks start opening up, forming etched pits. After etching away a thin layer by the plasma, cracks open up to a certain depth, and the isolated etched pits start creating over the entire workpiece surface, degrading the surface finish. Therefore, the surface finish is degraded as these etched pits appear over the whole surface of the workpiece. These pits make the surface slightly rougher. Similar results are also observed at 10 and 20 mbar, but the percentage change in surface roughness (i.e., % ΔR_a) at 20 mbar is lower than at 5 and 10 mbar pressure. It causes a physical bombardment (ions and radicals), and chemical reactions occur at lower pressure [105]. Further, it is observed that at 20 mbar, the surface roughness linearly increases with increased material removal depth up to 20 µm and later becomes constant. It could happen because only a chemical reaction is involved at high pressure. The % ΔR_a at 20 mbar total pressure is much lesser than other pressures, i.e., 5 and 10 mbar. This behavior is due to the bombardments of

ions and radicals that dominate at lower pressures and chemical reactions at high pressures. The energy of electrons in plasma is affected by pressure and electric field; as pressure increases, electron energy decreases [103]. With increased pressure at constant power, the electron mean-free path reduces, and the chance of gaining energy decreases between collisions. It leads to the interaction of molecules at the surface with less energy, obtaining a better surface finish at higher pressure. The scan area is 844.56 x 706.56 μm, and three profiles at different locations are captured to measure each sample's initial and final surface roughness values. It is observed that the surface roughness values are approximately the same at various places on the surface. The material is approximately isotropic in terms of surface roughness values at the measured locations (along X and Y directions). These profiles calculate the average surface roughness (R_a) value. R_a is commonly used to quantify the average deviation of a surface from its mean line or plane. It provides a measure of the roughness of a surface by calculating the arithmetic average of the absolute values of the height deviations from the mean line or plane within a sampling length. The surface roughness (i.e., R_a) [130] and change in surface roughness (ΔR_a) are calculated using Eqs. (5.1) and (5.2), respectively.

$$\text{Surface roughness } (R_a) = (1 / \text{Lm}) \int |\text{y(x)}|\, \text{dx} \tag{5.1}$$

$$\text{Change in surface roughness } (\Delta R_a) = \text{Final } R_a - \text{Initial } R_a \tag{5.2}$$

Where R_a is the average roughness, L_m is the sampling length, y(x) represents the height deviation of the surface from the mean line or plane at a given position x, the integral represents the summation of the absolute values of the height deviations over the sampling length, and dividing by the sampling length gives the average. The variation of surface roughness with material removal depth at different pressures is shown in Fig. 5.4. The percentage change in surface roughness (i.e., % ΔR_a) is calculated using Eq. (5.3).

$$\text{Percentage change in surface roughness } (\%\Delta R_a) = \left(\frac{\text{Final } R_a - \text{Initial } R_a}{\text{Initial } R_a}\right) \times 100 \tag{5.3}$$

Material removal depth	Total pressure of plasma chamber		
	5 mbar	**10 mbar**	**20 mbar**
Initial surface	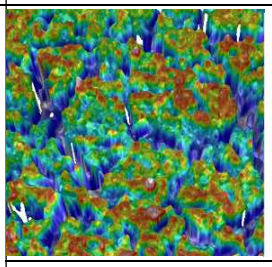	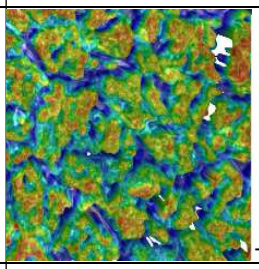	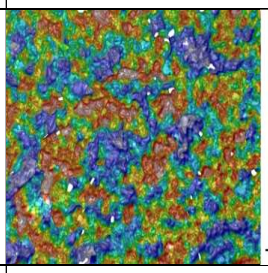
	R_a = 2.50 µm	R_a = 2.49 µm	R_a = 2.51 µm
5 µm	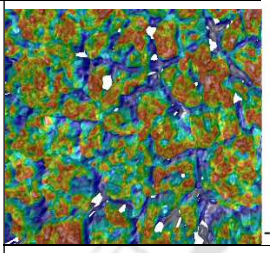	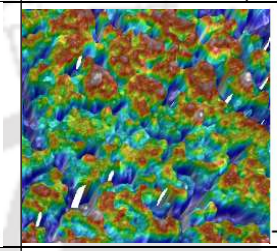	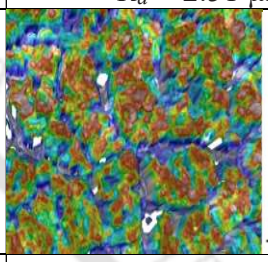
	R_a = 4.82 µm	R_a =4.70 µm	R_a = 2.60 µm
10 µm	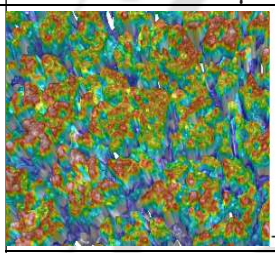	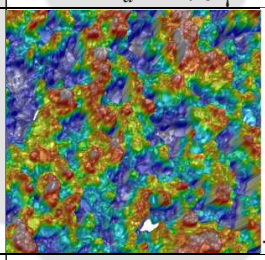	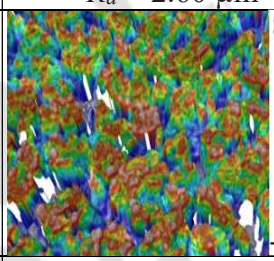
	R_a = 6.74 µm	R_a = 6.30 µm	R_a = 3.30 µm
15 µm	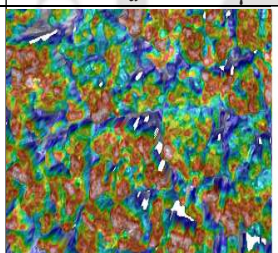	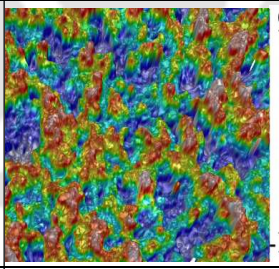	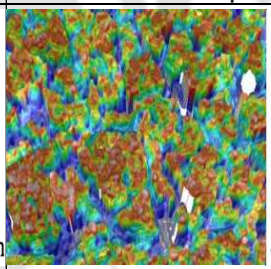
	R_a = 8.08 µm	R_a = 7.43 µm	R_a = 4.02 µm
20 µm	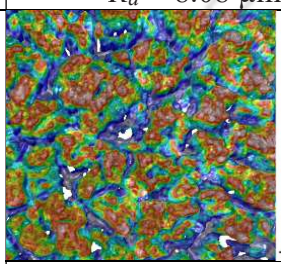	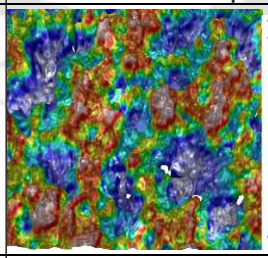	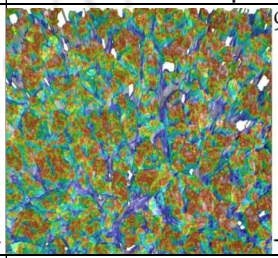
	R_a = 10.42 µm	R_a = 9.43µm	R_a = 4.57 µm
25 µm	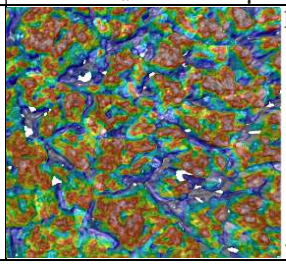	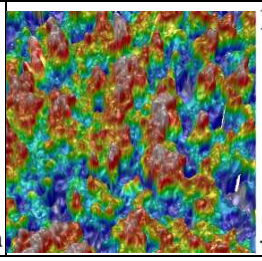	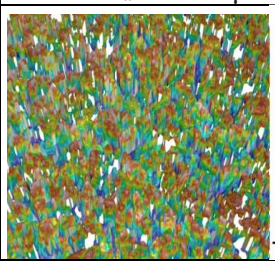

	R_a = 11.46 µm	R_a = 10.27 µm	R_a = 4.60 µm
30 µm	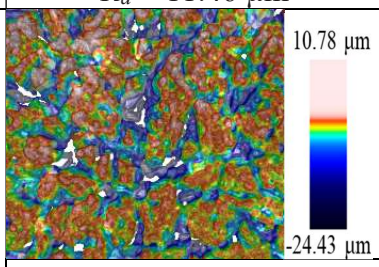	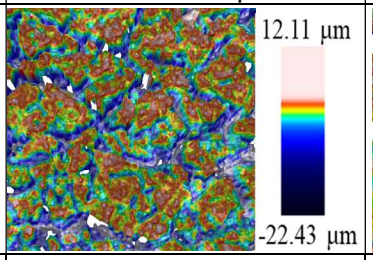	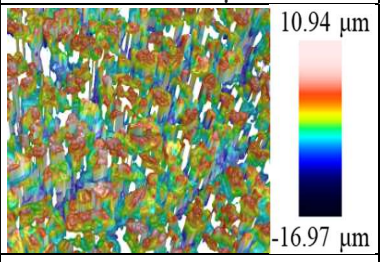
	R_a = 13.98 µm	R_a =12.32 µm	R_a = 4.64 µm

Fig. 5.3 Coarse machined surfaces after plasma polishing at different pressures

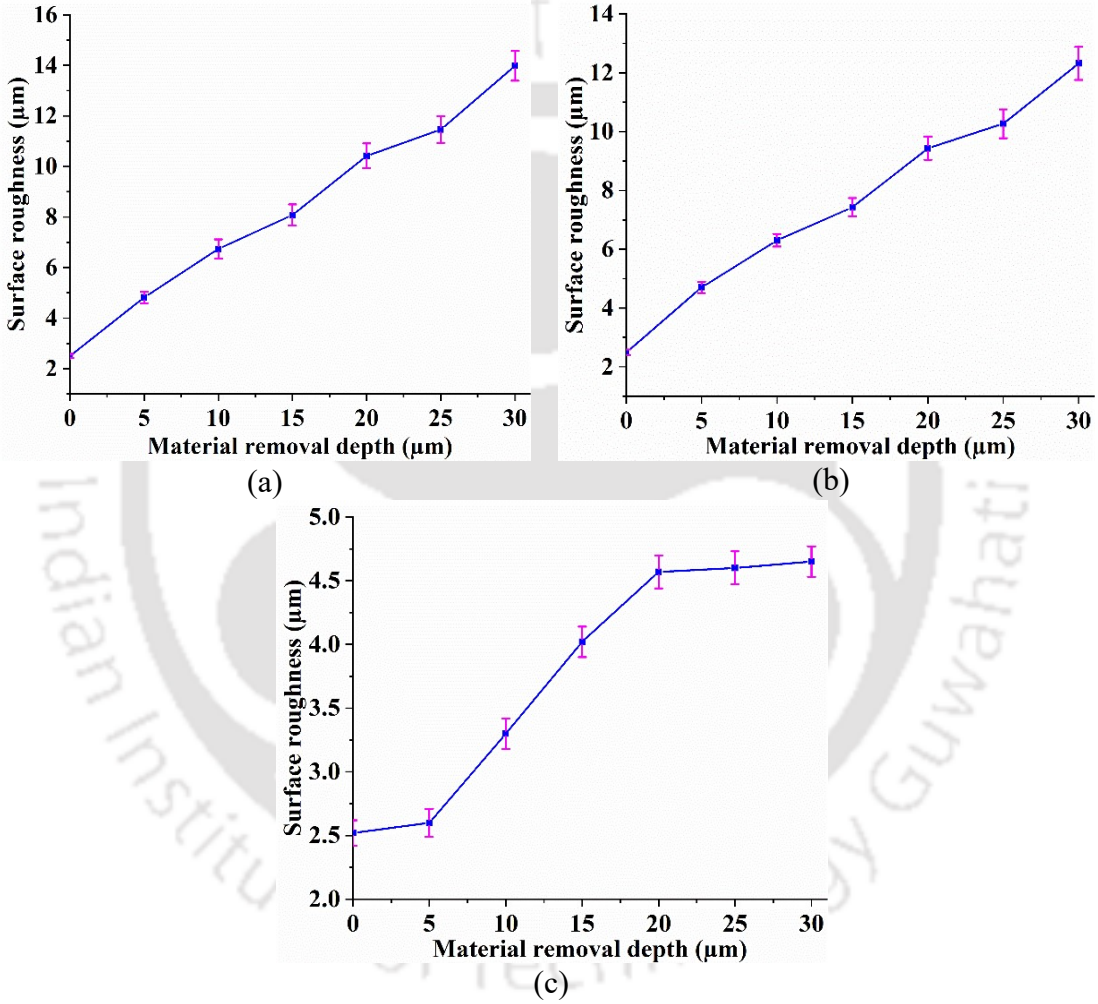

Fig. 5.4 Variation of surface roughness with material removal depth of coarse machined surface at (a) 5 mbar, (b) 10 mbar, and (c) 20 mbar pressures and 80 W fixed RF power

5.3.1.2 Lapped Surface

Initially, the samples are prepared using lapping followed by plasma polishing. During lapping, the material removal is realized through mechanical effects. The cracks get filled up/closed due to the plowing action by abrasives, and the surface becomes smooth. This pre-polished surface is further plasma processed to achieve a highly uniform polished surface

over the entire substrate. The variation of surface topography of lapped fused silica substrate with material removal depth at different pressures, i.e., 5, 10, and 20 mbar, is demonstrated in Fig. 5.5. The result reveals that the surface roughness increases linearly with increased material removal depth, i.e., between 5–30 µm at 5 mbar pressure. Similar results are observed at 10 and 20 mbar total pressure, but the percentage changes in surface roughness (i.e., % ΔR_a) at 20 mbar are lower than at 5 and 10 mbar. It causes fluorine radicals that react with the sidewalls of the micro-cracks on the substrate surface. The micro-cracks are smaller than the coarse surface. Thus, the micro-cracks start opening up, forming etched pits. After etching away a thin layer by the plasma, cracks get opened up, and the isolated etched pits start creating. Therefore, the surface finish is marginally degraded over the entire surface of the workpiece. Moreover, at 20 mbar initially, the surface roughness increases linearly up to 20 µm material removal depth and becomes constant later. It has been observed from the results that the better finish is achieved at 20 mbar because of higher pressure, i.e., the energy of the atom is less, which leads to less penetration on the surface. The % ΔR_a at 5, 10, and 20 mbar pressure on the lapped surface is lower than the coarse machined surface. The reason behind that is the surface crack of the coarse machined surface is more than the lapped surface. The radical reaction affects the sidewalls of the microcracks, which causes the microcracks to open and form etched pits. The variation of surface roughness with material removal depth at different pressures is demonstrated in Fig. 5.6.

Material removal depth	**Total pressure of plasma chamber**		
	5 mbar	**10 mbar**	**20 mbar**
Initial surface	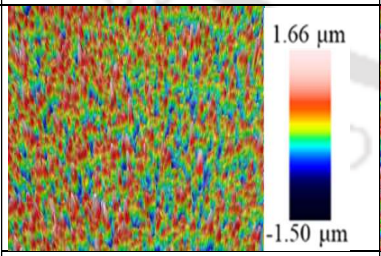	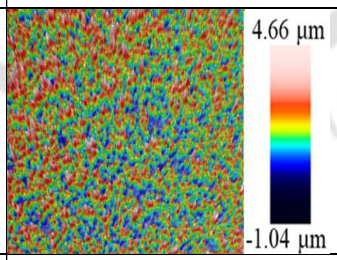	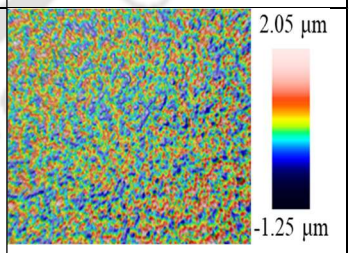
	R_a = 0.13 µm	R_a = 0.13 µm	R_a = 0.13 µm
5 µm	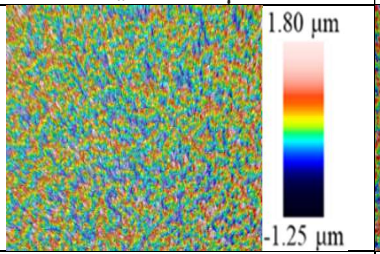	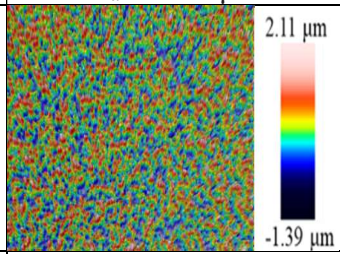	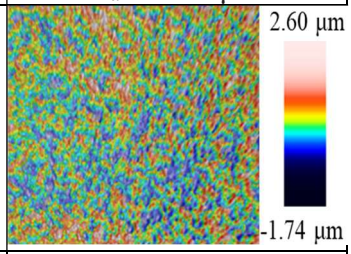
	R_a = 0.16 µm	R_a = 0.15 µm	R_a = 0.14 µm

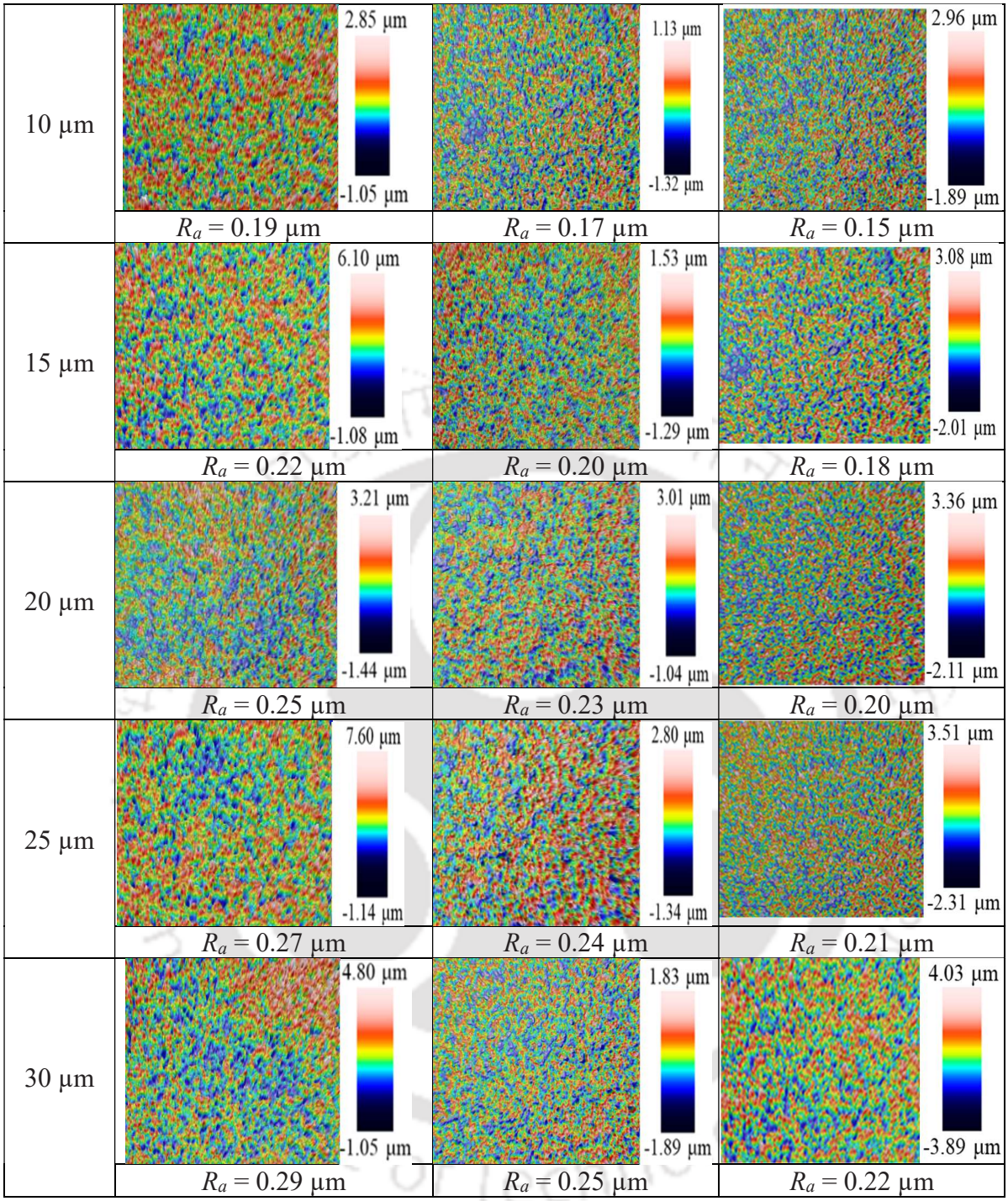

Fig. 5.5 Lapped surface after plasma processing with different total pressures

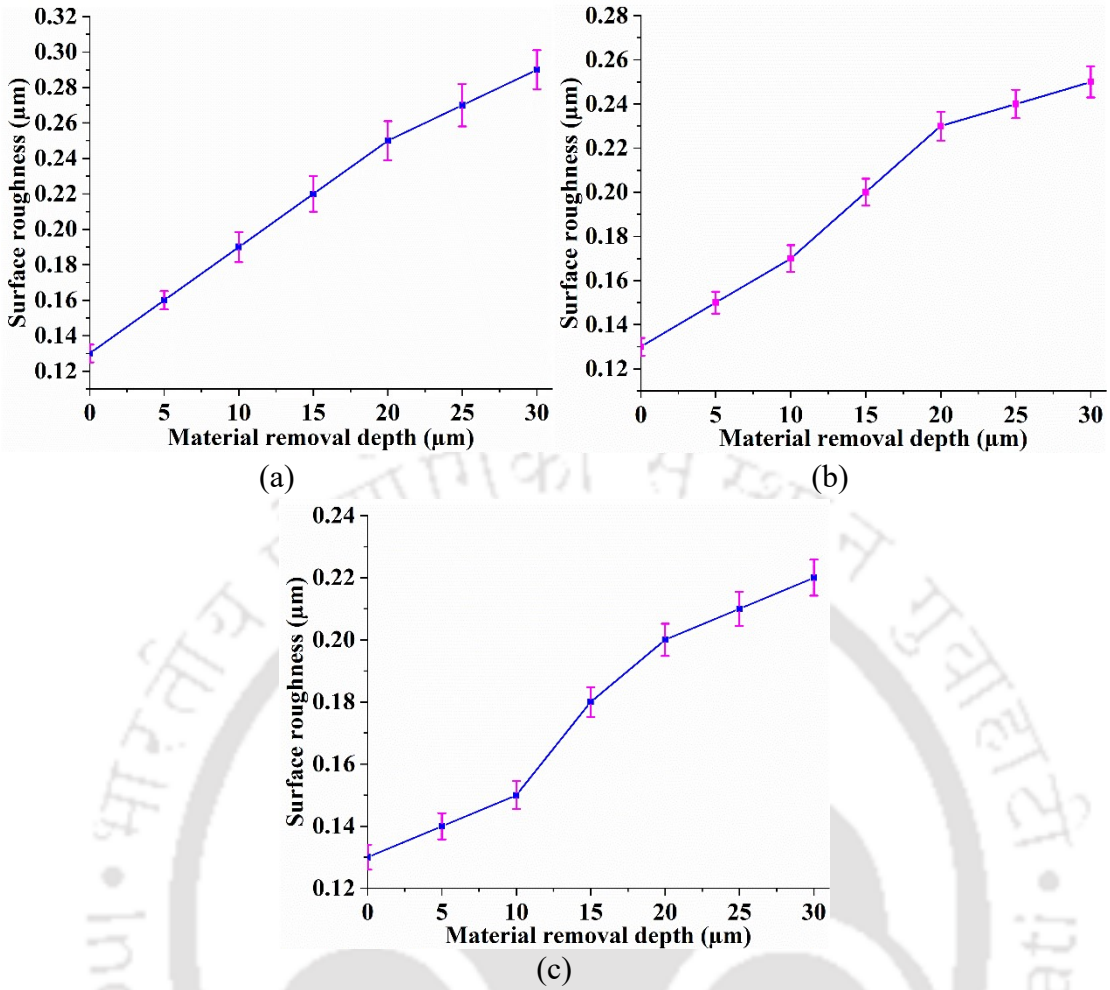

Fig. 5.6 Variation of surface roughness with material removal depth of lapped surface at (a) 5, (b) 10, and (c) 20 mbar pressures and 80 W fixed RF power

5.3.1.3 Comparative Study of Coarse and Lapped Surfaces using MPPP

Fig. 5.7 depicts the comparative analysis of surface roughness variation with material removal depth of coarse machined and lapped surfaces. Fig. 5.7(a) shows the surface roughness change for the coarse and lapped surfaces at 5 mbar pressure. The result shows that surface roughness increases more with the coarse surface than the lapped surface. This is due to the larger surface crack on the coarse surface compared to the lapped surface. In addition, the species' energy remains high during processing at lower pressure, leading to more material removal from the base material, which consists of several surface cracks. During processing, the fluorine radical reacts with the sidewalls of the microcracks, which causes more openings of microcracks and etched pits than the lapped surface. The etched pits coalesce with each other and transform into irregular convex-concave structures, leading to surface degradation. Similar results are also obtained at 10 and 20 mbar pressure (as shown in Fig. 5.7(b) and (c)), and it has been observed that the changes of surface roughness with

material removal depth are more for coarse surface compared to lapped surface. It can be observed that higher surface roughness has been achieved at 5 mbar, followed by 10 and 20 mbar for coarse and lapped surfaces. At higher pressure, electrons have less chance to gain enough energy between collisions to perform excitation and ionization, i.e., the discharge quantity decreases with increased pressure in the plasma chamber. Etched pits are much smaller and shallower at 10 and 20 mbar pressure compared to 5 mbar pressure. With increased material removal depth, these etched pits become wider. At higher removal depth, the etched pits start to intersect gradually and coalesce with each other. After coalescing the separated pits, the surface texture transfers to irregular concave-convex structures. Therefore, surface roughness is increased with material removal depth. With further material removal, the irregular texture almost remains unchanged at higher pressure (i.e., 20 mbar) owing to the restriction of surface roughness changes. In conclusion, the medium-pressure plasma process is suitable for finishing lapped fused silica substrate. It also improves the subsurface defects without any surface contamination.

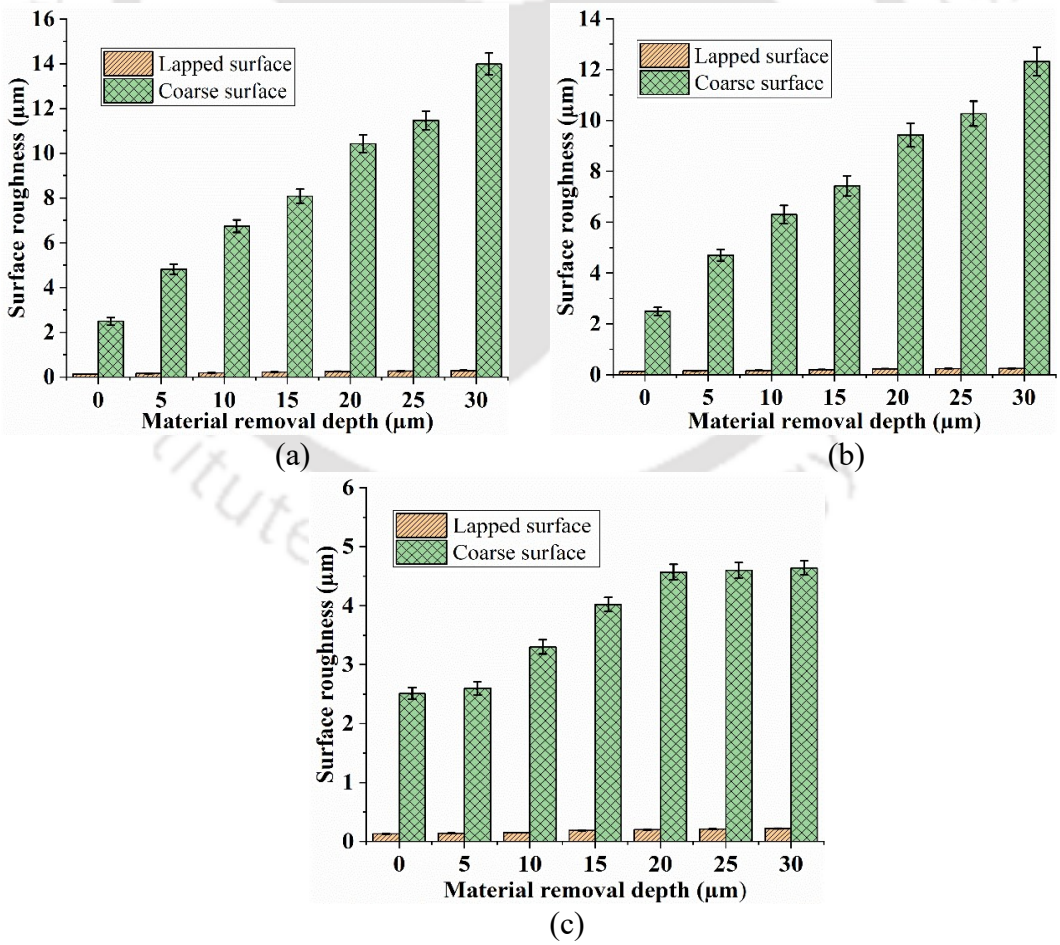

Fig. 5.7 Comparison of surface roughness in coarse and lapped surfaces at different pressures (a) 5, (b) 10, and (c) 20 mbar after plasma processing

5.3.2 Part B: Effect of Wet Chemical Etching on Fused silica

The experiments are conducted with coarse machined and lapped fused silica substrates using wet chemical etching. The initial R_a value of the tested samples represents the surface condition in which they are received/obtained without any post-processing. The best finishing performance is achieved from plasma polishing at 20 mbar pressure with initial surface roughness values of 2.51 µm on the coarse machined surface and 0.13 µm on the lapped surface. Lapped fused silica substrates are prepared on a lapping machine, followed by ultrasonic cleaning, and dried with nitrogen to achieve the required surface conditions. The substrates are processed up to 30 µm material removal depth on the coarse machined and lapped surface using wet chemical etching. The surface roughness (R_a) is increased from 2.52 to 5.01 µm for the coarse surface and 0.13 to 1.29 µm for the lapped surface after wet chemical etching, as presented in Table 5.4. This outcome can be attributed to the replication of scratches and the expansion of cracks as the etching depth increases. Cheng et al. [131] reported that the surface roughness of fused silica increases for an etching depth larger than 2.15 µm. Wet chemical etching of fused silica optical components can open up surface cracks for diagnostic reasons, produce surface topology, and be a potential mitigation approach for removing damaged materials [132]. The $\%\Delta R_a$ is lesser for coarse machined surfaces (i.e., 98.81%) than lapped surfaces (i.e., 892.3%) for the same time intervals of 30 min. During wet chemical etching, a sudden change in surface roughness on the lapped surface might be due to the higher contact area of the lapped surface with the etching agent. A lapped surface is typically smoother and has reduced peak-to-valley height compared to a coarse surface. The irregularities on a lapped surface are minimum, resulting in a more flat and uniform appearance. Hence, the contact between the surface area and the etching agent is higher, leading to faster material removal than the coarse surface. In addition, the control of etching parameters, such as etching time, temperature, agitation, and etchant composition, play an important role in surface roughness.

Table 5.4 Substrate details before and after wet chemical etching

Before processing R_a value (µm)	**Substrate condition**	**Material removal depth (µm)**	**After processing R_a value (µm)**	**% ΔR_a**
2.52	Coarse machined	30	5.01	98.81
0.13	Lapped	30	1.29	892.3

Moreover, wet chemical etching is only a pure chemical reaction. Opening cracks with increased etching depth is responsible for the increased surface roughness. The surface

topography is measured using a 3D optical profiler of coarse and lapped surfaces before and after wet chemical etching, as shown in Fig. 5.8.

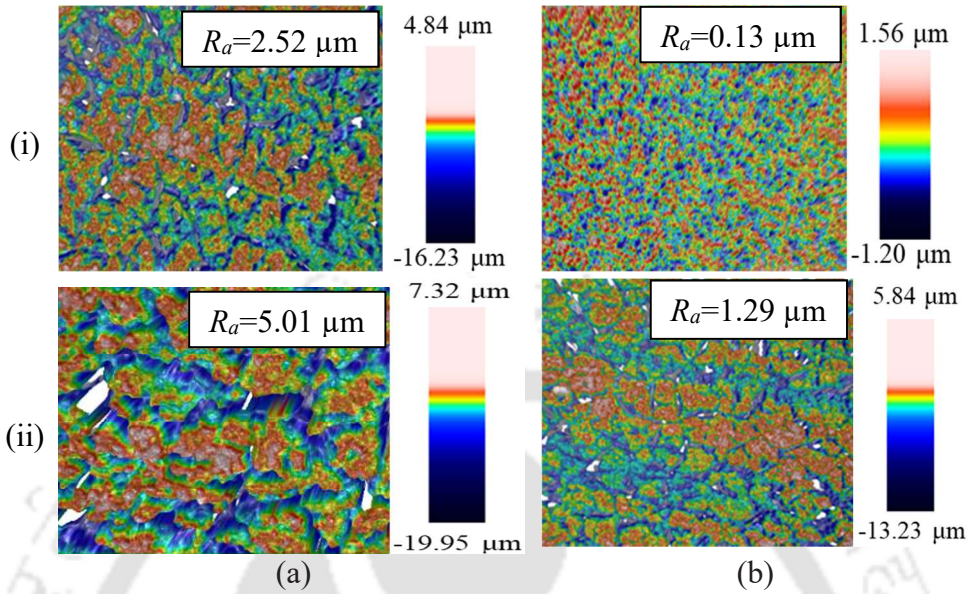

Fig. 5.8 2D surface roughness profiles of fused silica surfaces (i) before and (ii) after wet chemical etching on (a) coarse machined and (b) lapped surfaces

5.3.3 Comparative Study of MPPP and WCE

Fig. 5.9 compares the $\%\Delta R_a$ of the substrate surface using the plasma process (at 20 mbar total pressure) and wet chemical etching. The increased $\%\Delta R_a$ of coarse machined and lapped surfaces are 84.8% and 69.23%, respectively, using the MPPP process at 20 mbar. Moreover, using wet chemical etching, the increased $\%\Delta R_a$ of coarse machined and lapped surfaces are 98.81% and 892.3%, respectively. The increase in surface roughness is mainly due to the chemical reactions and ion bombardments using the plasma process. However, wet chemical etching is only a pure chemical reaction. The opening of cracks with increased etching depth should be responsible for this increase in surface roughness [131]. The result reveals that the percentage change in surface roughness of fused silica for coarse and lapped surfaces is higher in wet chemical etching than in the plasma process.

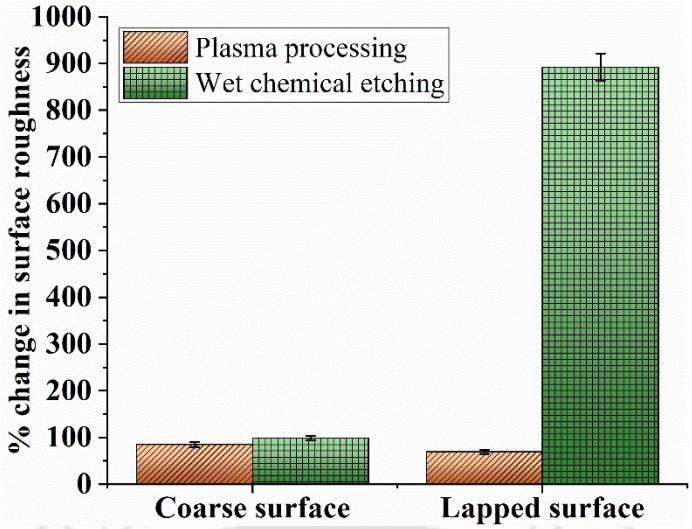

Fig. 5.9 Comparative study of percentage change in surface roughness (i.e., % ΔR_a) between plasma processed and wet chemical etched substrates

5.4 Surface Characterization

This section discusses surface morphology, chemical composition, and crystallography of materials using FESEM, EDX, and XRD.

5.4.1 Morphological Analysis

FESEM is used to analyze the surface microstructure of the substrate surface. FESEM images of coarse-machined and lapped fused silica substrates without processing and after plasma processing and wet chemical etching are provided in Fig. 5.10. Initially, micro-cracks, adhered material, and micro-holes are observed on both coarse machined (Fig. 5.10(i)(a)) and lapped surfaces (Fig. 5.10(i)(b)) before processing. The surface morphology after plasma processing is depicted in Fig. 5.10(ii)(a) for coarse machined and in Fig. 5.10(ii)(b) for the lapped surface. After plasma processing, the irregular surface, etched pit, and micro-cracks are reduced on the coarse machined surface. Comparatively, the lapped surface shows some deposition and reduced cracks after plasma processing. Fig. 5.10(iii) reveals the surface microstructure after wet chemical etching of (a) coarse machined and (b) lapped surfaces. Line patterns are visible on the FESEM image of the coarse machined surface (Fig. 5.10(iii)(a)) after wet chemical etching, and more distinct and denser line patterns are observed on the lapped surface (Fig. 5.10(iii)(b)).

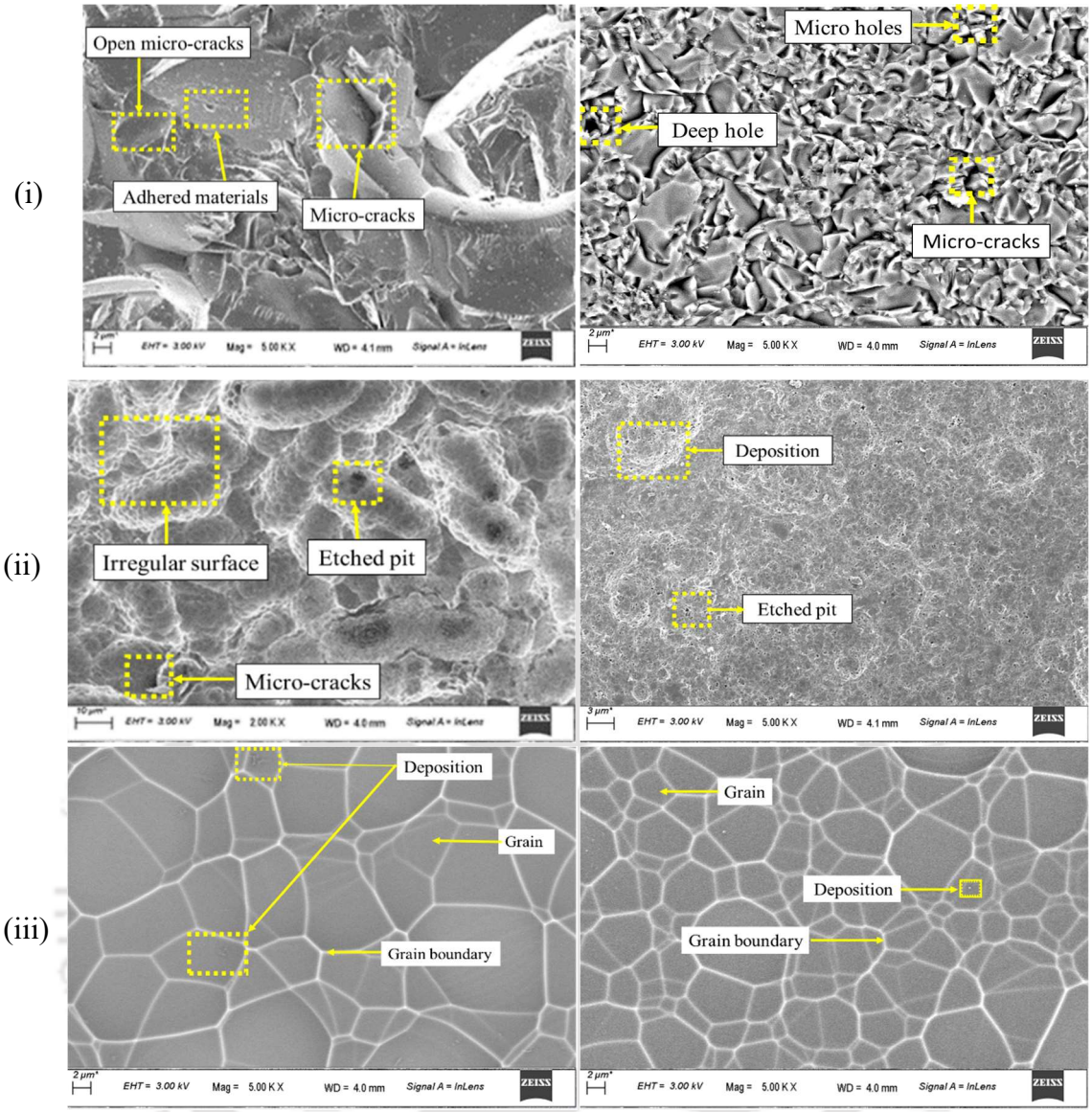

Fig. 5.10 FESEM images on (a) coarse machined and (b) lapped surfaces (i) without processing; After (ii) plasma processing at 20 mbar, 80 W and (iii) wet chemical etching

Energy-dispersive X-ray (EDX) results depict the elemental composition of fused silica before (Fig. 5.11(a)) and, after plasma processing (Fig. 5.11(b)), and after wet chemical etching (Fig. 5.11(c)). Two elements, i.e., Si and O, appear before the process (Fig. 5.11(a)). A higher atomic % of O than Si is observed on the substrate surface before plasma processing, indicating that these are the main elements of fused silica. The elements silicon (Si), fluorine (F), oxygen (O), and carbon (C) appear on the plasma processed surface as shown in Fig. 5.11(b), where the C elements came from the O ring that is used to restrict the leakage of air on the top of the plasma chamber. Most of the O and C elements are from the air and deposited on the surface when the surface is exposed to the environment. Some parts may be from the recipe gas when the chemical reaction progresses. The main elements

involved in this reaction are Si and F, which can combine in various ways. Some F atoms bond with the Si atoms on the outer layers and perform chemical adsorption on the surface. Thus, the existing F element offers evidence of the anticipated main reactions. An additional element, S, is shown in Fig. 5.11(c), although its weight % and atomic % are meager and come from the etching solution.

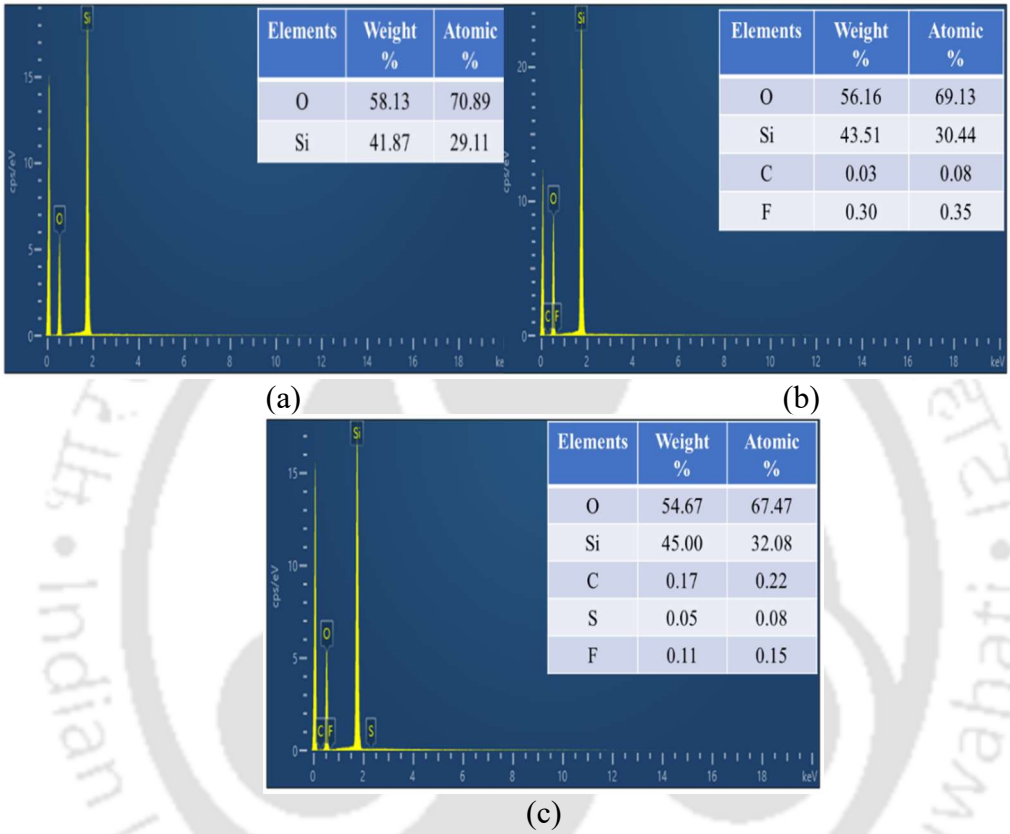

Fig. 5.11 EDX analysis of fused silica surface (a) without processing; after (b) plasma processing and (c) wet chemical etching

5.4.2 XRD Analysis

X-ray diffraction (XRD) is a rapid analytical technique primarily used for phase identification of crystalline material. The XRD analysis is further carried out on plasma-processed substrates as it provides better polishing performances. The non-destructive XRD method can provide a detailed description of the chemical compositions, the material's crystallographic structure, and physical characteristics [133]. The XRD pattern shows no obvious diffraction peaks, indicating the substance is amorphous fused silica [134]. The XRD result shows that while using plasma polishing, there is no change in the pattern (as shown in Fig. 5.12) before and after processing, indicating no addition of any impurity involved after processing. The XRD result shows no apparent sharp diffraction pattern of fused silica before and after

processing, suggesting no significant change after processing. These results confirm that no crystallization occurs during plasma processing. Liu et al. [135] reported the XRD spectra of fused silica and did not observe any sharp diffraction peak on the fused silica substrate. The obtained results confirm no occurrence of crystallization after plasma processing.

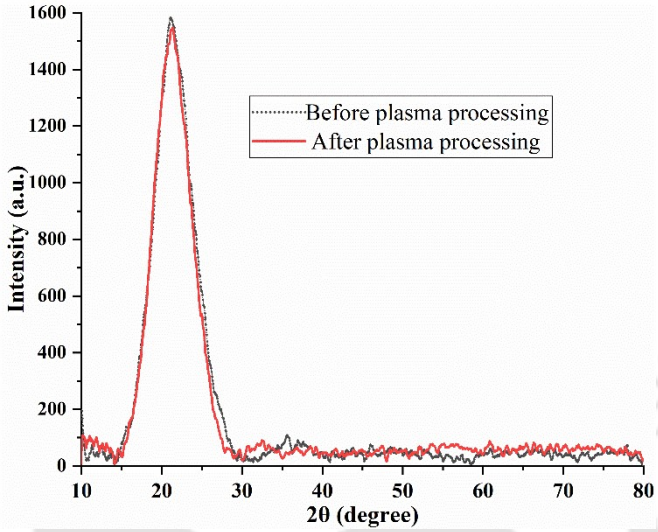

Fig. 5.12 XRD pattern of fused silica before and after plasma processing

5.5 Summary

A comparative analysis of the surface finish between the coarse machined and lapped surfaces of the fused silica substrate is investigated using a medium-pressure plasma process and wet chemical etching. In MPPP, the surface roughness linearly increases with increased material removal depth, i.e., up to 30 µm at a total pressure of 5 mbar for the coarse machined surface. Similar results are also observed at 10 mbar pressure; however, the percentage change in surface roughness is lower than 5 mbar. Further, it has been observed that at 20 mbar pressure, the surface roughness linearly increases up to 20 µm depth, and beyond that, surface roughness remains constant. The lapped surface also follows a similar trend in MPPP. However, the percentage increase in surface roughness of the lapped surface is lower than that of the coarse machined surface. MPPP is suggested for finishing lapped surfaces instead of coarse surfaces. The percentage increase in surface roughness is 84.8 % and 98.81 % on coarse machined surfaces and 69.23 % and 892.3 % on a lapped surface using MPPP (at 20 mbar pressure) and wet chemical etching, respectively. The micro-cracks and uneven surfaces are present on the coarse and lapped surface of the base substrate. After plasma processing, reduced surface defects (i.e., micro-cracks etched pits and deposition) have been obtained on the coarse machined and lapped surface. FESEM image shows line patterns on

the coarse machined surface, and more distinct and denser line patterns are observed on the lapped surface using wet chemical etching. Si, O, C, and F elements appear on the plasma processed surface, indicating reactions during plasma processing. The sharp diffraction peaks have not been observed in XRD patterns, suggesting the material is amorphous in fused silica.

Chapter 6 Surface Finishing Evolution of Prism using MPPP

6.1 Introduction

The rising demand for precision optics, which are widely employed in ground and space-based astronomical instruments and other scientific instrumentation, requires a highly efficient advanced fabrication process. Due to complex-shaped fused silica substrate surfaces like freeform or aspheres with strong curvatures or very small-sized components, a novel non-contact medium-pressure plasma-based method has been developed to finish optical components. This study critically compares the polished optical surfaces, i.e., prism, with a medium-pressure plasma process and wet chemical etching to provide insight into their smoothing, i.e., surface roughness, morphology, and topography. Field emission scanning electron microscopy (FESEM), energy dispersive X-ray (EDX), and atomic force microscopy (AFM) have been utilized to investigate surface morphology, elemental composition, and surface topography, respectively.

6.2 Experimental Details

MPPP is designed and developed to uniformly finish optical components up to 45 mm in substrate length. The system comprises a vacuum pump and various gas-feeding lines that are linked to the plasma chamber. The electrodes are positioned externally to the plasma chamber and are not in touch with the plasma chamber. Medium pressure is chosen for plasma processing to prevent ions from impacting the substrate. Furthermore, an RF excitation scheme with a dielectric barrier is employed to minimize electron heating and facilitate the chemical interaction of reactive free radicals with the surface atoms of the workpiece. An RF excitation frequency of 40.68 MHz is chosen to reduce ion bombardment to a minimum. The plasma chamber is linked to the vacuum system and connected to three gas supply lines. The fiber optic probe head of the optical emission spectrometer is employed to measure the species' densities in the energized states, which is very useful for interpreting the mechanism of material processing under the plasma process. In MPPP, working gases, such as reactive gas, i.e., SF_6, and processing gases (He, O_2), are admitted into the process chamber. The specifications of the plasma processing setup and its operating parameters are illustrated in Table 6.1 and Table 6.2, respectively.

Table 6.1 Specification of plasma processing setup

Gap between electrodes and plasma chamber	Plasma chamber body	Discharge frequency	Substrate material	Processing and reactive gases
1 to 2 mm	Zerodur	40.68 MHz	Fused silica	O_2, He, and SF_6

Table 6.2 Process parameters of medium-pressure plasma process

Parameters	Range	Unit
RF power	80	W
SF_6 flow rate	1.9	sccm
O_2 flow rate	0.49	sccm
He flow rate	10	sccm
Chamber pressure	5, 20	mbar
Processing time	40	mins

Wet chemical etching is used to remove material from freeform and complex surfaces. Initially, the substrate is prepared using the traditional machining processes. The substrate is then dried at room temperature after being thoroughly cleaned in deionized water using an ultrasonic cleaner. Substrates are processed by being submerged in the solution of HF and H_2SO_4 as illustrated in Fig. 6.1. During wet chemical etching, the etchant reacts with the substrate. During experiments, the fused silica substrate is subjected to wet chemical etching using a mixed solution consisting of hydrofluoric acid and sulfuric acid with a volume ratio of 2:1.

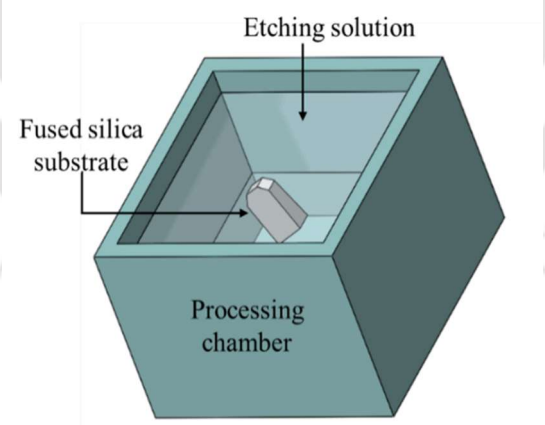

Fig. 6.1 Schematic of wet chemical etching setup

6.3 Results and Discussion

This section discusses the polishing of optical components before and after processing. A comparative study between the plasma process and wet chemical etching of complex substrate, i.e., prism, is also discussed.

6.3.1 Qualitative Analysis of Plasma Discharge for Prism

Preliminary experiments involving the use of a helium (He) plasma are conducted to study and analyze the extent of plasma discharge occurring within a plasma chamber for prism. Such experiments are often essential to understand the behavior of the plasma discharge. Experiments are conducted at varying pressures with different RF power to compare the plasma discharge within the plasma chamber. An increase in plasma discharge directly influences the MRR and surface roughness. A complete plasma discharge uniformly removes material from the substrate [13]. Fig. 6.2 shows qualitative measurements of plasma discharge at various RF power levels and pressures. The removal of material from the substrate during processing depends on the quantity of discharge inside the plasma chamber. The flow rate (sccm) of He gas corresponds to the individual plasma chamber pressure, as illustrated in Fig. 6.2.

Pressure (mbar)	**Flow rate (sccm)**	**Plasma discharge at various RF powers**		
		20 W	**40 W**	**80 W**
5 mbar	8 sccm			
		80-85%	90-92%	100%
10 mbar	17 sccm			
		85-90%	92-95%	100%
15 mbar	32 sccm			
		90-92%	95-97%	100%
20 mbar	45 sccm			
		75-80%	80-82%	100%

30 mbar	80 sccm			
		60-70%	60-70%	60-70%
40 mbar	125 sccm			
		25-30%	30-32%	30-35%
50 mbar	177 sccm			
		17-20%	20-25%	25-30%
60 mbar	235 sccm			
		10-12%	12-14%	12-15%

Fig. 6.2 Qualitative discharge percentage at various pressures and RF power

6.3.2 Comparative study of Prism using MPPP and WCE

This section compares the medium-pressure plasma process and wet chemical etching of a fused silica cuboidal prism to analyze their smoothness, surface roughness, morphology, and topography.

6.3.2.1 Surface Roughness Analysis

The plasma processing experiments are carried out at optimized process parameters, i.e., 90:10 gas composition, 1:1 pressure ratio, and 80 W RF power. The parameter settings were chosen based on preliminary experimental studies and a literature review [129]. Surface roughness (R_a) of SiO_2 substrate is investigated before and after the plasma polishing with a polishing time of 40 mins. Fig. 6.3(a) and (b) show the R_a profiles before and after plasma processing, respectively, at 5 mbar. The results in Fig. 6.3 depict that the surface roughness value increases from its initial value of 0.54 nm to 2.61 nm after plasma polishing. During processing, the chemical reaction occurs between fluorine radicals (F*) and fused silica

surface atoms, which removes material from the substrate. Moreover, a physical bombardment of radicals and ions with substrate surface atoms also happens during processing at lower pressure, i.e., 5 mbar. The 3D surface image/topography and 2D surface roughness profile are obtained using a 3D optical profilometer, as illustrated in Fig. 6.3.

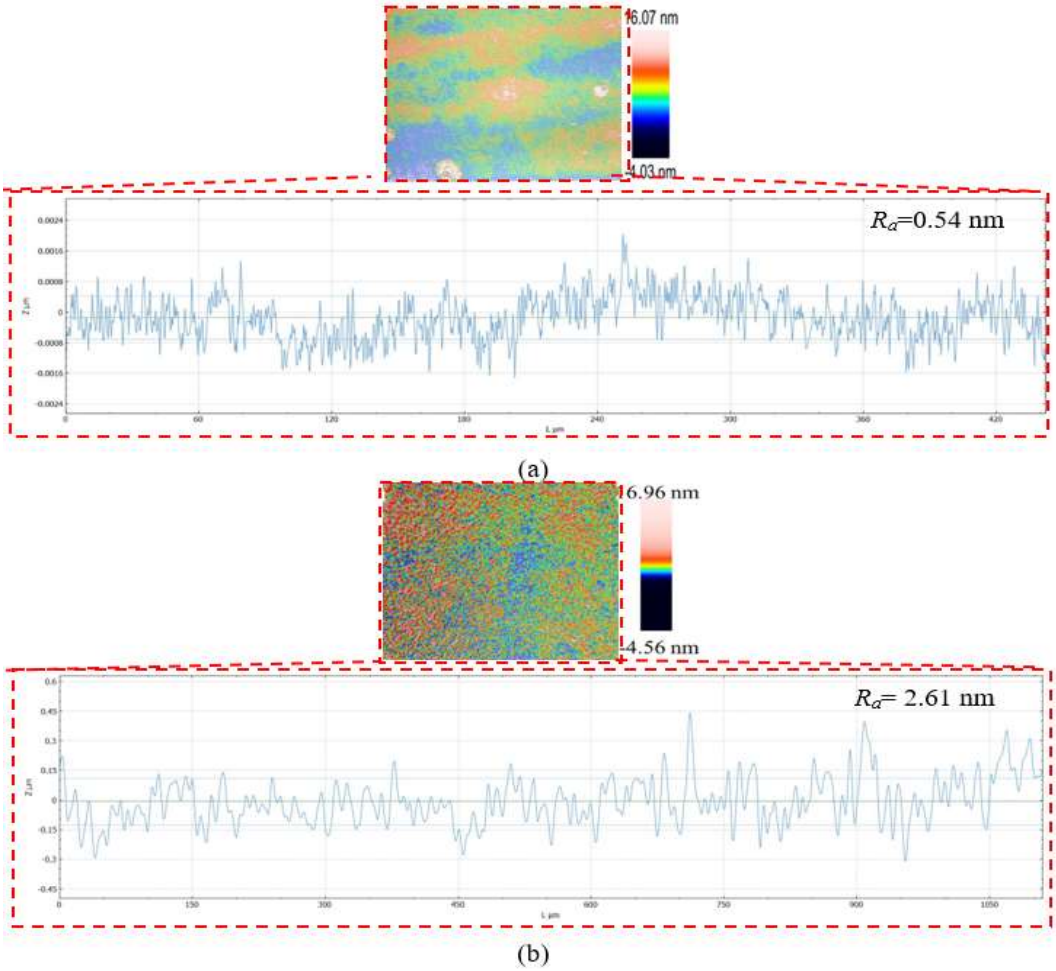

Fig. 6.3 2D and 3D profiles (a) before and (b) after plasma processing of fused silica prism at 5 mbar total pressure

Fig. 6.4(a) and (b) show surface roughness profiles (R_a) before and after the plasma processing of fused silica substrate at 20 mbar total pressure. The result reveals that the surface roughness increases from an initial value of 0.53 nm to 0.57 nm after plasma processing. Each sample's measurements are repeated three times, and the mean roughness value is further calculated. The 3D surface image and 2D surface roughness profiles are illustrated in Fig. 6.4. The surface roughness is much higher at 5 mbar total pressure than 20 mbar because of the high energy of species reacting with surface atoms. The plasma polished surface displays reduced defects and surface cracks after plasma processing because the fluorine radicals come into contact with the surface, and F* radicals react with micro-cracks

sidewalls. Gradually, the etched holes begin to intersect and merge. The surface roughness changes to irregular concave-convex shapes once the isolated pits coalesce. Microcracks and bond strain become eliminated, but surface topography changes after the plasma process. Consequently, micro-cracks and etched pits are diminished following the plasma processing.

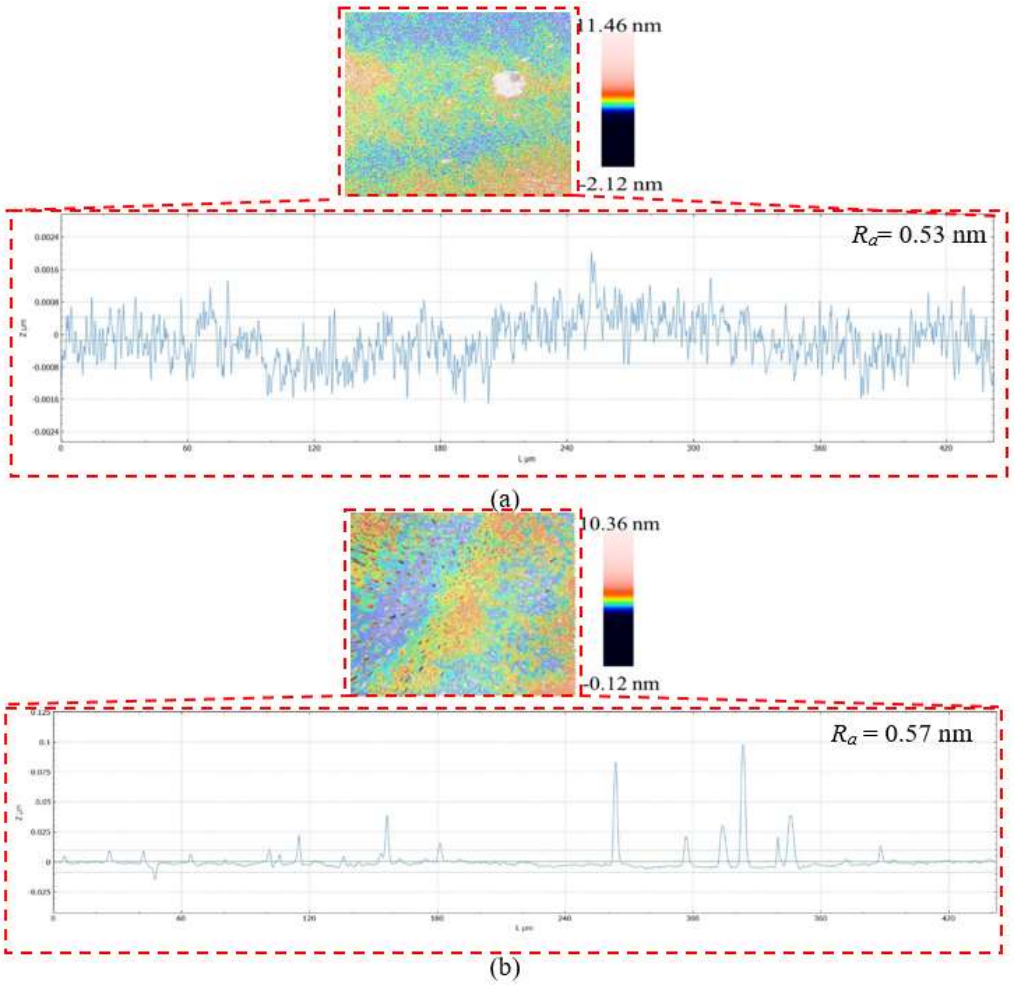

Fig. 6.4 2D and 3D roughness profiles (a) before and (b) after plasma processing of fused silica prism at 20 mbar total pressure

Further wet chemical etching was performed under the HF and H2SO4 solution for 2 mins of etching time. Preliminary experiments are conducted to remove material using wet chemical etching. The removal depth of material is controlled by processing time, and this has been known from the preliminary experiments. Fig. 6.5(a) and (b) illustrate the initial and final surface profiles before and after wet chemical etching.

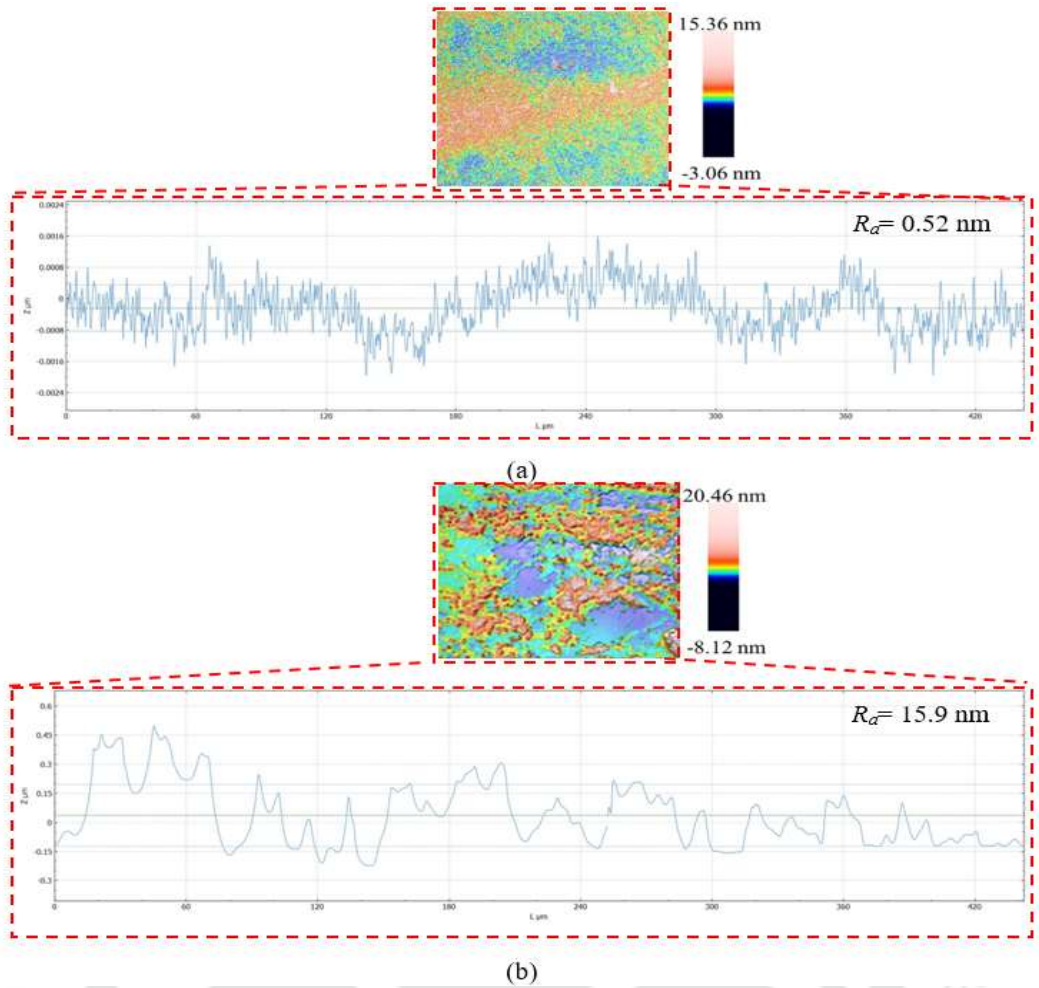

Fig. 6.5 2D and 3D surface roughness profiles (a) before and (b) after wet chemical etching of fused silica prism

The result reveals that the surface roughness increases from its initial value of 0.52 nm to 15.9 nm after wet chemical etching. Moreover, the scratches are enlarged, and the microcracks open up and become blunt due to wet chemical etching. The initial area surface roughness (R_a) value on fused silica substrate increases after wet chemical etching because of the uncontrolled chemical reactions. Wet etching severely damages the substrate's surface topography while eliminating microcracks. Although microcracks and bond strain are reduced, surface topography changes. The 3D surface image/topography and 2D surface roughness profiles are obtained after wet chemical etching using a 3D optical profilometer, as illustrated in Fig. 6.5.

The cuboidal-shaped fused silica prism substrates are investigated using a medium-pressure plasma process and wet chemical etching. The plasma process has been performed at 5 and 20 mbar, 80 W RF power, for a machining time of 40 minutes. The increased surface roughness after plasma processing is higher at 5 mbar total pressure than 20 mbar due to the

higher energy ions and radicals at low pressure; thus, a smooth surface has been observed at higher pressure, i.e., 20 mbar. Moreover, wet chemical etching is performed in the solution of HF and H_2SO_4 for 2 mins etching time. The results show that the surface roughness becomes higher in wet chemical etching than in the plasma process for both 5 and 20 mbar total pressures. The comparison of surface roughness values between the plasma process and wet chemical etching is illustrated in Fig. 6.6.

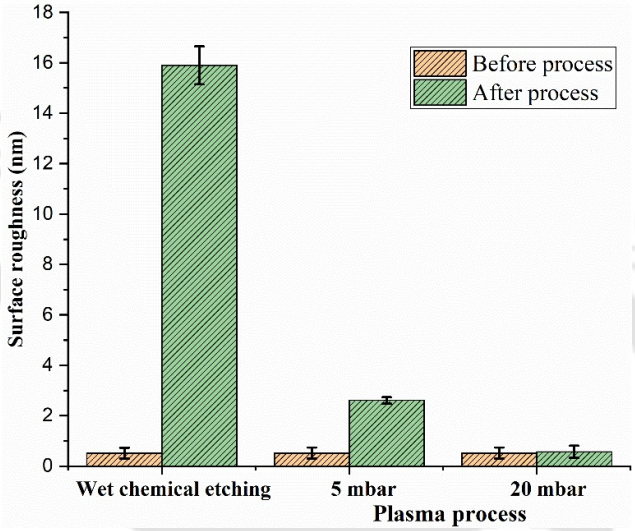

Fig. 6.6 Comparison between surface roughness values of substrates before and after wet chemical etching and plasma processing at different pressures

However, wet chemical etching offers simplicity, cost-effectiveness, and higher material removal. Wet etching consistently leads to significant degradation of surface topography while eliminating microcracks. Microcracks and bond strain are eliminated [44]; however, surface topography changes. It is concluded that the plasma polishing process provides anisotropic etching, which means it etches vertically rather than isotropically. This allows for precise control over the etching profile. However, wet chemical etching allows for faster material removal during fabrication.

6.3.2.2 Analysis of Surface Morphology and Elemental Composition

FESEM analysis is a powerful imaging technique used to obtain high-resolution, detailed images of the surface morphology and topography of a wide range of materials. The surface morphology of fused silica (i.e., optical material) before and after the plasma process and wet chemical etching are shown in Fig. 6.7. Fig. 6.7(a) shows surface morphology before plasma processing, and Fig. 6.7(b) and (c) show the surface morphology after plasma processing at 5

and 20 mbar total pressure, respectively. The surface morphology in Fig. 6.7(b) shows that the microstructure becomes refined and regular, and the cracks are reduced after plasma processing at 5 mbar total pressure. A similar result is also observed at 20 mbar total pressure, and the cracks have been removed from the surface, as shown in Fig. 6.7(c). Moreover, the results show that the etched pits mostly disappeared after the plasma process at both 5 and 20 mbar pressure.

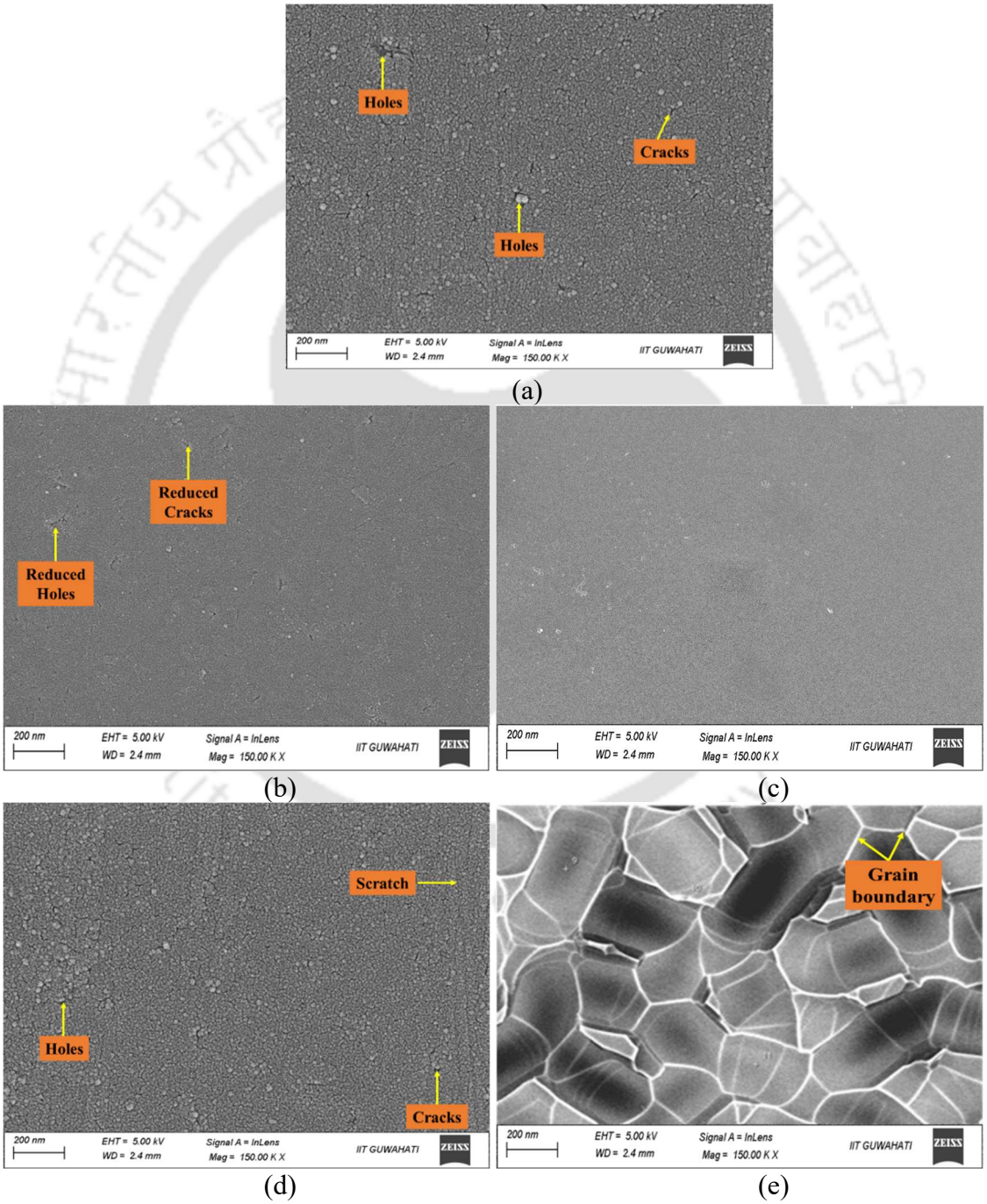

Fig. 6.7 FESEM images of substrate (a) initial and plasma polished surfaces at (b) 5 and (c) 20 mbar pressures; FESEM images (d) before and (e) after wet chemical etching

The surface microstructure of fused silica prism before and after wet chemical etching is shown in Fig. 6.7(d) and (e). Some cracks, holes, and scratches are visible on the initial surface (Fig. 6.7(d)). Also, microstructures are small and regular before processing. The shape of the microstructure and grain boundary has been enlarged and visible after wet chemical etching. The FESEM results show that the grain size (Fig. 6.7(e)) is large and irregular after wet chemical etching, i.e., showing a typical wet chemically etched surface. The results reveal that the wet chemical method produces etched pits that merge and change into irregular convex-concave structures with deteriorated roughness.

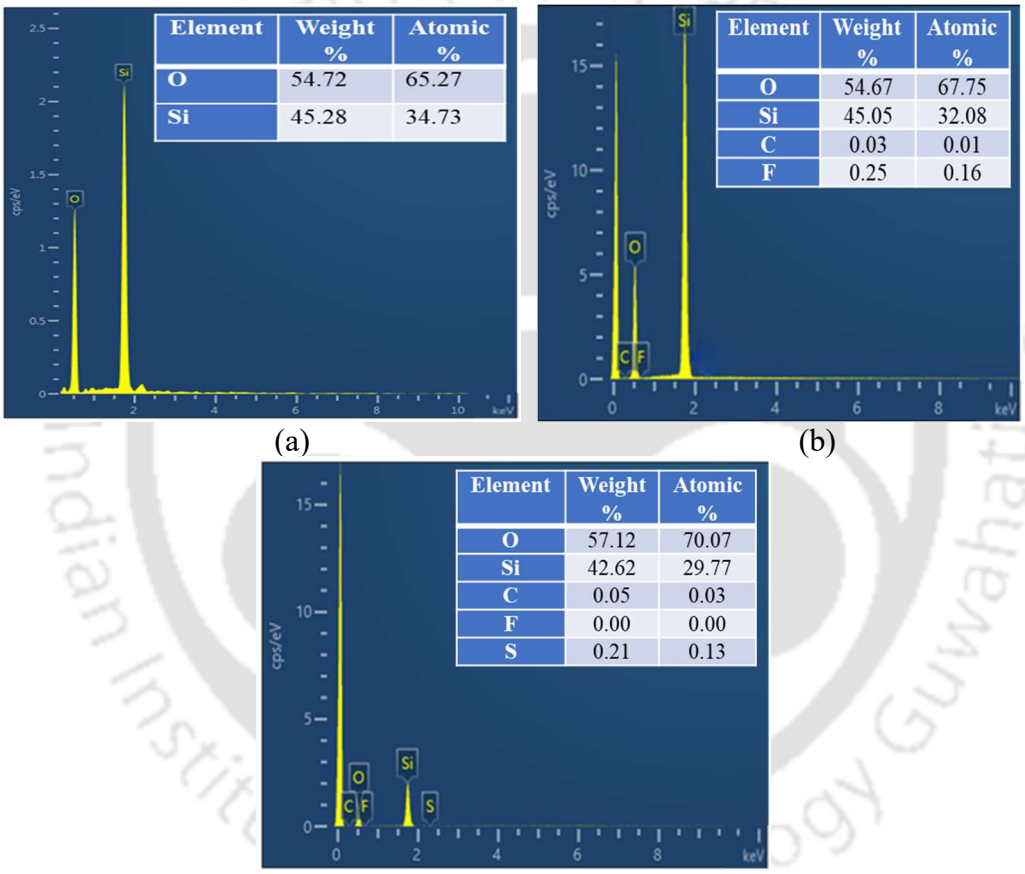

Fig. 6.8 EDX images of fused silica prism substrates on (a) initial surface, (b) after plasma processing, and (c) after wet chemical etching

EDX analysis is a technique used to reveal the elemental composition of the substrate. Fig. 6.8 shows the elemental analysis of fused silica using the plasma process and wet chemical etching. Fig. 6.8(a) shows the two elements, i.e., O and Si, are present on an initial fused silica sample. After processing, the plasma-processed surface shows the elements, i.e., Si, F, O, and C, as illustrated in Fig. 6.8(b). The additional F element is due to the reaction that occurred with the substrate surface. However, the C element comes from the atmosphere

and the O ring. After wet chemical etching, the etched substrate shows the presence of Si, O, F, S, and C elements, as illustrated in Fig. 6.8(c). The additional element, sulfur (S), is observed on the substrate surface after wet chemical etching due to the chemical reactions that happened while processing with the substrate.

6.3.2.3 Atomic Force Microscopy Analysis

Atomic force microscopy (AFM) analysis is a powerful imaging technique used to study materials' surface topography, roughness, and other surface properties. Fig. 6.9(a and c) depicts the initial surface topography of the substrate before processing. Fig. 6.9(b) shows the surface topography of fused silica after the plasma process without any surface defect or contamination using the plasma process at 20 mbar total pressure. The results show the roughness peaks are reduced (Fig. 6.9 (b)) after plasma processing. However, the roughness peaks became irregular, and their height increased after wet chemical etching, as illustrated in Fig. 6.9(d) compared to the initial surface (Fig. 6.9(c)).

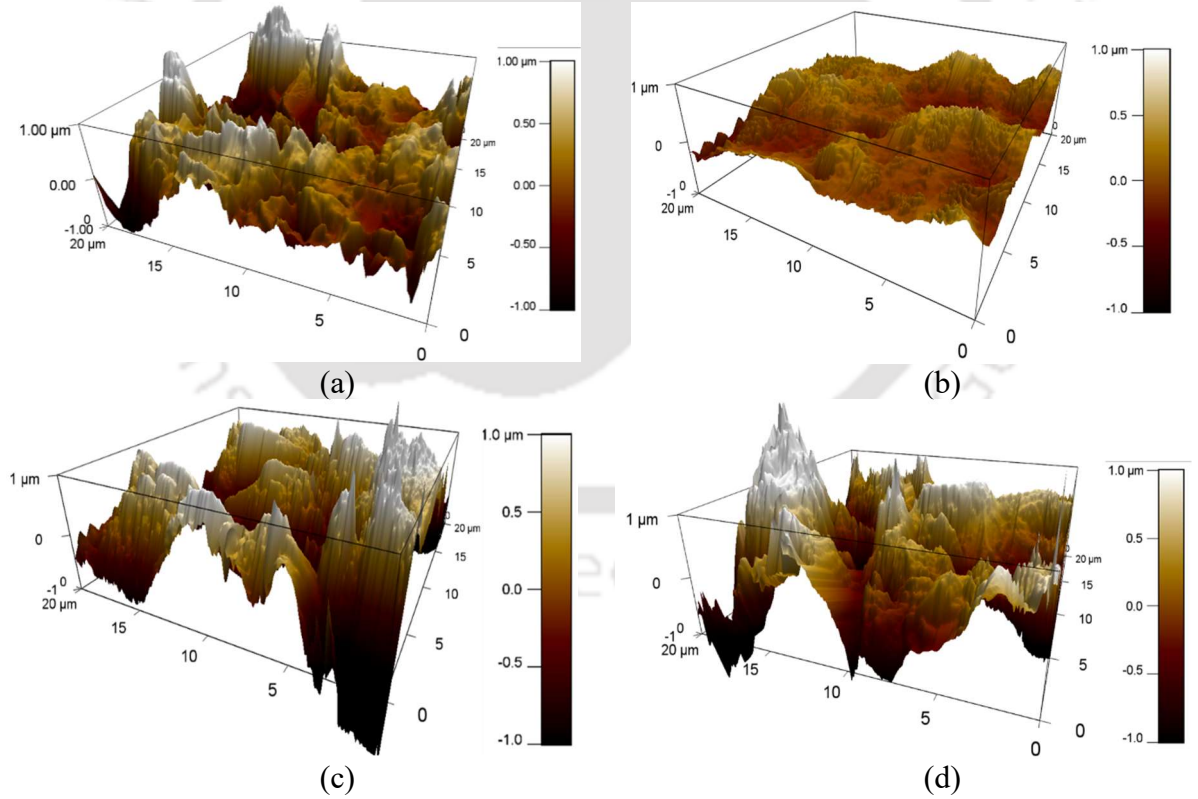

Fig. 6.9 AFM images of substrates (a) before and (b) after plasma polishing at 20 mbar total pressure; (c) before and (d) after wet chemical etching

6.4 Summary

In this section, two different polishing techniques, i.e., medium-pressure plasma and wet chemical etching, lead to obtaining a smooth surface finish without introducing defects and subsurface damage, have been compared. The surface roughness (R_a) is slightly improved from 0.54 nm to 2.61 nm (i.e., 5 mbar) and 0.53 nm to 0.57 nm (at 20 mbar); utilizing MPPP ensures the absence of surface contamination. A higher surface roughness (R_a) value is observed at 5 mbar total pressure than 20 mbar. It is caused by the greater excitation and ionization of ions inside the plasma chamber at 5 mbar. The molecules achieved higher energy at low pressure than at higher pressure. The surface roughness is measured before (R_a = 0.52 nm) and after (R_a = 15.9 nm) wet chemical etching. FESEM images reveal that the grain size was reduced and remained regular in shape after plasma processing. However, the grain size became very fine at 20 mbar, a total pressure greater than 5 mbar. Also, irregular and larger grain boundaries are observed after wet chemical etching. Also, EDX images reveal the reaction involved during the plasma process and wet chemical etching. The additional elements F, C, and sulfur (S) are observed after the plasma processes and wet chemical etching. It shows the reactions that happened while processing with the substrate. Moreover, AFM images reveal that MPPP has reached an outstanding surface topography of optical material without any surface defect or contamination. The finding shows the surface topography peak is reduced after the plasma process. However, a higher increase in surface roughness peak is observed in the case of wet chemical etching.

Chapter 7 Conclusions and Scope for Future Work

7.1 Conclusions

The fabrication and further finishing of fused silica optics often pose challenges for manufacturing industries. In order to achieve surface integrity of the precision optical components, few researchers quantified the damages caused by conventional machining. The physical action of traditional machining processes induces surface and subsurface damage to the brittle fused silica optics. The presence of defects on the critical optics can significantly reduce the device's required performance.

Plasma processing with a medium-pressure region contains the energy advantages of a low-pressure plasma system and chemical reactivity, similar to atmospheric plasma processing. Hence, the entire freeform substrate can be polished simultaneously and uniformly without surface contamination. Medium-pressure plasma processing utilizes a chemical reaction of reactive gases with the substrate atoms. Hence, the surface topography and sub-surface defects improve after plasma processing, unlike low-pressure plasma processing. This technique effectively mitigates damages due to physical contact machining without inducing any further damage to the optical substrate. The MPPP technique is a vital replacement for hazardous chemical etching with HF and H_2SO_4 acids. The final finishing using MPPP can achieve ultra-smooth precision optics.

In the present study, initial experiments are conducted to examine plasma discharge through preliminary modeling and optimization of the plasma chamber's dimension to fabricate fused silica in a medium-pressure plasma process. Further investigations of process parameters and workpiece dimensions are carried out to influence surface finish and material removal rate. Moreover, surface finishing evolution of freeform fused silica by He:(SF_6/O_2) based medium-pressure plasma process and wet chemical etching are also carried out. The MPPP process is fine-tuned and implemented as a superfinishing process on prisms to remove its previously fine-finished molecular or atomic level defects by ultra-high finishing processes like chemo-mechanical polishing. The physical action of conventional machining processes induces surface and subsurface damage to the brittle fused silica optics. The novelty of this process is that it combines the merits of an isotropic etching by low-pressure plasma and atmospheric pressure plasma process. The process can simultaneously polish entire complex 3D surfaces, including cavities where no tool or beam can reach. The

presence of defects on the critical optics can significantly reduce the device's helpful performance. Hence, it is essential to understand the defects and quantify the depth of the damage. Based on experimental investigations, the following conclusions are drawn from the work reported in the thesis.

7.1.1 Design and Development of MPPP setup

A medium-pressure plasma processing setup is designed and developed to achieve isotropic and atomistic polishing on 3D surfaces and establish chemical plasma for achieving stress-free material removal. Plasma process parameters, i.e., gas composition, flow rate, RF power, machining time, pressure ratio, and total pressure, are chosen, and preliminary experiments are performed to get the range of plasma parameters while polishing fused silica optical components having lengths up to 45 mm. The following conclusions are drawn from the present study:

- Process parameters, i.e., gas composition of 90:10, pressure ratio of 1:1, total pressure of 5 mbar, and RF power of 80 W have been obtained as the optimized parameters based on preliminary experiments. The material removal rate has been improved up to 0.10036 mm^3/min at the optimized parameter condition.
- Raman spectroscopy results show that the average ratio ω1/D1 (at different depths) improves from 1.88 before processing to 2.12 after plasma processing, enhancing 13% reduction in damaged and strained layers after plasma processing on the substrate surface.

7.1.2 Investigations of Workpiece Dimension in MPPP

An experimental investigation of atomistic isotropic material removal on fused silica surfaces and a further understanding of the material removal mechanism is carried out. Also, the MRR and surface roughness variation have been performed at different total plasma pressures with varying substrate dimensions/lengths. The conclusions drawn from this study are as follows:

- MRR increases with increased substrate dimension/length at higher total pressure. Also, MRR decreases with increased plasma chamber pressure for smaller substrate dimensions/lengths. The highest and lowest MRR achieved at 5 mbar and 30 mbar pressure are 0.039 mm^3/min and 0.0061 mm^3/min for substrate dimensions/lengths of 45×5×2 mm^3 and 5×5×2 mm^3, respectively.

- The highest and lowest changes in surface roughness have been observed at a total pressure of 5 mbar and 30 mbar. The dimension of the smallest substrate (5×5×2 mm^3) shows the highest change in surface roughness because of more radicals surrounding the substrate.
- The morphological changes reveal that the cracks and holes are removed after plasma processing. The presence of fluorine elements on the processed surface indicates that the reactions occurred on the substrate surface of fused silica.

7.1.3 Parametric Investigations of Plasma Polishing Parameters

The statistical analysis of the plasma process for MRR and % ΔR_a with different RF power, pressure ratio, and total pressure are performed to find a suitable relationship between input and output parameters. Based on this analysis, it has been found that further parametric optimization is needed, considering machining time, which is included as an input parameter for better responses. The conclusions drawn from this study are as follows:

- MRR and % ΔR_a are significantly affected by RF power, pressure ratio, and total pressure of the process chamber. A low-pressure ratio and low power with constant total pressure during the reaction resulted in lower MRR and % ΔR_a.
- The maximum value of MRR achieved throughout all experiments is 0.013 mm^3/min. The maximum achieved value of % ΔR_a is 21.36.
- The RF power has the highest contribution (39.7%), followed by the pressure ratio (30.18%) for MRR. In the case of % ΔR_a, the combined effect of power and total pressure of the plasma chamber has the highest contribution (47.5%).
- The desirability approach has been employed to optimize the parametric conditions. The optimum values of the responses achieved after the optimization study of MRR and % ΔR_a are 0.012 mm^3/min and 3.59, respectively, for RF power, pressure ratio, and total pressure of 60 W, 3, and 14.3 mbar, respectively. The obtained desirability is 74.90%, which is acceptable.
- Subsequently, considering the machining time as the input process parameter, the MRR and % ΔR_a are significantly affected by RF power, total pressure, and machining time. A low RF power and higher total pressure resulted in lower MRR, and higher RF power with lower total pressure resulted in a higher % ΔR_a.
- The maximum value of MRR achieved throughout all experiments is 0.049 mm^3/min, whereas the maximum achieved value of % ΔR_a is 7.5.

- The total pressure of the plasma chamber has the highest contribution (76.7%), followed by the RF power (4.9%) for MRR. In the case of % ΔR_a, machining time has the highest contribution (52.8%), followed by the combined effect of RF power and total pressure of the plasma chamber with the highest contribution (24.5%).
- The desirability approach has been employed to optimize the parametric conditions. The values achieved after the optimization study of MRR and % ΔR_a are 0.029 mm^3/min and 3.4 for RF power, total pressure of plasma chamber, and machining time of 60 W, 18 mbar, and 60 min, respectively. The obtained desirability is 89.7%, which is acceptable.

7.1.4 Comparative Study of Finishing between MPPP and WCE

A comparative analysis of the surface finish of the coarse machined and lapped surfaces of the fused silica substrate has been investigated between the medium-pressure plasma process and wet chemical etching. The conclusions drawn from this study are as follows:

- In MPPP, the surface roughness linearly increases with increased material removal depth, i.e., up to 30 μm at a total pressure of 5 mbar for the coarse machined surface. Similar results are also observed at 10 mbar pressure; however, the percentage change in surface roughness is lower than 5 mbar. Further, it has been observed that at 20 mbar pressure, the surface roughness linearly increases up to 20 μm depth, and beyond that, surface roughness remains constant.
- The lapped surface also follows a similar trend in MPPP. However, the percentage increase in surface roughness of the lapped surface is lower than that of the coarse machined surface. MPPP is suggested for finishing lapped surfaces instead of coarse surfaces.
- The percentage increase in surface roughness is 84.8% and 98.81% on coarse machined surfaces and 69.23% and 892.3% on a lapped surface using MPPP (at 20 mbar pressure) and wet chemical etching, respectively.
- The micro-cracks and uneven surfaces are present on the coarse and lapped surfaces of the base substrate. After plasma processing, reduced surface defects (i.e., micro-cracks etched pits and deposition) have been obtained on the coarse machined and lapped surfaces.
- The sharp diffraction peaks have not been observed in XRD patterns, suggesting the material is amorphous in fused silica.

7.1.5 Surface Finishing Evolution of Prism

The polishing techniques, i.e., medium-pressure plasma process and wet chemical etching, are proposed to obtain a smooth surface finish without introducing defects and subsurface damage. This section also emphasizes a comparative study of surface roughness between medium-pressure plasma processes and wet chemical etching. The conclusions drawn from this study are as follows:

- The surface roughness (R_a) of prisms is slightly improved from 0.54 nm to 2.61 nm (at 5 mbar) and 0.53 nm to 0.57 nm (at 20 mbar) utilizing MPPP. This process ensures the absence of surface contamination. A higher surface roughness (R_a) value is observed at 5 mbar total pressure than 20 mbar. It is caused by the more significant excitation and ionization of ions inside the plasma chamber at 5 mbar total pressure. The molecules achieved higher energy at low pressure than at higher pressure.
- 2D and 3D surface roughness profiles are measured before and after wet chemical etching. The results show that R_a is increased from an initial value of 0.52 nm to 15.9 nm after etching.
- FESEM images reveal that the grain size was reduced and remained regular in shape after plasma processing. However, the grain size became very fine at 20 mbar total pressure than 5 mbar. Also, irregular and larger grain boundaries are observed after wet chemical etching.
- EDX images reveal the reactions involved during the plasma process and wet chemical etching. The additional elements F, C, and sulfur (S) are observed after the plasma processes and wet chemical etching. It shows the reactions that happened while processing with the substrate.
- AFM images reveal that MPPP has reached an outstanding surface topography of optical material without any surface defect or contamination. The finding shows the surface topography peak is reduced after the plasma process. However, a higher increase in surface roughness peak is observed in the case of wet chemical etching.

7.2 Scope for Future Work

The work presented here offers several avenues for further exploration of the plasma process. Some of these possible avenues are listed below.

- A simulation study using Comsol Multiphysics® can be performed to model the plasma process. This study can simulate the chemical interaction of reactive radicals with the substrate surface. Hence, comprehensive molecular modeling may be performed to simulate plasma interactions effectively.
- Modeling of plasma process parameters can be performed for optimum chamber configuration using Comsol® with SF_6, He, and O_2 gases on Hemispherical Gyro (HRG) component and further validation with experimental results.
- Process gas (Ar) and reactive/etching gas (CF_4) can be used for other optical materials, i.e., zerodur, silicon wafer, etc.
- The plasma process can be further optimized and automated using soft computing techniques.
- Periodic plasma cleaning of the plasma chamber and the component surface is mandated to ensure continued polishing for further analysis.
- The depth of damage was quantitatively analyzed by Confocal Raman spectroscopy. However, this study failed to quantify the plastic deformation of machine-induced stresses.

References

[1] J.P. Davim, Surface integrity in machining, Springer London, 2010. https://doi.org/10.1007/978-1-84882-874-2.

[2] Z.W. Zhong, Recent Advances in Polishing of Advanced Materials, Materials and Manufacturing Processes. 23 (2008) 449–456. https://doi.org/10.1080/10426910802103486.

[3] H. Takino, Plasma Chemical Vaporization Machining with a Pipe Electrode for Optical Fabrication : a Review, International Journal of Electrical Machining. (2012) 1–6.

[4] Y. Li, Y. Wu, J. Wang, W. Yang, Y. Guo, Q. Xu, Tentative investigation towards precision polishing of optical components with ultrasonically vibrating bound-abrasive pellets, Optics Express. 20 (2012) 568. https://doi.org/10.1364/oe.20.000568.

[5] W. Peng, C. Guan, S. Li, Ultrasmooth surface polishing based on the hydrodynamic effect, Applied Optics. 52 (2013) 6411–6416. https://doi.org/10.1364/AO.52.006411.

[6] D.S.D. Dev, E. Krishna, M. Das, Development of a non-contact plasma processing technique to mitigate chemical network defects of fused silica with life enhancement of He-Ne laser device, Optics and Laser Technology. 113 (2019) 289–302.

[7] X. Liu, R.. DeVor, S. Kapoor, K.. Ehmann, The mechanics of machining at the microscale: assessment of the current state of the science, J. Manuf. Sci. Eng. 4 (2004) 666–678.

[8] X. Luo, K. Cheng, D. Webb, F. Wardle, Design of ultraprecision machine tools with applications to manufacture of miniature and micro components, Journal of Materials Processing Technology. 167 (2005) 515–528. https://doi.org/10.1016/j.jmatprotec.2005.05.050.

[9] K. Ehmann, D. Bourell, M. Culpepper, R.. DeVor, T. Hodgson, T. Kurfess, M. Madou, K. Rajurkar, An international assessment of micro-manufacturing research technology, Mechanical & Materials Engineering. 155 (2005) 211–224.

[10] M. Kumar, A. Kumar, A. Alok, M. Das, Magnetorheological method applied to optics polishing: A review, IOP Conference Series: Materials Science and Engineering. 804 (2020) 321–328. https://doi.org/10.1088/1757-899X/804/1/012012.

[11] H.N.S. Yadav, H. Bishwakarma, N. Kumar, S. Kumar, P.K. Singh, S. Mohanty, A.K. Das, Production of tungsten carbide nanoparticles through Micro-EDM and its characterization, Materials Today: Proceedings. 18 (2019) 1192–1197. https://doi.org/10.1016/j.matpr.2019.06.580.

[12] A. Barman, M. Das, Generation of Nano-Level Surface Finish by Advanced Nano-Finishing Processes, in: Springer, Singapore, 2020: pp. 199–214. https://doi.org/10.1007/978-981-15-2117-1_10.

[13] C. Chang, B. Kiseung, WetzsteinGordon, B. Lee, L. Gao, Toward the next-generation VR/AR optics: a review of holographic near-eye displays from a human-centric perspective, Optical Society of America. 7 (2020) 1563. https://doi.org/10.1364/OPTICA.406004.

[14] T. Arnold, G. Böhm, H. Paetzelt, Precision asphere and freeform optics manufacturing using plasma jet machining technology, PROCEEDINGS OF SPIE. 1044814 (2017) 43. https://doi.org/10.1117/12.2279786.

[15] V. Sudarsan, Optical materials: Fundamentals and applications, in: Functional Materials, Elsevier Inc., 2012: pp. 285–322. https://doi.org/10.1016/B978-0-12-385142-0.00008-8.

[16] M.R. Shabgard, A. Ivanov, A. Rees, Influence of EDM machining on surface integrity of WC-Co, in: 4M 2006 - Second International Conference on Multi-Material Micro

Manufacture, Elsevier, 2006: pp. 331–334. https://doi.org/10.1016/b978-008045263-0/50075-1.

[17] N. Kumar, N. Mandal, A.K. Das, Micro-machining through electrochemical discharge processes: a review, Materials and Manufacturing Processes. 35 (2020) 363–404. https://doi.org/10.1080/10426914.2020.1711922.

[18] M. Kumar, V. Kumar, A. Kumar, H.N.S. Yadav, M. Das, CFD analysis of MR fluid applied for finishing of gear in MRAFF process, Materials Today: Proceedings. 8 (2021) 245–252. https://doi.org/10.1016/j.matpr.2021.01.116.

[19] N.R. Dhar, M. Kamruzzaman, M. Ahmed, Effect of minimum quantity lubrication (MQL) on tool wear and surface roughness in turning AISI-4340 steel, Journal of Materials Processing Technology. 172 (2006) 299–304. https://doi.org/10.1016/j.jmatprotec.2005.09.022.

[20] X. Liu, F. Zhang, J. Liu, J. Zhang, Y. Chen, Z. Zhang, H. Shen, J. Kong, J. Sun, Atmospheric pressure plasma-assisted precision turning of pure iron material, International Journal of Advanced Manufacturing Technology. 106 (2020) 5187–5197. https://doi.org/10.1007/s00170-019-04798-5.

[21] D.L. Flamm, Mechanisms of silicon etching in fluorine-and chlorine-containing plasmas, Degruyter.Com. 62 (1990) 170–1720. https://doi.org/10.1351/pac199062091709.

[22] S. Al-Hawat, M.A. Polonica, Spatial Structure of Emission Intensity in Capacitive RF Discharge of He: Ne Mixture at Moderate Pressures., Acta Physica Polonica. 117 (2010) 911–916.

[23] F.A. Harb, Noha H and Mutlak, Effect of etching current density on spectroscopic, structural and electrical properties of porous silicon photodetector, Optik. 249 (2022) 168298.

[24] H. Jin, B. Wang, F.Z.-5th I.S. On, U. 2010, Effect on surface roughness of zerodur material in atmospheric pressure plasma jet processing, SPIE. 7655 (2010).

[25] C. Fanara, P. Shore, J.R. Nicholls, N. Lyford, J. Kelley, J. Carr, P. Sommer, A New Reactive Atom Plasma Technology (RAPT) for Precision Machining: the Etching of ULE® Surfaces, Advanced Engineering Materials. 8 (2006) 933–939. https://doi.org/10.1002/ADEM.200600028.

[26] D. Vana, R. Suba, M. Hurajt, The change of surface properties on tested smooth stainless steel surfaces after plasma polishing, International Journal of Engineering Science Invention. 2 (2013) 7–11.

[27] K. Sowmiya, K. Ramachandran, R. Abiyazhini, V.R. Barath, Numerical evaluation on the performance of CO_2 plasma in material processing applications, Materials and Manufacturing Processes. 34 (2019) 1775–1782. https://doi.org/10.1080/10426914.2019.1683575.

[28] C. Gerhard, T. Weihs, D. Tasche, S. Brückner, S. Wieneke, W. Viöl, Atmospheric pressure plasma treatment of fused silica, related surface and near-surface effects and applications, Plasma Chemistry and Plasma Processing. 33 (2013) 895–905. https://doi.org/10.1007/s11090-013-9471-7.

[29] D.S.D. Dev, E. Krishna, M. Das, A novel plasma-assisted atomistic surface finishing on freeform surfaces of fused silica, International Journal of Precision Technology. 6 (2016) 262.

[30] J. Zhang, B. Wang, S. Dong, Application of atmospheric pressure plasma polishing method in machining of silicon ultra-smooth surfaces, Frontiers of Electrical and Electronic Engineering in China. 3 (2008) 480–487.

[31] M. Gupta, D. Dinakar, I. Chhabra, S.J.- Optik, U. 2021, Experimental investigation and machine parameter optimization for nano finishing of fused silica using

magnetorheological finishing process, Optik. 226 (2021) 165908.
[32] L.A. Moore, C.M. Smith, Fused silica as an optical material, Optical Materials Express. 12 (2022) 3043. https://doi.org/10.1364/ome.463349.
[33] J. Ye, J. Yu, H. He, Y. Zhang, Effect of water on wear of phosphate laser glass and BK7 glass, Wear. 376–377 (2017) 393–402. https://doi.org/10.1016/j.wear.2017.01.048.
[34] A.A. Wereszczak, C.E. Anderson, Borofloat and Starphire Float Glasses: A Comparison, International Journal of Applied Glass Science. 5 (2014) 334–344. https://doi.org/10.1111/ijag.12095.
[35] A. Moghaddam, Archive of SID Nonlinear optical response and optical properties modification in crown B270 glass sample with fs laser pulses Archive of SID, Journal of Theoretical and Applied Physics. 25 (2010) 21–25.
[36] R. Yimnirun, P.J. Moses, R.E. Newnham, R.J. Meyer, Electrostrictive strain in low-permittivity dielectrics, Journal of Electroceramics. 8 (2002) 87–98. https://doi.org/10.1023/A:1020543610685.
[37] L.A.B. Pilkington, Review Lecture: The float glass process, Proceedings of the Royal Society of London. A. Mathematical and Physical Sciences. 314 (1969) 1–25. https://doi.org/10.1098/rspa.1969.0212.
[38] A. Esmaeilzare, A. Rahimi, S.M. Rezaei, Investigation of subsurface damages and surface roughness in grinding process of Zerodur® glass–ceramic, Applied Surface Science. 313 (2014) 67–75. https://doi.org/10.1016/J.APSUSC.2014.05.137.
[39] N.J. Kreidl, Recent applications of glass science, Journal of Non-Crystalline Solids. 123 (1990) 377–384. https://doi.org/10.1016/0022-3093(90)90810-9.
[40] Y. Izawa, N. Miyanaga, J. Kawanaka, K. Yamakawa, High power lasers and their new applications, Journal of the Optical Society of Korea. 12 (2008) 178–185. https://doi.org/10.3807/JOSK.2008.12.3.178.
[41] W.M. Steen, Laser material processing - An overview, Journal of Optics A: Pure and Applied Optics. 5 (2003) S3. https://doi.org/10.1088/1464-4258/5/4/351.
[42] H.N.S. Yadav, M. Das, Surface characteristics of fused silica in medium-pressure plasma process, Materials Today: Proceedings. (2023) 1–5.
[43] G. Müller, G. Krötz, J. Schalk, New Sensors for Automotive and Aerospace Applications, Physica Status Solidi (A). 185 (2001) 1–14. https://doi.org/10.1002/1521-396x(200105)185:1<1::aid-pssa1>3.3.co;2-l.
[44] D.S.D. Dev, K. Enni, M. Das, Novel Finishing Process Development for Precision Complex-Shaped Hemispherical Shell by Bulk Plasma Processing, in: Precision Product-Process Design and Optimization, 2018: pp. 313–335.
[45] E. Krishna, K. Sreelakshmy, D.S.D. Dev, M. Das, Medium Pressure Plasma Processing of Fused Silica: A Comparative Study for Material Removal Rate, Plasma Chemistry and Plasma Processing. (2024). https://doi.org/10.1007/s11090-023-10440-w.
[46] What is Surface Finish and Surface Roughness? - ExtruDesign, (n.d.). https://extrudesign.com/surface-finish-surface-roughness-waviness/.
[47] Y. Mizugaki, M. Sakamoto, K. Kamijo, N. Taniguchi, Development of Metal-Mold Polishing Robot System with Contact Pressure Control Using CAD/CAM Data, CIRP Annals - Manufacturing Technology. 39 (1990) 523–526. https://doi.org/10.1016/S0007-8506(07)61111-1.
[48] H. Huang, Z.M. Gong, X.Q. Chen, L. Zhou, Robotic grinding and polishing for turbine-vane overhaul, Journal of Materials Processing Technology. 127 (2002) 140–145. https://doi.org/10.1016/S0924-0136(02)00114-0.
[49] F.J. Shiou, C.C.A. Chen, W.T. Li, Automated surface finishing of plastic injection

mold steel with spherical grinding and ball burnishing processes, International Journal of Advanced Manufacturing Technology. 28 (2006) 61–66. https://doi.org/10.1007/s00170-004-2328-8.

[50] F.J. Shiou, J. Te Chiu, Surface finishing of plastic injection mold steel with ball burnishing and spherical polishing processes on a machining center, Materials Science Forum. 505–507 (2006) 799–804. https://doi.org/10.4028/0-87849-990-3.799.

[51] H. Weule, S. Timmermann, W. Eversheim, Automation of the Surface Finishing in the Manufacturing of Dies and Molds, CIRP Annals - Manufacturing Technology. 39 (1990) 299–303. https://doi.org/10.1016/S0007-8506(07)61058-0.

[52] B. Nowicki, M. Szafarczyk, The new method of freeforms surface honing, CIRP Annals - Manufacturing Technology. 42 (1993) 425–428. https://doi.org/10.1016/S0007-8506(07)62477-9.

[53] J. Masseth, M. Kolivand, Lapping and superfinishing effects on hypoid gears surface finish and transmission errors, in: Proceedings of the ASME International Design Engineering Technical Conferences and Computers and Information in Engineering Conference, 2008: pp. 759–765. https://doi.org/10.1115/DETC2007-34010.

[54] G.W. Chang, B.H. Yan, R.T. Hsu, Study on cylindrical magnetic abrasive finishing using unbonded magnetic abrasives, International Journal of Machine Tools and Manufacture. 42 (2002) 575–583. https://doi.org/10.1016/S0890-6955(01)00153-5.

[55] B.H. Yan, Y.C. Lin, F.Y. Huang, Development of magneto abrasive flow machining process, International Journal of Machine Tools and Manufacture. 42 (2002) 953–959. https://doi.org/10.1016/S0890-6955(02)00021-4.

[56] S. Singh, H.S. Shan, P. Kumar, Wear behavior of materials in magnetically assisted abrasive flow machining, Journal of Materials Processing Technology. 128 (2002) 155–161. https://doi.org/10.1016/S0924-0136(02)00442-9.

[57] P. Singh, L. Singh, S. Singh, Manufacturing and performance analysis of mechanically alloyed magnetic abrasives for magneto abrasive flow finishing, Journal of Manufacturing Processes. 50 (2020) 161–169. https://doi.org/10.1016/j.jmapro.2019.12.033.

[58] N. Saka, T. Eusner, J.H. Chun, Nano-scale scratching in chemical-mechanical polishing, CIRP Annals - Manufacturing Technology. 57 (2008) 341–344. https://doi.org/10.1016/j.cirp.2008.03.098.

[59] Y. Tani, K. Kawata, K. Nakayama, Development of High-Efficient Fine Finishing Process Using Magnetic Fluid, CIRP Annals - Manufacturing Technology. 33 (1984) 217–220. https://doi.org/10.1016/S0007-8506(07)61412-7.

[60] V.K. Jain, ABRASIVE-BASED NANO-FINISHING TECHNIQUES: AN OVERVIEW, Machining Science and Technology. 12 (2008) 257–294. https://doi.org/10.1080/10910340802278133.

[61] S. Gao, H. Huang, X. Zhu, R. Kang, Surface integrity and removal mechanism of silicon wafers in chemo-mechanical grinding using a newly developed soft abrasive grinding wheel, Materials Science in Semiconductor Processing. 63 (2017) 97–106. https://doi.org/10.1016/j.mssp.2017.02.001.

[62] H.N.S. Yadav, M. Kumar, A. Kumar, M. Das, Plasma polishing processes applied on optical materials: A review, Journal of Micromanufacturing. 6 (2023) 27–39. https://doi.org/10.1177/25165984211038882.

[63] W.I. Kordonski, D. Golini, Fundamentals of magnetorheological fluid utilization in high precision finishing, Journal of Intelligent Material Systems and Structures. 10 (1999) 683–689. https://doi.org/10.1106/011M-CJ25-64QC-F3A6.

[64] N.I. Chkhalo, S.A. Churin, A.E. Pestov, N. Salashchenko, Y.A. Vainer, M. V Zorina, Y. Platonov, J. Rodriguez, M. Kriese, E. Gullikson, T. Harada, T. Watanabe, H.

Kinoshita, Roughness measurement and ion-beam polishing of super-smooth optical surfaces of fused quartz and optical ceramics, Optics Express. 22 (2014) 20094–20106.
[65] J.R. McNeil, S.R. Wilson, Neutral Ion Beam Figuring Of Large Optical Surfaces, Workshop on Optical Fabrication and Testing. (1987) FAA4.
[66] G. Sun, J. ShiLei, Z. Jin, Research on Ion beam polishing efficiency with changing different beam diameters, in: Fourth International Conference on Photonics and Optical Engineering, 2021: p. 23.
[67] G. Carter, M. Nobes, I. Katardjiev, The theory of ion beam polishing and machining, Vacuum. 44 (1993) 303–309.
[68] G. Carter, M.J. Nobes, I. V Katardjiev, The theory of ion beam polishing and machining, Vacuum. 44 (1993) 303–309.
[69] M. Xie, Y. Pan, Z. An, S. Huang, M. Dong, Review on Surface Polishing Methods of Optical Parts, Advances in Materials Science and Engineering. (2022).
[70] Y. Namba, H. Tsuwa, R. Wada, N. Ikawa, Ultra-Precision Float Polishing Machine, CIRP Annals. 36 (1987) 211–214.
[71] A. Manna, Finishing of Curved Surface by Rotary Abrasive Float Polishing, in: Advances in Abrasive Based Machining and Finishing Processes, Springer, Cham, 2020: pp. 255–268.
[72] K. Shimada, Y. Matsuo, K. Yamamoto, Y. Wu, A new float-polishing technique with large clearance utilising magnetic compound fluid, International Journal of Abrasive Technology. 1 (2008) 302–315. https://doi.org/10.1504/IJAT.2008.020564.
[73] Y. Namba, Y. Shibano, J.M. Bennett, J.J. Shaffer, Float polishing of optical materials, Applied Optics. 26 (1987) 696–703.
[74] K. Shimada, Y. Wu, Y. Matsuo, K. Yamamoto, Float polishing technique using new tool consisting of micro magnetic clusters, Journal of Materials Processing Technology. 162–163 (2005) 690–695.
[75] A. Kubota, Y. Shinbayashi, H. Mimura, Y. Sano, K. Inagaki, Y. Mori, K. Yamauchi, Investigation of the Surface Removal Process of Silicon Carbide in Elastic Emission Machining, Journal of Electronic Materials. 36 (2006) 92–97.
[76] Y. Mori, K. Yamauchi, K. Endo, Elastic emission machining, Precision Engineering. 9 (1987) 123–128.
[77] K. Yamauchi, H. Mimura, K. Inagaki, Y. Mori, Figuring with subnanometer-level accuracy by numerically controlled elastic emission machining, Review of Scientific Instruments. 73 (2002) 4028.
[78] K. Yamauchi, K. Hirose, H. Goto, K. Sugiyama, K. Inagaki, K. Yamamura, Y. Sano, Y. Mori, First-principles simulations of removal process in EEM (Elastic Emission Machining), Computational Materials Science. 14 (1999) 232–235.
[79] Y.T. Su, S.Y. Wang, P.Y. Chao, Y.D. Hwang, J.S. Hsiau, Investigation of elastic emission machining process: lubrication effects, Precision Engineering. 17 (1995) 164–172.
[80] T. Hirata, Y. Takei, H. Mimura, Machining Property in Smoothing of Steeply Curved Surfaces by Elastic Emission Machining, Procedia CIRP. 13 (2014) 198–202.
[81] Y. Mori, K. Yamauchi, K. Endo, Mechanism of atomic removal in elastic emission machining, Precision Engineering. 10 (1988) 24–28. https://doi.org/10.1016/0141-6359(88)90091-8.
[82] K. Yamamura, T. Takiguchi, M. Ueda, A.N. Hattori, N. Zettsu, High-Integrity Finishing of 4H-SiC (0001) by Plasma-Assisted Polishing, Advanced Materials Research. 126–128 (2010) 423–428.
[83] K. Yamamura, T. Takiguchi, M. Ueda, H. Deng, A.N. Hattori, N. Zettsu, Plasma assisted polishing of single crystal SiC for obtaining atomically flat strain-free surface,

CIRP Annals. 60 (2011) 571–574.
[84] S. Reuter, J. Santos Sousa, G. Daniel Stancu, A. -, Atmospheric pressure plasma jets: an overview of devices and new directions, Plasma Sources Science and Technology. 24 (2015) 64001. https://doi.org/10.1088/0963-0252/24/6/064001.
[85] T. Arnold, G. Böhm, R. Fechner, J. Meister, A. Nickel, F. Frost, T. Hänsel, A. Schindler, Ultra-precision surface finishing by ion beam and plasma jet techniques-status and outlook, Nuclear Instruments and Methods in Physics Research, Section A: Accelerators, Spectrometers, Detectors and Associated Equipment. 616 (2010) 147–156. https://doi.org/10.1016/j.nima.2009.11.013.
[86] A. Schütze, J.Y. Jeong, S.E. Babayan, J. Park, G.S. Selwyn, R.F. Hicks, The atmospheric-pressure plasma jet: A review and comparison to other plasma sources, IEEE Transactions on Plasma Science. 26 (1998) 1685–1694. https://doi.org/10.1109/27.747887.
[87] H. Deng, M. Ueda, K. Yamamura, Chemical and Morphological Analysis of 4H-SiC Surface Processed by Plasma Assisted Polishing, Key Engineering Materials. 516 (2012) 186–191.
[88] J. Laimer, H. Störi, Recent advances in the research on non-equilibrium atmospheric pressure plasma jets, Plasma Processes and Polymers. 4 (2007) 266–274. https://doi.org/10.1002/PPAP.200600114.
[89] T. Yasui, S. Kimura, R. Nishikawa, M. Fukumoto, Carbon nitride deposition onto steel substrates by radio frequency plasma assisted pulsed laser deposition with substrate heating, Thin Solid Films. 523 (2012) 20–24.
[90] D.R. Cote, S. V. Nguyen, A.K. Stamper, D.S. Armbrust, D. Többen, R.A. Conti, G.Y. Lee, Plasma-assisted chemical vapor deposition of dielectric thin films for ULSI semiconductor circuits, IBM Journal of Research and Development. 43 (1999) 5–37.
[91] K. Yamamura, T. Takiguchi, M. Ueda, H. Deng, A.N. Hattori, N. Zettsu, Plasma assisted polishing of single crystal SiC for obtaining atomically flat strain-free surface, CIRP Annals - Manufacturing Technology. 60 (2011) 571–574.
[92] J. Watanabe, J. Suzuki, A. Kobayashi, High Precision Polishing of Semiconductor Materials Using Hydrodynamic Principle, CIRP Annals. 30 (1981) 91–95.
[93] W. Liu, D. Wang, M. Hu, Y. Wang, H. Liang, L. Hang, Roughness evolution of fused silica during plasma polishing processes, Optical Manufacturing Technologies. 7282 (2009) 478–486.
[94] H. Qi, Z. Xie, T. Hong, Y. yu Wang, F. zhi Kong, D. hui Wen, CFD modelling of a novel hydrodynamic suspension polishing process for ultra-smooth surface with low residual stress, Powder Technology. 317 (2017) 320–328.
[95] J. Watanabe, J. Suzuki, A. Kobayashi, High Precision Polishing of Semiconductor Materials Using Hydrodynamic Principle, CIRP Annals. 30 (1981) 91–95.
[96] J. Watanabe, J. Suzuki, A. Kobayashi, High Precision Polishing of Semiconductor Materials Using Hydrodynamic Principle, CIRP Annals. 30 (1981) 91–95. https://doi.org/10.1016/S0007-8506(07)60902-0.
[97] K.T.A.L. Burm, Plasma: The fourth state of matter, Plasma Chemistry and Plasma Processing. 32 (2012) 401–407. https://doi.org/10.1007/s11090-012-9356-1.
[98] A. Fridman, Plasma Chemistry, 2008.
[99] L. Tonks, I. Langmuir, A general theory of the plasma of an arc, Physical Review. 34 (1929) 876–922. https://doi.org/10.1103/PhysRev.34.876.
[100] H.L. Jin, B. Wang, F.H. Zhang, Effect on surface roughness of zerodur material in atmospheric pressure plasma jet processing, Advanced Optical Manufacturing Technologies. 7655 (2010) 423–429. https://doi.org/10.1117/12.866683.
[101] S. Yao, YX and Wang, B and Wang, JH and Jin, HL and Zhang, YF and Dong,

Chemical machining of Zerodur material with atmospheric pressure plasma jet, CIRP Annals. 59 (2010) 337–340.
[102] H. Thomas Arnold, G. Boehm, H. Paetzelt, T. Arnold, Precision asphere and freeform optics manufacturing using plasma jet machining technology, PROCEEDINGS OF SPIE. 10448 1044 (2017). https://doi.org/10.1117/12.2279786.
[103] B. Wang, Q. Zhao, L. Wang, D. S, Application of atmospheric pressure plasma in the ultrasmooth polishing of SiC optics, Materials Science Forum. 532–533 (2006) 532–533.
[104] S. Zhang, Jufan and Wang, Bo and Dong, Application of atmospheric pressure plasma polishing method in machining of silicon ultra-smooth surfaces, Frontiers of Electrical and Electronic Engineering in China. 245 (2008) 480–487.
[105] Shi et al., A high efficiency machining method of SiC: ion-enhanced atmospheric pressure plasma machining, PROCEEDINGS OF SPIE. 9281 (2014) 928104. https://doi.org/10.1117/12.2069012.
[106] M. Castelli, R. Jourdain, G. McMeeking, P. Morantz, P. Shore, D. Proscia, P. Subrahmanyan, Initial strategies for 3D RAP processing of optical surfaces based on a temperature adaptation approach, in: Proceedings of the 36th International MATADOR Conference, 2010: pp. 569–572. https://doi.org/10.1007/978-1-84996-432-6_124.
[107] D. Wang, W. Liu, Y. Wu, L. Hang, H. Yu, N. Jin, Material removal function of the capacitive coupled hollow cathode plasma source for plasma polishing, Physics Procedia. 19 (2011) 408–411.
[108] L. Liu, Weiguo and Wang, Dasen and Hu, Minda and Wang, Yingnan and Liang, Haifeng and Hang, Roughness evolution of fused silica during plasma polishing processes, PROCEEDINGS OF SPIE. 7282 (2009) 72822T. https://doi.org/10.1117/12.831002.
[109] J. Meister, G. Böhm, I.M. Eichentopf, T. Arnold, Simulation of the substrate temperature field for plasma assisted chemical etching, Plasma Processes and Polymers. 6 (2009) 206–213.
[110] J. Hoffmeister, C. Gerhard, S. Brückner, Laser micro-structuring of fused silica subsequent to plasma-induced silicon suboxide generation and hydrogen implantation, Physics Procedia. 39 (2012) 613–620.
[111] A. Kolpaková, P. Kudrna, M. Tichý, Study of Plasma System by OES (Optical Emission Spectroscopy), in: WDS'11 Proceedings of Contributed Papers, 2011: pp. 180–185.
[112] A.K. Ray, A. Reisman, The Formation of SiO2 in an RF Generated Oxygen Plasma: I . The Pressure Range Below 10 mTorr, Journal of The Electrochemical Society. 128 (1981) 2460–2465. https://doi.org/10.1149/1.2127270.
[113] M. Engelhardt, R. Pothiraja, K. Kartaschew, al -, Plasma Sources Science and Technology Etching of silicon surfaces using atmospheric plasma jets Related content Interaction of an argon plasma jet with a silicon wafer, Plasma Sources Science and Technology. 24 (2015) 025002. https://doi.org/10.1088/0963-0252/24/2/025002.
[114] H.N.S. Yadav, M. Kumar, A. Kumar, M. Das, COMSOL simulation of microwave plasma polishing on different surfaces, Materials Today: Proceedings. 256 (2021) 1–7.
[115] S. Al-Hawat, Polonica, M. Akel, Spatial Structure of Emission Intensity in Capacitive RF Discharge of He: Ne Mixture at Moderate Pressures., Acta Physica Polonica. 117 (2010) 911–916.
[116] J. Meister, G. Böhm, I.M. Eichentopf, T. Arnold, Simulation of the Substrate Temperature Field for Plasma Assisted Chemical Etching, Plasma Processes and Polymers. 6 (2009) S209–S213.

[117] Q. Xin, N. Li, J. Wang, B. Wang, G. Li, F. Ding, H. Jin, Surface roughening of ground fused silica processed by atmospheric inductively coupled plasma, Applied Surface Science. 341 (2015) 142–148. https://doi.org/10.1016/J.APSUSC.2015.03.001.
[118] B. Su, Xing and Ji, Chenglong and Xu, Yang and Li, Duo and Walker, David and Yu, Guoyu and Li, Hongyu and Wang, Surface texture evolution of fused silica in a combined process of atmospheric pressure plasma processing and bonnet polishing, Coatings. 9 (2019) 676–689.
[119] G. Greczynski, L. Hultman, A step-by-step guide to perform x-ray photoelectron spectroscopy, Journal of Applied Physics. 132 (2022). https://doi.org/10.1063/5.0086359/2837063.
[120] G. Greczynski, L. Hultman, X-ray photoelectron spectroscopy: Towards reliable binding energy referencing, Progress in Materials Science. 107 (2020) 100591.
[121] H.T. Sahin, RF-plasma vapor deposition of siloxane on paper. Part 2: Chemical evolution of paper surface, Applied Surface Science. 265 (2013) 564–569.
[122] G. Greczynski, L. Hultman, Reliable determination of chemical state in x-ray photoelectron spectroscopy based on sample-work-function referencing to adventitious carbon: Resolving the myth of apparent constant binding energy of the C 1s peak, Applied Surface Science. 451 (2018) 99–103.
[123] M. Kumar, M. Das, Effect of optimum process parameters in rotational-magnetorheological poppet valve polishing, Materials and Manufacturing Processes. 37 (2022) 393–406. https://doi.org/10.1080/10426914.2021.2016818.
[124] G. Derringer, R. Suich, Simultaneous Optimization of Several Response Variables, Journal of Quality Technology. 12 (1980) 214–219.
[125] I. Jeong, K.K. Research, An interactive desirability function method to multiresponse optimization, European Journal of Operational Research. 195 (2009) 412–426.
[126] M. Kumar, S. Ahmad, M. Das, Magnetorheological-finishing of miniature gear teeth profiles using uniform flow restrictor, Materials and Manufacturing Processes. 37 (2022) 467–482.
[127] Y.X. Yao, B. Wang, J.H. Wang, H.L. Jin, Y.F. Zhang, S. Dong, Chemical machining of Zerodur material with atmospheric pressure plasma jet, CIRP Annals - Manufacturing Technology. 59 (2010) 337–340.
[128] F. Jin, HL and Wang, B and Zhang, Effect on surface roughness of zerodur material in atmospheric pressure plasma jet processing, in: 5th International Symposium on Advanced Optical Manufacturing and Testing Technologies: Advanced Optical Manufacturing Technologies, Dalian, China, 2010: p. 76552X.
[129] H. Narayan, S. Yadav, E. Krishna, S. Kombath, S. Dayala, M. Das, S. Dayala Dev, Investigation of MRR and surface characterization using plasma process, Materials and Manufacturing Processes. 38 (2023) 1–13.
[130] E. Sancaktar, R. Gomatam, A Study on the Effects of Surface Roughness on the Strength of Single Lap Joints, 1998. https://doi.org/10.1115/IMECE1998-1121.
[131] J. Cheng, J. Wang, J. Hou, H. Wang, L. Zhang, Effect of polishing-induced subsurface impurity defects on laser damage resistance of fused silica optics and their removal with HF acid etching, Applied Sciences. 7 (2017) 1–23. https://doi.org/10.3390/app7080838.
[132] M.D. Feit, T.I. Suratwala, L.L. Wong, W.A. Steele, P.E. Miller, J.D. Bude, Modeling wet chemical etching of surface flaws on fused silica, Laser-Induced Damage in Optical Materials. 7504 (2009) 75040L. https://doi.org/10.1117/12.836912.
[133] P. Raja, K. Munusamy, V Perumal, Characterization of nanomaterial used in nanobioremediation, in: Nano-Bioremediation: Fundamentals and Applications, 2022: p. 57–83.

[134] W. Wan, Y. Feng, J. Yang, W. Bu, Microstructure, mechanical and high-temperature dielectric properties of zirconia-reinforced fused silica ceramics, Ceramics International. 42 (2016) 6436–6443.
[135] C. Liu, B. Qian, X. Liu, L. Tong, J. Qiu, Additive manufacturing of silica glass using laser stereolithography with a top-down approach and fast debinding, RSC Advances. 8 (2018) 16344–16348.

List of Publications

Journal Publications

1. Hari Narayan Singh Yadav, Manjesh Kumar, Abhinav Kumar, Manas Das, Plasma polishing processes applied on optical materials: A review, Journal of Micromanufacturing, 6 (2021) 251659842110388.

2. Hari Narayan Singh Yadav, Enni Krishna, Sreelakshmy Kombath, D. Sam Dayala Dev, Manas Das, Investigation of MRR and surface characterization using plasma process, Materials and Manufacturing Processes, 38 (2023) 1–13.

3. Hari Narayan Singh Yadav, Manas Das, Experimental investigations through modeling and optimization for fabrication of fused silica in medium-pressure plasma process, Optical Materials, 143 (2023) 114157.

4. Hari Narayan Singh Yadav, Manas Das, Parametric optimisation of plasma polishing process using response surface methodology, Surface Engineering, 39 (2023) 1–14.

5. Hari Narayan Singh Yadav, and Manas Das. "Design and development of medium-pressure plasma process for optical substrate finishing: A comparative study with wet chemical etching." Journal of Manufacturing Processes, 109 (2024): 628-642.

6. Hari Narayan Singh Yadav, and Manas Das. Development and performance evolution of medium-pressure He/SF_6/O_2-based plasma and wet chemical etching process for surface modification of fused silica. Plasma Chemistry and Plasma Processing, 10.1007/s11090-024-10447-x.

7. Hari Narayan Singh Yadav, and Manas Das. Evaluation of plasma parameters' impact on MRR and surface roughness in plasma polishing of fused silica: An investigation of surface characterization. Vacuum, 225 (2024): 113263.

8. Hari Narayan Singh Yadav, and Manas Das. Advances in finishing of optical complex substrates: A comprehensive review, Optics and Laser Technology, 176 (2024): 110938.

9. Hari Narayan Singh Yadav, and Manas Das. Interactions of generated plasma with fused silica in novel medium-pressure plasma process for sub-surface defects minimization, Plasma Sources Science and Technology, (**Under review**).

Conference Details

1. Hari Narayan Singh Yadav, Manjesh Kumar, Abhinav Kumar, Manas Das. "COMSOL simulation of microwave plasma polishing on different surfaces,",2nd International

Conference on Aspects of Materials Science and Engineering (ICAMSE 2021), Panjab University, Chandigarh, India, 05th – 06th March, 2021.

2. Hari Narayan Singh Yadav, and Manas Das. "Investigation of plasma process for finishing of fused silica and its characterization," International Conference on Precision, Meso, Micro & Nano Engineering (COPEN-12), IIT Kanpur, Uttar Pradesh, India, 8th -10th Dec, 2022.

3. Hari Narayan Singh Yadav, and Manas Das. "Surface characteristics of fused silica in a medium-pressure plasma process," 7th International Conference on Production & Industrial Engineering (CPIE 2023), Dr. B R Ambedkar National Institute of Technology, Jalandhar (Punjab) India, 10th - 12th March, 2023.

4. Hari Narayan Singh Yadav, and Manas Das. "Advanced plasma polishing process: Principle, Recent applications, Challenges, and Future scope," 7th International Conference on Production & Industrial Engineering (CPIE 2023), Dr. B R Ambedkar National Institute of Technology, Jalandhar (Punjab) India, 10th - 12th March, 2023.

5. Hari Narayan Singh Yadav, and Manas Das. "Investigation of plasma process for finishing of fused silica and its characterization," 2nd International Conference On Advances in Mechanical Engineering And Material Science (ICAMEMS-23), VIT-AP University, India, 20th- 22nd April, 2023.

6. Hari Narayan Singh Yadav, and Manas Das. "Plasma-based finishing process applied on optical component and its characterization" Research & industrial conclave, IIT Guwahati, India, 14th -16th May, 2023.

7. Hari Narayan Singh Yadav, and Manas Das. "The evolution of morphology and chemistry in fused silica surface after He:(SF_6/O_2) medium pressure plasma processing". 9th International & 30th All India Manufacturing Technology, Design and Research (AIMTDR-2023), IIT BHU, India, 8th - 10th Dec, 2023.

8. Hari Narayan Singh Yadav, Anand Mohan Pandey and Manas Das. "Plasma Polishing Processes–Outlook, Challenges, and Opportunities" 2nd International Conference on Mechanical Engineering: Researches and Evolutionary Challenges (ICMech-REC-2024), Organised by Department of Mechanical Engineering National Institute of Technology Warangal, Warangal Telangana State, India, May 29-31, 2024.

9. Hari Narayan Singh Yadav, Anand Mohan Pandey and Manas Das. "Study on Medium-Pressure Plasma Processing of Fused Silica and its Applications" 2nd International Conference on Mechanical Engineering: Researches and Evolutionary Challenges (ICMech-

REC-2024), Organised by Department of Mechanical Engineering National Institute of Technology Warangal, Warangal Telangana State, India, May 29-31, 2024. **(Paper Id: 64 Received best paper award)**

Book Chapters

1. Hari Narayan Singh Yadav, Manjesh Kumar, and Manas Das, Fundamentals of Plasma polishing. In Advanced machining Science, ISBN: 9781482211092, CRC Press (Taylor & Francis), 2022, DOI: 10.1201/9780429160011-8.

2. Hari Narayan Singh Yadav, and Manas Das. "Advanced Plasma Polishing Process: Principle, Recent Applications, Challenges, and Future Scope." In International Conference on Production and Industrial Engineering, pp. 169-181. Singapore: Springer Nature Singapore, 2023.

3. Hari Narayan Singh Yadav, and Manas Das. The evolution of morphology and chemistry in fused silica surface after He:(SF_6/O_2) medium pressure plasma processing. (**Accepted**)

Patent

1. Hari Narayan Singh Yadav, Manas Das, Process and apparatus for a non-contact medium-pressure plasma for finishing of optical components, Indian Patent, Patent Application Number: 202231064559, Nov 2022 |**Patent Published.**